KING FAHD UNIVERSITY OF PETROLEUM AND MINERALS

DHAHRAN 31261, SAUDI ARABIA

DEANSHIP OF GRADUATE STUDIES

This thesis, written by

MOHAMMED ABDALLA AYOUB

Under the direction of his thesis advisor and approved by this thesis committee, has been presented to and accepted by the Dean of Graduate Studies, in partial fulfillment of the requirements for the degree of

MASTER OF SCIENCE IN PETROLEUM ENGINEERING

Thesis Committee

M. A. Aggour

Prof. Mohamed Ahmed Aggour (Thesis Advisor)

S. Osman

Dr. El-Sayed Ahmed Osman (Co-Advisor)

Dr. Sidqi A. Abu-Khamsin (Member)

H. Y. Al-Yousef

Dr. Hasan Y. Al-Yousef (Member)

A. A. Almajed

Dr. Abdulaziz A. Al-Majed (Member)

Dr. Sidqi A. Abu-Khamsin
(Department Chairman)

Prof. Osama A. Jannadi
(Dean of Graduate Studies)

1550 / 5/5

Date May 9, 2004

خلاصة الرسالة

اسم الطالب: محمد عبدالله ايوب

عنوان الدراسة: تطوير واختبار نموذج لشبكة الاعصاب الاصطناعية للتنبؤ بضغط الآبارالسفلى ذات السريان العمودى للموائع المتعددة الاطوار.

التخصص: هندسة البترول
تأريخ الشهادة: مارس 2004 م

أُستخدمت تقنية الشبكات العصبية بنجاح لعمل نموذج للتنبؤ بضغط البئر السفلى فى آبار النفط ذات السريان العمودى المتعددة الاطوار. وقد تم تطوير النموذج الجديد بإستخدام خوارزمية للتعلم (التوجيه الخلفى للاخطاء). وقد أُستخدمت 206 نقطة بيانات حقلية فى تطوير النموذج مأخوذة من عدّة حقول من منطقة الشرق الاوسط. وتغطى البيانات المستخدمة فى تطوير النموذج معدل انتاج نفطى يتراوح ما بين 280 الى 19618 برميل فى اليوم، نسبة وجود الماء فى الموائع من 0.0% الى 44.8% ووصلت نسبة الغاز الى النفط حتى 675.5 قدم مكعب لكل برميل. وعند تقسيم البيانات المتاحة (زمرة التدريب، الصلاحية، والأختبار) بنسبة 3:1:1 تم الحصول على أعلى أداء بالنسبة للنموذج المطور.

وقد تم إجراء دراسة مقارنة لأداء النموذج المطور ومقارنته بالعلاقات التجريبية والنماذج الميكانيستية الاخرى باستخدام مقاييس احصائية وقد وُجد ان اداء النموذج المُطور يفوق النماذج الاخرى والعلاقات التجريبية بحصوله على أعلى معدل إرتباط وأقل أخطاء وإنحراف معيارى.

وعند تطبيق النموذج الجديد، ينبغى الأخذ بعين الاعتبار نطاق البيانات الحقلية التى أُستخدمت فى تطوير النموذج.

درجة الماجستير فى العلوم
جامعة الملك فهد للبترول والمعادن
الظهران-المملكة العربية السعودية

مارس 2004 م

Thesis Abstract

Full Name of Student: Mohammed Abdalla Ayoub

Title of Study: DEVELOPMENT AND TESTING OF AN ARTIFICIAL NEURAL NETWORK MODEL FOR PREDICTING BOTTOMHOLE PRESSURE IN VERTICAL MULTIPHASE FLOW

Date of Degree: March 2004

A Neural Network technique has been used successfully for developing a model for predicting bottomhole pressure in vertical multiphase flow in oil wells. The new model has been developed using the most robust learning algorithm (back-propagation). A total number of 206 data sets; collected from Middle East fields; has been used in developing the model. The data used for developing the model covers an oil rate from 280 to 19618 BPD, water cut up to 44.8%, and gas oil ratios up to 675.5 SCF/STB. A ratio of 3:1:1 between training, validation, and testing sets yielded the best training/testing performance. The best available empirical correlations and mechanistic models have been tested against the data and the developed model.

Graphical and statistical tools have been utilized for the sake of comparing the performance of the new model and other empirical correlations and mechanistic models. Thorough verifications indicated that the new developed model outperforms all tested empirical correlations and mechanistic models in terms of highest correlation coefficient, lowest average absolute percent error, lowest standard deviation, lowest maximum error, and lowest root mean square error. The new developed model results can only be used within the range of used data; hence care should be taken if other data beyond this limit is implemented.

MASTER OF SCIENCE DEGREE

KING FAHD UNIVERSITY OF PETROLEUM AND MINERALS

Dhahran-Saudi Arabia

Date: March 2004

ACKNOWLEDGEMENT

All praise is due to Allah the most beneficent, the most compassionate, and peace is upon his prophet Mohammed. I wish firstly to express my sincere gratitude and thanks to KFUPM for providing me full financial support during the entire research period. My deep thanks go to my main advisor professor Mohamed Ahmed Aggour and co-advisor Dr. El-Sayed Ahmed Osman, for their continuous guidance, encouragement and advice that made this work possible. Special thanks and appreciation are due to Dr. Osman who has introduced the science of artificial neural networks to me and guided me through the learning process.

I would like also to thank Dr Sidqi Abu-Khamsin, Dr Hasan Yousef Al-Yousef, and Dr Abdulaziz Al-Majed for serving as committee members. My special appreciation is to the late Dr K. Al-Fossail who had served on my thesis committee. A word of thank is also due Mr. Khalid El-Badawi who helped me a lot in developing the last step of the model.

Special recognition is given to my family in my home country for their patience and sacrifices during the course of my study.

THIS WORK IS DEDICATED TO MY

FATHER'S MEMORY, "MAY ALLAH REST HIS SOUL"

List of Contents

List of Figures

List of Tables

CHAPTER 1

INTRODUCTION

Multiphase flow in pipes can be defined as the process of simultaneous flow of two phases or more namely; liquid and gas. It occurs in almost all oil production wells, in many gas production wells, and in some types of injection wells. This process has raised considerable attention from nuclear and chemical engineering disciplines as well as petroleum engineering. The phenomenon is governed mainly by bubble point pressure; whenever the pressure drops below bubble point, gas will evolve from liquid, and from that point to surface, gas-liquid flow will occur. Furthermore, certain flow patterns will develop while the pressure decreases gradually below the bubble point, as illustrated in Figure 1.1. The flow patterns depend mainly on the gas and liquid velocities, and gas/liquid ratio. Needless to say that sharp distinction between these regimes is not possible.

The present study focuses on prediction of the pressure losses in vertical pipes carrying multiphase mixtures (gas and liquid). These pressure losses need to be estimated with good precision in order to implement certain design considerations. Such considerations include tubing sizing and operating wellhead pressure in a flowing well; well completion or re-completion schemes; artificial lift during either gas-lift or pump

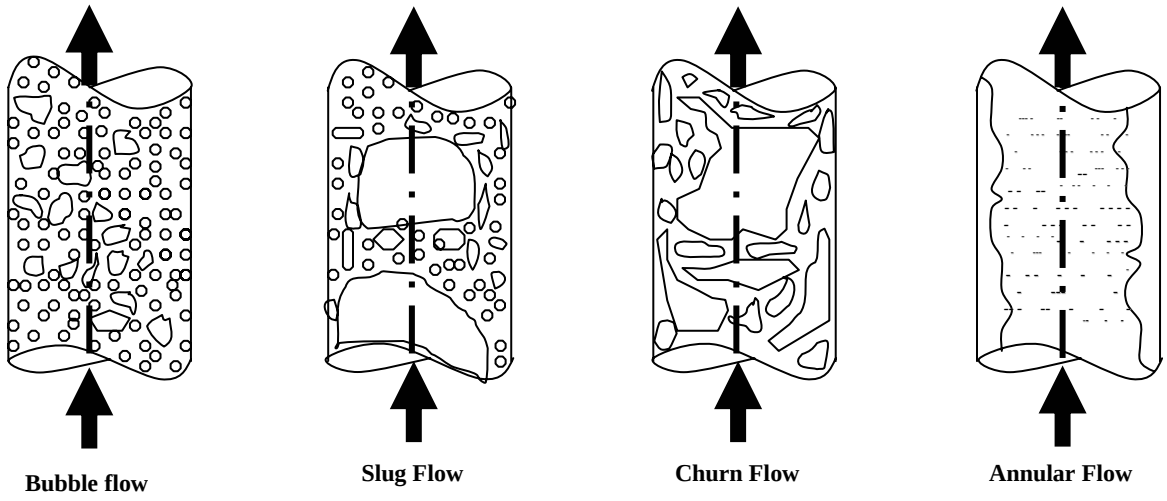

Figure 1.1: Vertical Flow Patterns.

operation in a low energy reservoir; liquid unloading in gas wells; direct input for surface flow line and equipment design calculations.

In the present study, Chapter 2 reviews and discusses literature relevant to the topics addressed in this work. Chapter 3 presents the statement of the problem and defines the general objectives. In Chapter 4 a general framework for the concept of artificial neural networks is presented. Great emphasis is placed on a back propagation learning algorithm that was utilized in developing a model for predicting pressure drop in multiphase flow wells. Also, the model parameters are discussed along with general network optimization. Chapter 5 presents the model optimization and results of the developed model along with a comparison to the best available empirical correlations and mechanistic models. Finally, Chapter 6 concludes and summarizes the findings of this study and discusses potential future developments for the used approach.

CHAPTER 2

LITERATURE REVIEW

This chapter provides a revision of the most commonly used correlations and mechanistic models and their drawbacks. The concept of artificial neural network is, in brief, being presented along with its applications in petroleum industry as well as in multiphase flow area. Special emphasis is devoted to pressure drop calculations in multiphase flow wells using the best available empirical correlations and mechanistic models.

2.1 Empirical Correlations

Numerous correlations have been developed since the early 1940s on the subject of vertical multiphase flow. Most of these correlations were developed under laboratory conditions and are, consequently, inaccurate when scaled-up to oil field conditions[1]. A detailed description of these correlations is given in *Appendix A* for reference. The most commonly used correlations are those of Hagedorn and Brown[2], Duns and Ros[3], Orkiszewski[4], Beggs and Brill[5], Aziz and Govier[6], and Mukherjee and Brill[7]. These correlations, discussed in Appendix A, have been evaluated and studied carefully by numerous researchers to validate their applicability under different ranges of data.

Espanol[8] has shown that Orkiszewski[4] correlation was found more accurate than other correlations in determining pressure drop especially when three-phase flow is introduced in wellbores.

Camacho[9] collected data from 111 wells with high gas-liquid ratios to test five correlations. None of these wells encountered a mist flow regime defined by Duns and Ros[3] or Orkiszewski[4] correlations. He reported that no single method was sufficiently accurate to cover all ranges of gas-liquid ratios. Duns and Ros[3] and Orkiszewski[4] correlations performed better when forced to mist flow for gas liquid ratios exceed 10,000 SCF/STB.

Messulam[10] has also conducted a comparative study using data from 434 wells to test the performance of available correlations. Six methods were tested and no one was found to be superior for all data ranges. Hagedorn and Brown[2] followed by Orkiszewski[4] correlation were the most accurate over the other tested methods. Duns and Ros[3] method was the least accurate one.

Lawson and Brill[11] presented a study to ascertain the accuracy of seven pressure-loss prediction methods. The best method was Hagedorn and Brown[2] followed by Orkiszewski[4] correlation.

The same number of field data points (726, used by Lawson and Brill[11]) was used by Vohra *et al.*[12]**.** The purpose of their study was to include the new methods of Beggs and Brill[5], Aziz *et al.*[6], and Chierici *et al.*[13]. It was found that Aziz *et al.*[6] performed the best followed by the Beggs and Brill[5] and Chierici *et al.*[13] correlations.

Chierici *et al.*[13] proposed a new method to be used in slug flow regime only. They suggested using the Griffith and Wallis[14] correlation in bubble flow and the Duns and

Ros[3] method in mist flow. Besides, they specified which fluid property correlations have to be used for calculating two-phase flowing pressure gradients by their method. The Vohra *et al*.[12] study showed that this method overestimates pressure drop calculation in most cases.

Several correlations have been investigated using about 115 field data points by Kabir *et al*.[15]**.** Their correlation performed better than Aziz *et al*.[6] and Orkiszweski[4] correlations, when the slug and bubble flows are predominant. They claimed also that their correlation is outperforming the rest of correlations in the churn and annular flow regimes.

Aggour *et al.*[16] evaluated the performance of vertical multiphase flow correlations and the possibility of applying those set of correlations for conditions in Gulf region where large tubular and high flow rates are dominant. They concluded that Beggs and Brill[5] correlation outperforms the rest of correlations in pressure prediction. Hagedorn and Brown[2] correlation was found to be better for water cuts greater than 80%. Also, they reported that Aziz *et al*.[6] correlation could be improved when Orkiszewski flow pattern is applied.

Bharath[17] reported that the Orkiszewski[4] and Hagedorn and Brown[2] correlations are found to perform satisfactorily for vertical wells with or without water cut. Also, He concluded that Duns and Ros[3] correlation is not applicable for wells with water-cut and should be avoided for such cases. The Beggs and Brill[5] correlation is applicable for inclined wells with or without water-cut and is probably the best choice available for deviated wells.

Most researchers agreed upon the fact that no single correlation was found to be applicable over all ranges of variables with suitable accuracy[1]. It was found that correlations are basically statistically derived, global expressions with limited physical considerations, and thus do not render them to a true physical optimization

2.2 Mechanistic Models

Mechanistic models are semi-empirical models used to predict multiphase flow characteristics such as liquid hold up, mixture density, and flow patterns. Based on sound theoretical approach, most of these mechanistic models were generated to outperform the existing empirical correlations.

Four mechanistic models will be reviewed in this study; those of Hasan and Kabir[15], Ansari *et al.*[18], Chokshi *et al*.[19], and Gomez *et al*.[20]. Detailed description of these models is provided in Appendix A.

Hasan and Kabir[15] and Ansari *et al*.[18] models were evaluated thoroughly by Pucknell *et al.*[21] who reported that Hasan and Kabir[15] model was found to be no better than the traditional correlations while Ansari *et al.* model[18] gave reasonable accuracy. Kaya *et al.*[22] have proposed another comprehensive mechanistic model for predicting flow patterns in inclined upward and vertical pipes with five flow patterns used; bubbly, dispersed, bubble, slug, churn and annular flows. Their model was tested against four mechanistic models and two empirical correlations and was found to perform better than the rest. These different flow patterns are definitely resulting from the changing form of the interface between the two phases.

Tengesdal *et al.*[23] did the same as Kaya *et al.*[22], they identified five flow patterns and came up with vertical upward two-phase flow mechanistic model for predicting these flow patterns and liquid hold up plus pressure drop. He developed a new model for churn flow pattern and utilized some famous mechanistic model for the rest of flow regimes. The model also tested and gave satisfactory result compared to different schemes. Generally, each of these mechanistic models has an outstanding performance in specific flow pattern prediction and that is made the adoption for certain model of specific flow pattern by investigators to compare and yield different, advanced and capable mechanistic models.

Takacs[1] made a statistical study on the possible source errors in empirical correlation and mechanistic models. He concluded that there is no pronounced advantage for mechanistic models over the current empirical correlations in pressure prediction ability when fallacious values are excluded. Actually, there is no privilege for mechanistic models over the existing empirical correlation but they behave similarly when mistaken data from the former is taken out.

2.3 Artificial Neural Networks

Artificial neural networks are collections of mathematical models that emulate some of the observed properties of biological nervous systems and draw on the analogies of adaptive biological learning. The concept of artificial neural network and how it works will be discussed in details in chapter 4.

2.3.1 The Use of Artificial Neural Networks in Petroleum Industry

The use of artificial intelligence in petroleum industry can be tracked back just almost ten years[24]**.** The use Artificial Neural Network (ANN) in solving many petroleum industry problems was reported in the literature by several authors.

Conventional computing tools have failed to estimate a relationship between permeability and porosity. Knowing the behavior of this relationship is of utmost significance for estimating the spatial distribution of permeability in the reservoirs especially those of heterogeneous litho-facies. ANN was used successfully in determining the relationship between them and constructing excellent prediction or estimation[25]. For instance; ANN has a great share in solving problems related to drilling such as drill bit diagnosis and analysis[25, 26, 27, 28]. Moreover, ANN was used efficiently to optimize production, fracture fluid properties[30].

ANN has also been adopted in several other areas such as permeability predictions[30], well testing[31, 32, 33], reservoir engineering and enhance oil recovery specifically[34]; PVT properties prediction[35, 36, 37], identification of sandstone lithofacies, improvement of gas well production[38], prediction and optimization of well performance, and integrated reservoir characterization and portfolio management[39].

2.3.2 Artificial Neural Networks in Multiphase Flow

Recently, ANN has been applied in the multiphase flow area and achieved promising results compared to the conventional methods (correlations and mechanistic models). With regard to this field, a few researchers applied ANN technique to resolve

some problems associated with multiphase problems including flow patterns identification, liquid hold up, and gas and liquid superficial velocities.

Arirachakaran *et al*.[40] proposed an intelligent program, supported by a knowledge data base and human interaction to interpret the results obtained from prediction of flow pattern by mechanistic models. An expert systems approach that displays some sort of intelligence is capable of thinking like humans and have a learning talent was suggested by the author as a pioneering step of ANN. This expert system flow pattern simulator, the author suggests, can be intelligently utilized as a computer aided engineering tool in production system optimization.

Ternyik *et al***.**[41] presented a solution for predicting flowing bottomhole pressure in multiphase flow, both for wellbores and pipelines. He formulated separate neural networks for each case by using back-propagation method along with different set up and inclination angles. Their new approach, which is called virtual measurement in pipes (VMP), was designed to address the development of tools to predict pressure drops in pipes. It outperforms the conventional method (five empirical correlations were used to compare results) in its generality and high prediction capability. His approach worked reasonably with lower standard deviation and mean values when used for oil wells. The small number of data sets and high number of variables used in his study in hidden layer, which might limit their model generality. Also, they proceeded with the application of VMP in prediction of liquid holdup and flow regimes in pipes and wells. ANN utility of differentiating complex pattern has proved to be a good tool in this area especially where complex relationship between flow patterns present. The model can fit correctly at any inclination angle and might be claimed as a unified model for flow patterns and liquid

hold up prediction. Mukherjee[42] experimental data set was used due to wide coverage of inclination angles reported in to provide more generality and confidence to the output results. A Kohonen type network was utilized due to the ability of this network to self learning without depending on the output in each case. His model was restricted to a 1.5 inch tubing diameter and low operating condition, which limit the generality of his model.

The need for accurate hold up and flow patterns prediction stimulated Osman[43] to propose an artificial neural networks model for accurate prediction of these two variables under different conditions. 199-data points were used to construct his model. Neural Network performed perfectly in predicting liquid hold up in terms of lowest standard deviation and average absolute percent error when compared to published models. His model did not work efficiently in the transition phases.

Osman *and* Aggour[44] presented an artificial neural networks model for predicting pressure drop in horizontal and near-horizontal multiphase flow. A three-layer back-propagation ANN model was developed using a wide range of data. Thirteen variables were considered as the most effective variables incorporated in pressure drop prediction. Their model achieved outstanding performance when compared to some of the existing correlations and two mechanistic models. The model was also found to correctly simulate the physical process.

Shippen *et al.*[45] confirmed the use of ANN as a good tool to predict liquid hold up in two phase horizontal flow. The author discussed the inapplicability of current mechanistic models and empirical correlation and the superiority of ANN over them. Large set of data was used to provide high degree of generality to their model. Highest

correlation factor (0.985), compared to cases tested, indicates the superior overall performance of the model.

As stated by different authors and researchers, and as discussed earlier, the empirical correlations and mechanistic models failed to provide a satisfactorily and a reliable tool for estimating pressure in multiphase flow wells. High errors are usually associated with these models and correlations which encouraged a new approach to be investigated for solving this problem. Artificial neural networks gained wide popularity in solving difficult and complex problems, especially in petroleum engineering. This new approach will be utilized for the first time in solving the problem of estimating pressure drop for multiphase flow in vertical oil wells.

CHAPTER 3

STATEMENT OF THE PROBLEM AND OBJECTIVES

This chapter describes the problem of estimating pressure drop for vertical multiphase flow in oil wells. The need for developing a model that can overcome the previous difficulties faced in utilizing empirical correlations and mechanistic models is addressed through stating the objective of this work.

3.1 Statement of the Problem

The need for accurate pressure prediction in vertical multiphase is of great importance in the oil industry. Prediction of pressure drop is quite difficult and complicated due to the complex relationships between the various parameters involved. These parameters include pipe diameter, slippage of gas past liquid, fluid properties, and the flow rate of each phase. Another parameter, which adds to the difficulty, is the flow patterns and their transition boundaries inside the wellbore along with changing temperature and pressure conditions. Therefore, an accurate analytical solution for this problem is difficult or impossible to achieve. However, numerous attempts have been tried since the early fifties to come up with precise methods to estimate pressure drop in vertical multiphase flow. These attempts varied from empirical correlations to semi empirical (mechanistic models) approaches. The first approach was based on development of empirical correlations from experimental data. The second approach was based on

fundamental physical laws, hence, provided some sort of reliability. As discussed in chapter 2, both solutions did not provide satisfactory and adequate results in all conditions.

Application of Artificial Neural Network (ANN) in solving difficult problems has gained wide popularity in the petroleum industry. This technique has the ability to acquire, store, and utilize experiential knowledge. Besides, it can differentiate, depending on the training data set, between complex patterns if it is well trained.

In this study, an artificial neural network model for prediction of pressure drop in vertical multiphase flow is developed and tested against field data. Some of the best available empirical correlations and mechanistic models are reviewed carefully using graphical and statistical analysis. These mechanistic models and empirical correlations are compared against the generated artificial neural network model.

3.2 Objective

The general objective of this study is to develop an artificial neural network model that provides more accurate prediction of pressure drop in vertical multiphase flow. Data from different Middle Eastern fields are used in this study. Specific objectives are:

1. To construct an ANN model for predicting pressure drop in vertical multiphase flow.
2. To test the constructed model against actual field data.
3. To compare the developed model against the best available empirical correlations and mechanistic models.

CHAPTER 4

NEURAL NETWORKS

This chapter deals with addressing the concept of artificial neural networks. First, historical background will be introduced, then, the fundamentals of ANN along with a deep insight to the mathematical representation of the developed model and the network optimization and configuration will be also discussed in details. The relationship between the mathematical and biological neuron is also explained. Besides, the way on how network functions is addressed through defining network structure, which deals also with solving many problems encountered during establishment of the model. Finally, the chapter concludes with presenting the robust learning algorithm that used in the training process.

4.1 Artificial Intelligence

The science of artificial intelligence or what is synonymously known as soft computing shows better performance over the conventional solutions. Sage[46] defined the aim of artificial intelligence as the development of paradigms or algorithms that require machines to perform tasks that apparently require cognition when performed by humans. This definition is widely broadened to include preceptrons, language, and problems

solving as well as conscious, unconscious processes[47]. Many techniques are classified under the name of artificial intelligence such as genetic algorithms, expert systems, and fuzzy logic because of their ability, one at least, to make certain reasoning, representation, problem solving, and generalization. Artificial neural network is also considered one of the important components of artificial intelligence system.

4.1.1 Artificial Neural Network

4.1.1.1 Historical Background

The research has been carried on neural network can be dated back to early 1940s. Specifically, McCulloch and Pitts[48] have tried to model the low-level structure of biological brain system. Hebb[49] published the book entitled "*the organization of behavior*" in which he focused mainly towards an explicit statement of a physiological learning rule for synaptic modification. Also, he proposed that the connectivity of the brain is continually changing as an organism learns differing functional tasks, and the neural assemblies are created by such changes. The book was a source of inspiration for the development of computational models of learning and adaptive systems.

However, Ashby[50] published another book entitled "*design for a brain; the origin of adaptive behavior*". The book focused on the basic notion that the adaptive behavior is not inborn but rather learned. The book emphasized the dynamic aspects of living organism as a machine and the related concepts of stability. While Gabor[51] proposed the idea of nonlinear adaptive filters. He mentioned that learning was accomplished in these filters through feeding samples of stochastic process into the machine, together with the target function that the machine was expected to produce. After 15 years of McCulloch

and Pitts[48] paper, a new approach to the pattern recognition problem was introduced by Rosenblatt[53] through what's called later, *preceptrons*. The latter, at the time when discovered, considered as an ideal achievement and the associative theorem "*preceptron convergence theorem*" was approved by several authors. The preceptron is the simplest form of a neural network that has been used for classifying patterns

This achievement followed by the introduction of *LMS* "least mean square algorithm" and *Adaline* "adaptive linear element" that followed by *Madaline* "multiple-Adaline" in 1962. Minskey and Papert[53] showed that there are several problems can not be solved by the theorem approved by Rosenblatt[52] and therefore countless effort to make such type of improvement will result in nothing. A decade of dormancy in neural network research was witnessed because of the Minskey's paper[53] results. In 1970_s, a competition learning algorithm was invented along with incorporation of self organizing maps. Since that time, several networks and learning algorithms were developed. A discovery of back-propagation learning algorithm was one of these fruitful revolutions that developed by Rumelhart *et al*.[54].

4.1.1.2 Definition

Generally, ANN is a machine that is designed to model the way in which the brain performs a particular task or function of interest. The system of ANN has received different definitions[55]. A widely accepted term is that adopted by Alexander and Morton[56]: "*A neural network is a massively parallel distributed processor that has a natural propensity for storing experiential knowledge and making it available for use*". ANN resembles the brain in two aspects; knowledge is acquired by the network through a

learning process, and the interneuron connection strengths known as synaptic weights are used to store the knowledge[55]. In other way, neural networks are simply a way of mapping a set of input variables to a set of output variables through a typical learning process. So, it has certain features in common with biological nervous system. The relationship between the two systems and the brain system mechanism is further explained in the next subsection.

4.1.1.2.1 Brain system

Human brain is a highly complex, nonlinear, and parallel information-processing system. It has the capability of organizing biological neurons in a fashion to perform certain tasks. In terms of speed, neurons are five to six orders of magnitude slower that silicon logic gates. However, human brain compensate for this shortcoming by having a massive interconnection between neurons. It is estimated that human brain consists of 10 billion neurons and 60 trillion synapses[57]. These neurons and synapses are expected to grow and increase in both number and connection over the time through learning.

Figure 4.1 is a schematic representation of biologic nerve cell. The biological neuron is mainly composed of three parts; dendrite, the soma, and the axon. A typical neuron collects signals from others through a host of fine structure (dendrite). The soma integrates its received input (over time and space) and thereafter activates an output depending on the total input.

The neuron sends out spikes of electrical activity through a long, thin stand known as an axon, which splits into thousands of branches (tree structure). At the end of each branch, a synapse converts the activity from the axon into electrical effects that inhibit or

excite activity in the connected neurons. Learning occurs by changing the effectiveness of synapses so that the influence of one neuron on another changes. Hence, artificial neuron network, more or less, is an information processing system that can be considered as a rough approximation of the above mentioned biological nerve system.

Figure 4.2 shows a typical neuron in an artificial neuron network. This mathematical neuron is a much simpler than the biological one; the integrated information received through input neurons take place only over space.

Output from other neurons is multiplied by the corresponding weight of the connection and enters the neuron as an input; therefore, an artificial neuron has many inputs and only one output. All signals in a neural network are typically normalized to operate within certain limit. A neuron can have a threshold level that must be exceeded before any signal is passed. The net input of the activation function may be increased by employing a bias term rather than a threshold; the bias is the negative of threshold. The inputs are summed and therefore applied to the activation function and finally the output is produced[51].

4.2 Fundamentals

In this section, artificial neural network basics will be presented, along with the close relationship between the technology and the biological nervous system. A full mathematical notation of the developed model and the network topology are also provided.

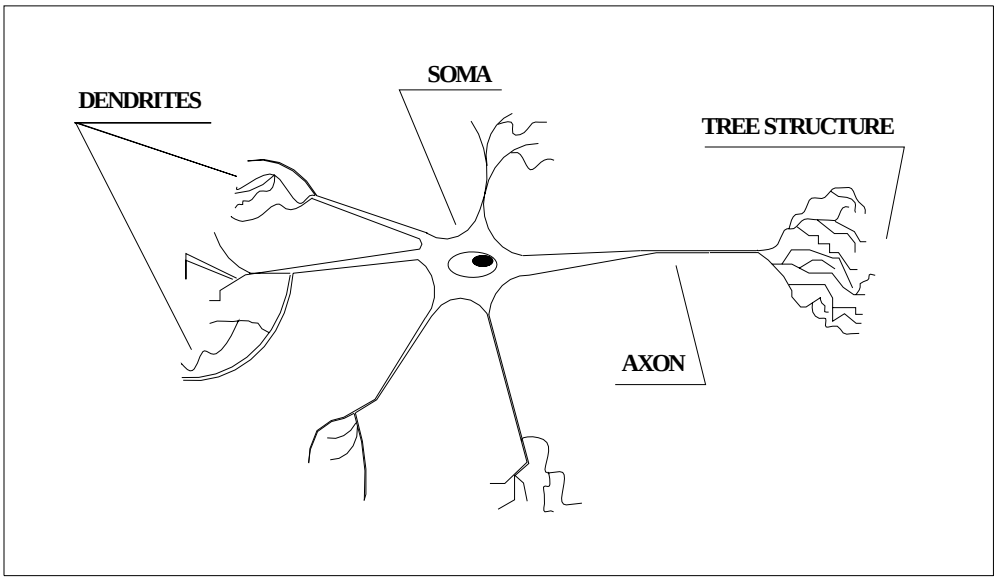

Figure 4.1: Major Structure of Biologic Nerve Cell (after Freeman[58]).

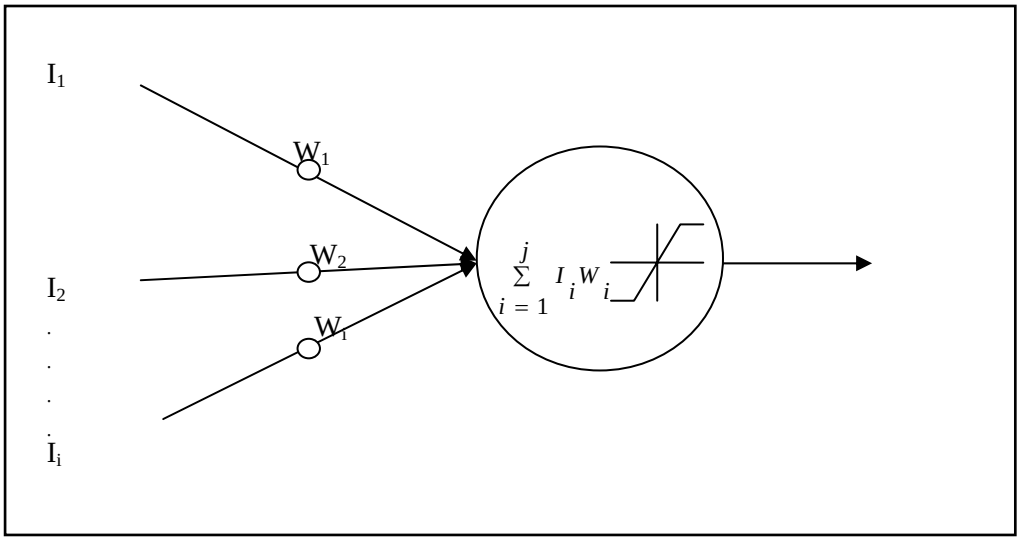

Figure 4.2: Artificial Neuron (after Freeman[58]).

4.2.1 Network Learning

The network is trained using supervised learning “providing the network with inputs and desired outputs”. The difference between the real outputs and the desired outputs is used by the algorithm to adapt the weights in the network. Figure 4.3 illustrates the supervised learning diagram. The net output is calculated and compared with the actual one, if the error between the desired and actual output is within the desired proximity, there will be no weights' changes; otherwise, the error will be back-propagated to adjust the weights between connections (feed backward cycle). After the weights are fixed the feed forward cycle will be utilized for the test set.

The other learning scheme is the unsupervised one where there is no feedback from the environment to indicate if the outputs of the network are correct. The network must discover features, rules, correlations, or classes in the input data by itself. As a matter of fact, for most kinds of unsupervised learning, the targets are the same as inputs. In other words, unsupervised learning usually performs the same task as an auto-associative network, compressing the information from the inputs.

4.2.2 Network Architecture

Network topology (architecture) is an important feature in designing a successful network. Typically, neurons are arranged in layers, each layer is responsible for performing a certain task. Based on how interconnections between neurons and layers are; neural network can be divided into two main categories (feed forward and recurrent).

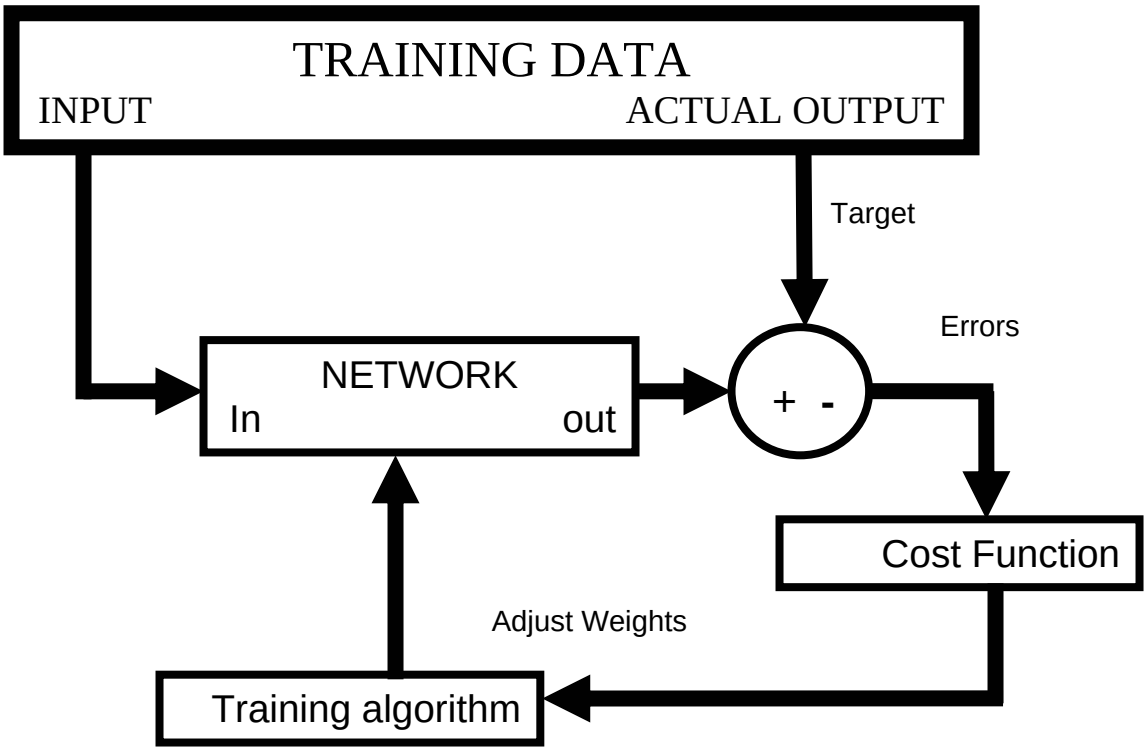

Figure 4.3: Supervised Learning Model.

4.2.2.1 Feed forward networks

In these networks the input data sweep directly through hidden layers and finally to the output layer. Hence, it does not allow an internal feedback of information. The essence of connectivity is primarily related to the fact that every node (neuron) in each layer of the network is connected to every other node in the adjacent forward layer. The number of neurons in the input layer should be equivalent to the number of input parameters being presented to the network as input. The same thing is correct for output layer, while the function of hidden layer is to intervene between the external input and the network output. Figure 4.4 is a schematic diagram of a fully connected network with two hidden layer and output layer. The overall response of the network is achieved through the final layer[55].

4.2.2.2 Recurrent networks

Feed-forward networks can be only used for dynamic relationship between input and output variable by including lagged values of input and output variables in the input layer. However, Recurrent Neural Network (RNN) allows for an internal feedback in the system. Internal feedback is a more successful way to account for dynamics in the model. It contains the entire history of inputs as well as outputs[55]. Two types of recurrent neural networks are presented here as examples; Jordan Recurrent Neural Network[55] (JRNN) and Elman Recurrent Neural Network [58] (ERNN). In JRNN, the output feeds back into the hidden layer with a time delay. The output of the previous periods becomes input in the

current period as illustrated in Figure 4.5 Thus, the current period output carries the history of past outputs, which in turn contain past values of inputs.

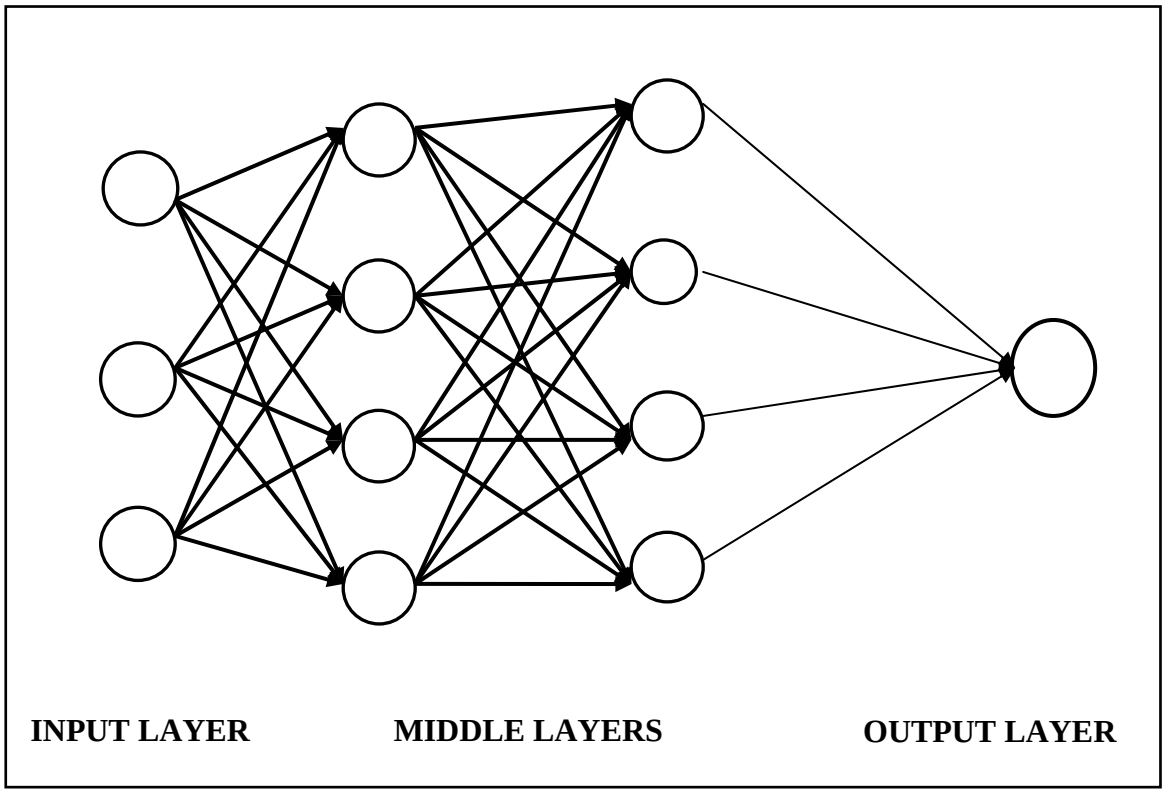

Figure 4.4: Fully Connected Network with Two Hidden Layers and Output Layer**.**

While a two-layer Elman Recurrent Neural Network (ERNN) is depicted in Figure 4.6. The ERNN accounts for internal feedback in such a way that the hidden layer output feeds back in itself with a time delay before sending signals to the output layer. RNN, however, requires complex computational processes that can only be performed by more powerful software. The back-propagation algorithm is used during the training process in the computation of estimates of parameters.

4.2.3 General Network Optimization

Any network should be well optimized in different senses in order to simulate the true physical behavior of the property under study. Certain parameters can be well optimized and rigorously manipulated such as selection of training algorithm, stages, and weight estimation. An unsatisfactory performance of the network can be directly related to an inadequacy of the selected network configuration or when the training algorithm traps in a local minimum or an unsuitable learning set.

In designing network configuration, the main concern is the number of hidden layers and neurons in each layer. Unfortunately, there is no sharp rule defining this feature and how it can be estimated. Trial and error procedure remains the available way to do so, while starting with small number of neurons and hidden layers “and monitoring the performance” may help to resolve this problem efficiently. Regarding the training algorithms, many algorithms are subjected to trapping in local minima where they stuck on it unless certain design criteria are modified. The existence of local minima is due to the fact that the error function is the superposition of nonlinear activation functions that

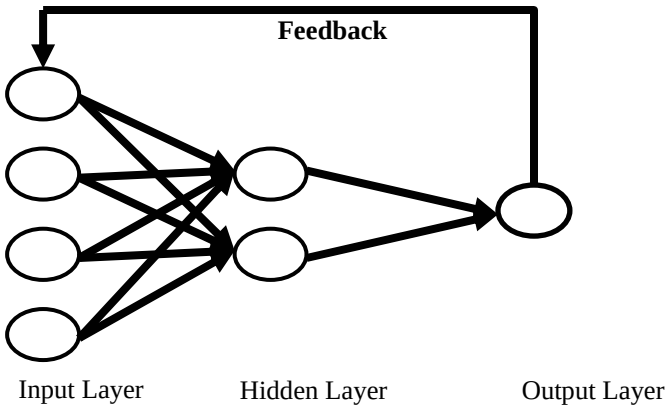

Figure 4.5: Jordan Recurrent Network.

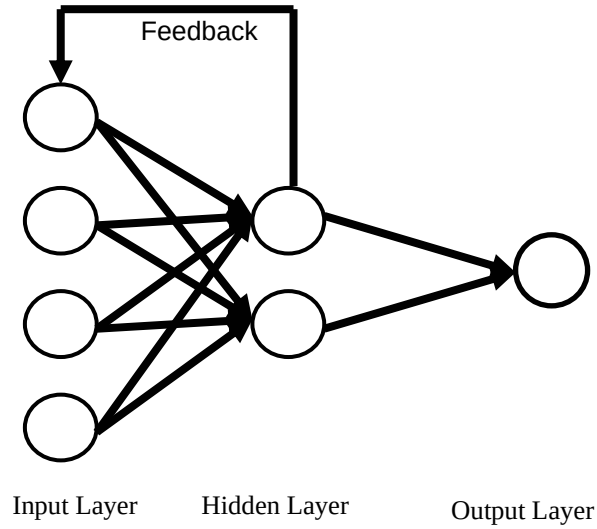

Figure 4.6: Elman Recurrent Network.

may have minima at different points, which sometimes results in a nonconvex error function. Using randomly initialized weight and inversion of the algorithm may become a solution for this problem.

The two most frequent problems that often encountered in network designing are the bad or unrepresentative learning set and overtraining. Therefore, selecting global ratios of data division may resolve it by using 2:1:1 or 3:1:1 or even 4:1:1 as suggested by Haykin[55]. Overtraining refers to the phenomenon when the network starts to model the noise associated with the training data. This phenomenon affects the generalization of network (network is able to accurately generalize when new cases that have not been seen during training are submitted to it). For this reason, cross-validation data are kept aside during training to provide an independent check on the progress of training algorithm. Besides, more confidence is gained where cross-validation data can minimize the error function as training progresses.

4.2.4 Activation Functions

As described earlier, the four basic elements of the neural network model are; synapses (that may receive a signal), adder **(**for summing up the input signals, weighted by respective synapses), an activation function, and an externally applied threshold. An activation function that limits (the amplitude of) the output of a neuron within a normalized value in a closed interval, say, between [0, 1] or [-1, 1], (see Figure 4.5). The activation function *squashes* the output signal in a 'permissible' (amplitude) range. When a neuron updates it passes the sum of the incoming signals through an activation function, or transfer function (linear or nonlinear). A particular transfer function is chosen to satisfy

some specification of the problem that the neuron is attempting to solve. In mathematical terms, a neuron j has two equations that can be written as follows[55]:

$$NET_{pj} = \sum_{i=1}^{N} w_{ji} x_{pi} \quad \text{.....(4.1)}$$

and

$$y_{pj} = \varphi(NET - \phi_{pj}) \quad \text{.....(4.2)}$$

Where; $x_{p1}, x_{p2}, \ldots, x_{pN}$ are the input signals; $w_{j1}, w_{j2}, \ldots, w_{jk}$ are the synaptic weights of neuron j; NET_{pj} is the linear combiner output, ϕ_{pj} is the threshold, φ is the activation function; and y_{pj} is the output signal of the neuron.

Four types of activation functions are identified based on their internal features. A simple threshold function has a form of:

$$y_{pj} = k(NET)_{pj} \quad \text{.....(4.3)}$$

Where k is a constant threshold function, i.e.:

$y_{pj} = 1$ if $(NET)_{pj} > T$

$y_{pj} = 0$ otherwise.

T is a constant threshold value, or a function that more accurately simulates the nonlinear transfer characteristics of the biological neuron and permits more general network functions as proposed by McCulloch-Pitts model[48]. However, this function is not widely used because it is not differentiable.

The second type of these transfer functions is the Gaussian function, which can be represented as:

$$y_{pj} = ce^{\left(-NET_{pj}^{2} \big/ \sigma^{2}\right)} \quad \text{.....(4.4)}$$

Where:

σ is the standard deviation of the function.

The third type is the Sigmoid Function, which is being tried in the present study for its performance. It applies a certain form of squashing or compressing the range of $(NET)_{pj}$ to a limit that is never exceeded by y_{pj} this function can be represented mathematically by:

$$y_{pj} = \frac{1}{\left(1 + e^{-a \times NET_{pj}}\right)} \quad \text{.....(4.5)}$$

Where;

a is the slope parameter of the sigmoid function.

By varying the slope parameter, different sigmoid function slopes are obtained. Another commonly used activation function is the hyperbolic function, which has the mathematical form of:

$$y_{pj} = \tanh(x) = \left(\frac{1 - e^{-NET_{pj}}}{1 + e^{-NET_{pj}}}\right) \quad \text{.....(4.6)}$$

This function is symmetrically shaped about the origin and looks like the sigmoid function in shape. However, this function produced good performance when compared to

sigmoid function. Hence, it is used as an activation function for the present model. Other functions are presented in Figure 4.7.

4.3 Back-Propagation Training Algorithm

Is probably the best known, and most widely used learning algorithm for neural networks. It is a gradient based optimization procedure. In this scheme, the network learns a predefined set of input-output sample pairs by using a two-phase propagate-adapt cycle. After the input data are provided as stimulus to the first layer of network unit, it is propagated through each upper layer until an output is generated. The latter, is then compared to the desired output, and an error signal is computed for each output unit. Furthermore, the error signals are transmitted backward from the output layer to each node in the hidden layer that mainly contributes directly to the output.

However, each unit in the hidden layer receives only a portion of the total error signal, based roughly on the relative contribution the unit made to the original output. This process repeats layer by layer, until each node in the network has received an error signal that describes its relative contribution to the total error. Based on the error signal received, connection weights are then updated by each unit to cause the network to converge toward a state that allows all the training set to be prearranged. After training, different nodes learn how to recognize different features within the input space. The way of updating the weights connections is done through the generalized delta rule "GDR". A full mathematical notion is presented in the next subsection.

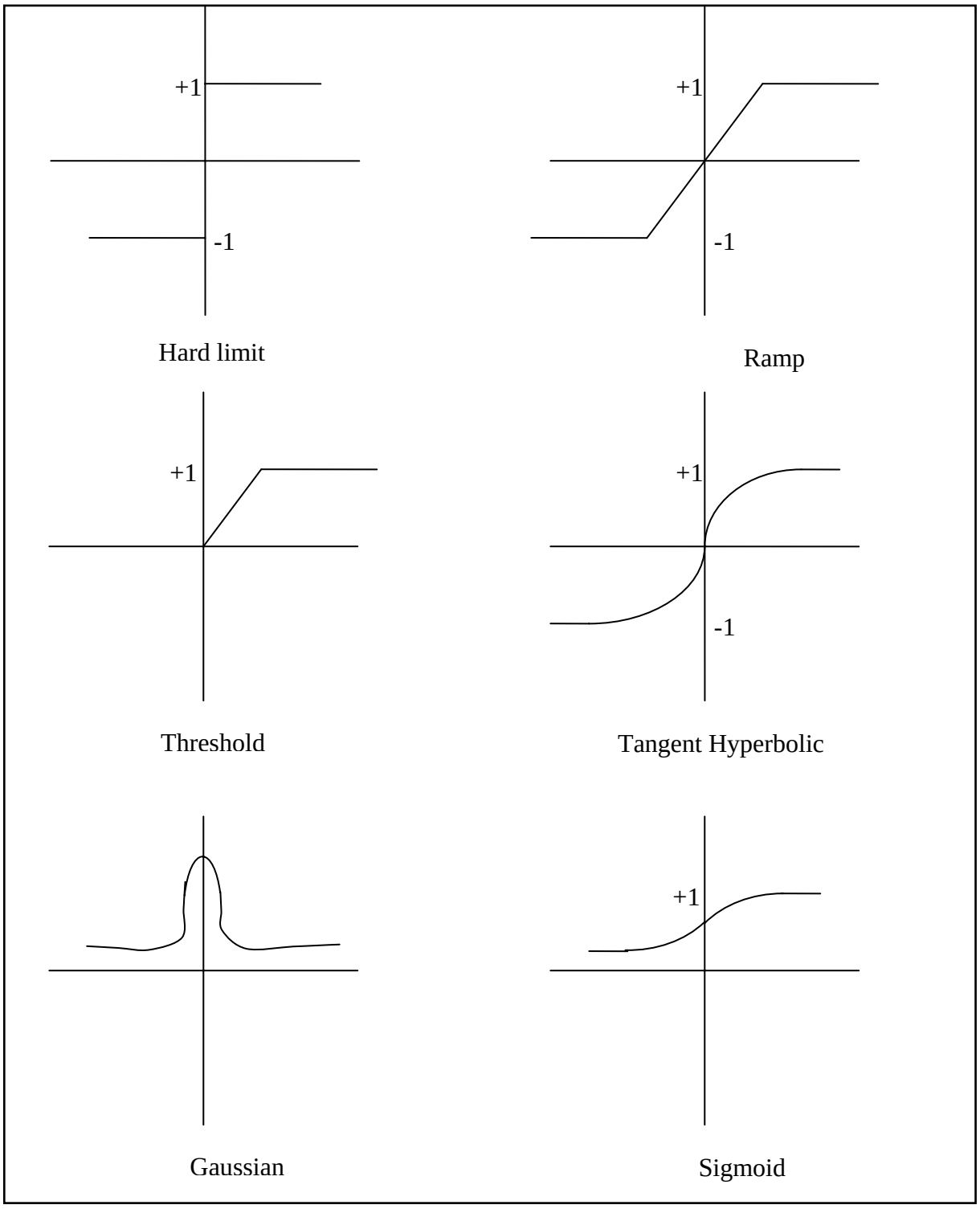

Figure 4.7: Activation Functions

4.3.1 Generalized Delta Rule

This section deals with the formal mathematical expression of Back-Propagation Network operation. The learning algorithm, or generalized delta rule, and its derivation will be discussed in details. This derivation is valid for any number of hidden layers.

Suppose the network has an input layer that contains an input vector;

$$x_p = \left(x_{p1}, x_{p2}, x_{p3}, ..., x_{pN}\right)^t \quad \text{.....(4.7)}$$

The input units distribute the values to the hidden layer units. The net output to the j th hidden unit is:

$$NET_{pj}^h = \sum_{i=1}^{N} w_{ji}^h x_{pi} + \theta_j^h \quad \text{.....(4.8)}$$

Where;

w_{ji}^h is the weight of the connection from the i th input unit, and

θ_j^h is the bias term

h is a subscript refer to the quantities on the hidden layer.

Assuming that the activation of this node is equal to the net input; then the output of this node is

$$i_{pj} = f_j^h\left(NET_{pj}^h\right) \quad \text{.....(4.8)}$$

The equations for the output nodes are:

$$NET_{pk}^o = \sum_{j=1}^{L} w_{kj}^o i_{pj} + \theta_k^o \quad \text{.....(4.10)}$$

$$o_{pk} = f_k^o\left(NET_{pk}^o\right) \quad \text{.....(4.11)}$$

Where:

o superscript refers to quantities of the output layer unit.

The basic procedure for training the network is embodied in the following description:

1. Apply an input vector to the network and calculate the corresponding output values.
2. Compare the actual outputs with the correct outputs and determine a measure of the error.
3. Determine in which direction (+ or -) to change each weight in order to reduce the error.
4. Determine the amount by which to change each weight.
5. Apply the correction to the weights.
6. Repeat steps 1 to 5 with all the training vectors until the error for all vectors in the training set is reduced to an acceptable tolerance.

4.3.1.1 Update of Output-Layer Weights

The general error for the k^{th} input vector can be defined as;

$$\varepsilon_k = \left(d_k - y_k\right) \quad \text{.....(4.12)}$$

Where:

d_k = desired output

y_k = actual output

Because the network consists of multiple units in a layer; the error at a single output unit will be defined as

$$\delta_{pk} = \left(y_{pk} - o_{pk}\right) \quad \text{.....(4.13)}$$

Where;

p subscript refers to the p^{th} training vector

k subscript refers to the k^{th} output unit

So,

y_{pk} = desired output value from the k_{th} unit.

o_{pk} = actual output value from the k_{th} unit.

The error that is minimized by the GDR is the sum of the squares of the errors for all output units;

$$E_p = \tfrac{1}{2}\sum_{k=1}^{M} \delta_{pk}^2 \quad \text{.....(4.14)}$$

To determine the direction in which to change the weights, the negative of the gradient of E_p and ∇E_p, with respect to the weights, w_{kj} should be calculated.

The next step is to adjust the values of weights in such a way that the total error is reduced.

From equation (4.14) and the definition of δ_{pk}, each component of ∇E_p can be considered separately as follows;

$$E_p = \tfrac{1}{2}\sum_{k} \left(y_{pk} - o_{pk}\right)^2 \quad \text{.....(4.15)}$$

and

$$\frac{\partial E_p}{\partial w_{kj}^o} = -\left(y_{pk} - o_{pk}\right)\frac{\partial f_k^o}{\partial\left(NET_{pk}^o\right)}\frac{\partial\left(NET_{pk}^o\right)}{\partial w_{kj}^o} \quad \text{.....(4.16)}$$

The chain rule is applied in equation (4.16)

The derivative of f_k^o will be denoted as $f_k^{o/}$

$$\frac{\partial\left(NET_{pk}^o\right)}{\partial w_{kj}^o} = \frac{\partial}{\partial w_{kj}^o}\sum_{j=1}^{L} w_{kj}^o i_{pj} + \theta_k^o = i_{pj} \text{.....(4.17)}$$

Combining equations (4.16) and (4.17) yields the negative gradient as follows

$$\frac{-\partial E_p}{\partial w_{kj}^o} = \left(y_{pk} - o_{pk}\right) f_k^{o/}\left(NET_{pk}^o\right) i_{pj} \text{.....(4.18)}$$

As far as the magnitude of the weight change is concerned, it is proportional to the negative gradient. Thus, the weights on the output layer are updated according to the following equation;

$$w_{kj}^o(t+1) = w_{kj}^o(t) + \Delta_p w_{kj}^o(t) \text{.....(4.19)}$$

Where;

$$\Delta_p w_{kj}^o(t) = \eta\left(y_{pk} - o_{pk}\right) f_k^{o/}\left(NET_{pk}^o\right) i_{pj} \text{.....(4.20)}$$

The factor η is called the learning-rate parameter, ($0 \prec \eta \prec 1$).

4.3.1.2 Output Function

The output function $f_k^o\left(NET_{jk}^o\right)$ should be differentiable as suggested in *section 4.2.4*. This requirement eliminates the possibility of using linear threshold unit since the output

function for such a unit is not differentiable at the threshold value. Output function is usually selected as linear function as illustrated below

$$f_k^o\left(NET_{jk}^o\right)=\left(NET_{jk}^o\right) \quad \text{.....(4.21)}$$

This defines the linear output unit.

In the first case:

$f_k^{o/}=1$

$$w_{kj}^o(t+1)=w_{kj}^o(t)+\eta\left(y_{pk}-o_{pk}\right)i_{pj} \quad \text{.....(4.22)}$$

The last equation can be used for the linear output regardless of the functional form of the output function f_k^o.

4.3.1.3 Update of Hidden-Layer Weights

The same procedure will be followed to derive the update of the hidden-layer weights. The problem arises when a measure of the error of the outputs of the hidden-layer units is needed. The total error, E_p, must be somehow related to the output values on the hidden layer. To do this, back to equation (4.15):

$$E_p=\tfrac{1}{2}\sum_k\left(y_{pk}-o_{pk}\right)^2 \quad \text{.....(4.15)}$$

$$E_p=\tfrac{1}{2}\sum_k\left(y_{pk}-f_k^o\left(NET_{pk}^o\right)\right)^2 \quad \text{.....(4.23)}$$

$$E_p = \frac{1}{2}\sum_k \left(y_{pk} - f_k^o \left(\sum_{j=1} w_{kj}^o i_{pj} + \theta_k^o \right) \right)^2 \quad \text{.....(4.24)}$$

Taking into consideration, i_{pj} depends on the weights of the hidden layer through equations (4.10) and (4.11). This fact can be exploited to calculate the gradient of E_p with respect to the hidden-layer weights

$$\frac{\partial E_p}{\partial w_{ji}^h} = \frac{1}{2}\sum_K \frac{\partial}{\partial w_{ji}^h}\left(y_{pk} - o_{pk}\right)^2 =$$

$$-\sum_K \left(y_{pk} - o_{pk}\right) \frac{\partial o_{pk}}{\partial \left(NET_{pk}^o\right)} \frac{\partial \left(NET_{pk}^o\right)}{\partial i_{pj}} \frac{\partial i_{pj}}{\partial \left(NET_{pj}^h\right)} \frac{\partial \left(NET_{pj}^h\right)}{\partial w_{ji}^h} \quad \text{.....(4.25)}$$

Each of the factors in equation (4.25) can be calculated explicitly from the previous equations. The result is;

$$\frac{\partial E_p}{\partial w_{ji}^h} = -\sum_K \left(y_{pk} - o_{pk}\right) f_k^{o/}\left(NET_{pk}^o\right) w_{kj}^o f_j^{h/}\left(NET_{pj}^h\right) x_{pi} \quad \text{.....(4.26)}$$

4.3.2 Stopping Criteria

Since back-propagation algorithm is a first-order approximation of the steepest-descent technique in the sense that it depends on the gradient of the instantaneous error surface in weight space[55]**.** Weight adjustments can be terminated under certain circumstances. Kramer and Sangiovanni-Vincentelli[60] formulated sensible convergence criterion for back-propagation learning; the back-propagation algorithm is considered to have converged when:

1. The Euclidean norm of the gradient vector reaches a sufficiently small gradient threshold.
2. The absolute rate of change in the average squared error per epoch is sufficiently small.
3. The generalization performance is adequate, or when it is apparent that the generalization performance has peaked.

CHAPTER 5

RESULTS AND DISCUSSIONS

In this chapter, first, data handling is discussed in terms of data collection and partitioning, pre-processing, and post-processing. Then, a detailed discussion of the developed neural network model, including model features, selected topology, and model optimization is presented. Next, a detailed trend analysis of the new developed model is presented to examine whether the model simulates the physical behavior. This is followed by a detailed discussion of the model superiority and robustness against some of the best available empirical correlations and mechanistic models. Finally, statistical and graphical comparisons of the developed model against other correlations and mechanistic models are presented.

5.1 Data Handling

Data handling is the most important step before feeding to the network because it determines the success of any neural network model. Neural network training can be made more efficient if certain pre-processing steps are performed on the network inputs and targets. Another post-processing step is needed to transform the output of the trained network to its original format. Theses two steps are explained below.

5.1.1 Data Pre-Processing (Normalization)

This step is needed to transform the data into a suitable form to the network inputs. The approach used for scaling network inputs and targets was to normalize the mean and standard deviation of the training set.

Normalizing the inputs and targets mean that they will have a zero mean and unity standard deviation if sorted and plotted against their frequencies. This step also involves selection of the most relevant data that network can take. The latter, was verified by most relevant input parameters that are used extensively in deriving correlations and mechanistic models. Normalized data are provided in *Appendix B.*

5.1.2 Post-processing of Results (Denormalization)

Presenting results in a way that is meaningful after model generation can be challenging, yet perhaps the most important task. This was needed to transform the outputs of the network to the required parameters. It is the stage that comes after the analysis of the data and is basically the reverse process of data pre-processing.

5.2 Data Collection and Partitioning

A total of 386 data sets were collected from Middle East fields. Real emphasis was drawn on selecting the most relevant parameters involved in estimation of bottomhole pressure. Validity of the collected data was first examined to remove the data that are suspected to be in error. For this purpose, the best available empirical correlations and mechanistic models were used to obtain predictions of the flowing bottomhole pressures

for all data. These were the mechanistic models of Hasan and Kabir[15], Ansari *et al.*[18], Chokshi *et al.*[19], Gomez *et al.*[20] and the correlations of Hagedorn and Brown[2], Duns and Ros[3], Orkiszewski[4], Beggs and Brill[5], and Mukherjee and Brill[7]. The reason for selecting the above mentioned models and correlations is that they represent the state-of-the-art in vertical pressure drop calculations; they proved accuracies relative to other available models and correlations as reported by several investigators[1, 18, 20, 61].

The measured (data) values of flowing bottomhole pressures were statistically compared and cross-plotted against the predicted values. The results of this comparison are summarized in Table 5.1. The data which consistently resulted in poor predictions by all correlations and mechanistic models were considered to be invalid and were, therefore, removed. A cut-off-error percentage (relative error) of 15% was implemented for the whole data. After completion of data screening and filtering, the final number of data sets used in developing the artificial neural network model was 206 data sets.

Partitioning the data is the process of dividing the data into three different sets: training sets, validation sets, and test sets. By definition, the *training set* is used to develop and adjust the weights in a network; the *validation set* is used to ensure the generalization of the developed network during the training phase, and the *test set* is used to examine the final performance of the network. The primary concerns should be to ensure that: (a) the training set contains enough data, and suitable data distribution to adequately cover the entire range of data, and (b) there is no unnecessary similarity between data in different data sets. Different partitioning ratios were tested (2:1:1, 3:1:1, and 4:1:1). The ratio of 4:1:1 (suggested by Haykin[62]) yielded better training and testing results. The problem with this ratio is that it is not frequently used by researchers.

Table 5.1: Performance of Empirical Correlations and Mechanistic Using All Data.

Correlation or Model Name	**AAPE "%"**	**R "fraction"**
Hasan and Kabir[15]	10.6016	0.6258
Ansari *et al.*[18]	8.7141	0.5601
Chokshi *et al.*[19]	7.3054	0.7798
Gomez *et al.*[20]	7.8187	0.7404
Hagedorn and Brown[2]	8.1703	0.6979
Duns and Ros[3]	7.5793	0.7499
Orkiszewski[4]	8.1549	0.7548
Beggs and Brill[5]	7.6804	0.7619
Mukherjee and Brill[7]	7.0574	0.7598
This Study (ANN model)	6.2825	0.7465

Normally, the more training cases are submitted to the network the better performance one can get, but the hazard of memorization becomes possible. Instead a ratio of 3:1:1 was followed in this study. Training, validation, and testing sets are presented in *Appendix B.*

5.3 Model Development

5.3.1 Introduction

Neural networks are used as computational tools with the capacity to learn, with or without teacher, and with the ability to generalize, based on parallelism and strong coherence between neurons in each layer. Among all types of available networks, the most widely used are a multiple-layer feed forward networks that are capable of representing non-linear functional mappings between inputs and outputs. The developed model consists of one input layer (containing nine input neurons or nodes), which represent the parameters involved in estimating bottomhole pressure (oil rate, water rate, gas rate, diameter of the pipe, length of pipe, wellhead pressure, oil density "API", surface temperature, and bottomhole temperature), three hidden layers (the first one contains six nodes, the second and third hidden layer each contains three nodes) and one output layer (contains one node) which is bottomhole pressure. This topology is achieved after a series of optimization processes by monitoring the performance of the network until the best network structure was accomplished.

5.3.2 Model Features

The developed model simply pivoted a set of processing units called neurons equivalent to nine input variables: oil rate, water rate, gas rate, diameter of the pipe, length of pipe, wellhead pressure, oil density "API", surface temperature, and bottomhole temperature. In addition to these nine input parameters, one input parameter (gas specific gravity) was discarded out because it was found insignificant.

Figure 5.1 illustrates the insignificance of gas specific gravity. As shown in the figure, predicted bottomhole pressure changes slightly for the entire range of gas specific gravity. The model also contains an activation state for each unit, which is equivalent to the output of the unit. Moreover, links between the units are utilized to determine the effect of the signal of each unit. Besides, a propagation rule is used to determine the effective input of the unit from its external inputs. An activation function (in this model tangent hyperbolic is used for hidden units and linear for output unit), which are applied to find out the new level of activation based on the effective input and the current activation. Additional term was included, which is an external input bias for each hidden layer to offer a constant offset and to minimize the number of iterations during training process. The key feature of the model is the ability to learn from the input environment through information gathering (learning rule).

5.3.3 Model Architecture

The number of layers, the number of processing units per layer, and the interconnection patterns between layers defines the architecture of the model. Therefore,

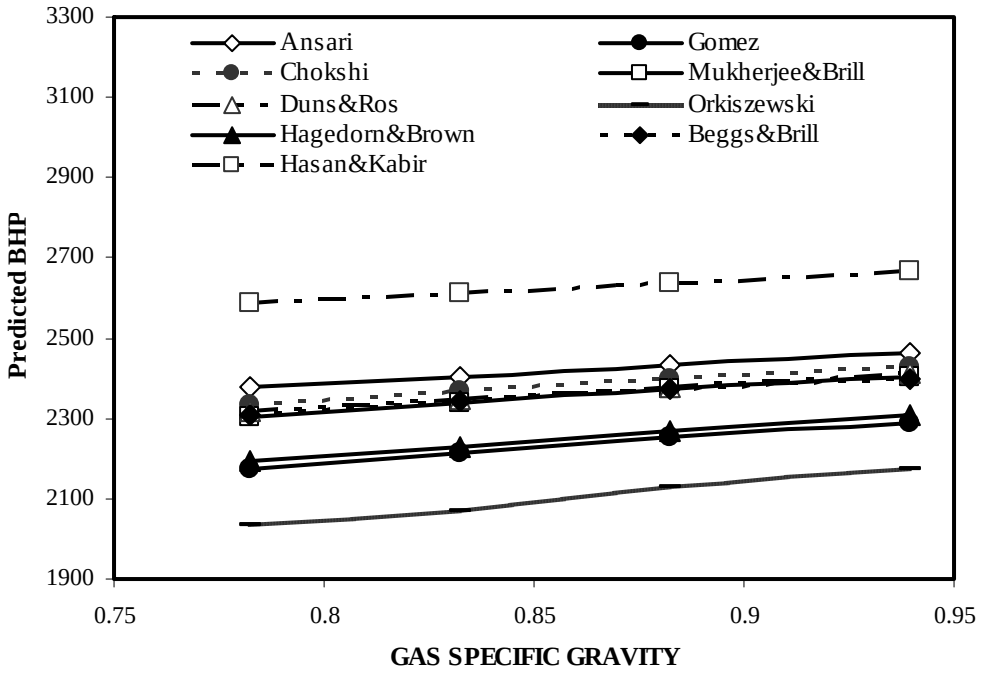

Figure 5.1: Effect of Changing Gas Specific Gravity.

defining the optimal network that simulates the actual behavior within the data sets is not an easy task. To achieve this task, certain performance criteria were followed. The design started with small number of hidden units in the only hidden layer that it acts as a feature detector. Some rules of thump were used as guides; for instance, the number of hidden units should not be greater than twice the number of input variables. In addition to this rules, several rules were suggested by different authors. Those rules can only be treated as a rough estimation for defining hidden layers size. Those rules ignore several facts such as the complexity and the discontinuities in the behavior under study. The basic approach used in constructing the successful network was trial and error. The generalization error of each inspected network design was visualized and monitored carefully through plotting the average absolute percent error of each inspected topology. Another statistical criterion (correlation coefficient) was utilized as a measure of tightness of estimated and measured values to a 45 degree line. Besides, a trend analysis for each inspected model was conducted to see whether that model simulates the real behavior. Data randomization is necessary in constructing a successful model, while a frequently found suggestion is that input data should describe events exhaustively; this rule of thumb can be translated into the use of all input variables that are thought to have a problem-oriented relevance. These nine selected input parameters were found to have pronounced effect in estimating pressure drop.

5.3.4 Model Optimization

The optimum number of hidden units depends on many factors: the number of input and output units, the number of training cases, the amount of noise in the targets, the

complexity of the error function, the network architecture, and the training algorithm. In most cases, there is no direct way to determine the optimal number of hidden units without training using different numbers of hidden units and estimating the generalization error of each.

To further describe the process of optimizing the model; Figures 5.2 and 5.3 and Table 5.2 illustrate the effect of changing number of neurons in the first hidden layer. As observed from Table 5.2, one hidden layer with three hidden neurons is achieving the highest correlation coefficient and the lowest average absolute percent error. But, on the other hand, the model failed in producing the correct physical trend across the data range. Instead of that, the second best model option was selected, which contains six neurons in the first hidden layer. The selection of this model was based on having the highest correlation coefficient for the training and validation sets. But still the performance of the model is not good enough and the inherent relationship between input variables and the output is not well extracted.

As shown in Table 5.3, two neurons in the second hidden layer are optimized while this selection failed in trend analysis. The next best option, which provides less number of neurons in the second hidden layer and the highest correlation coefficient and lowest AAPE, is selected (Table 5.3). A set contains three hidden neuron is selected based on the aforementioned criteria. Figures 5.4 and 5.5 provide a good insight on how this selection was made.

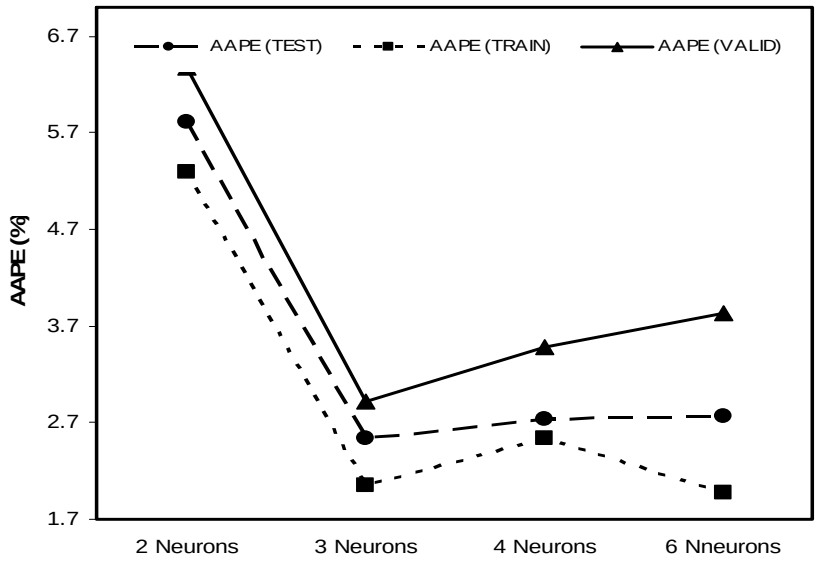

Figure 5.2: Effect of Changing Number of Neurons in the First Hidden Layer on Average Absolute Percent Error.

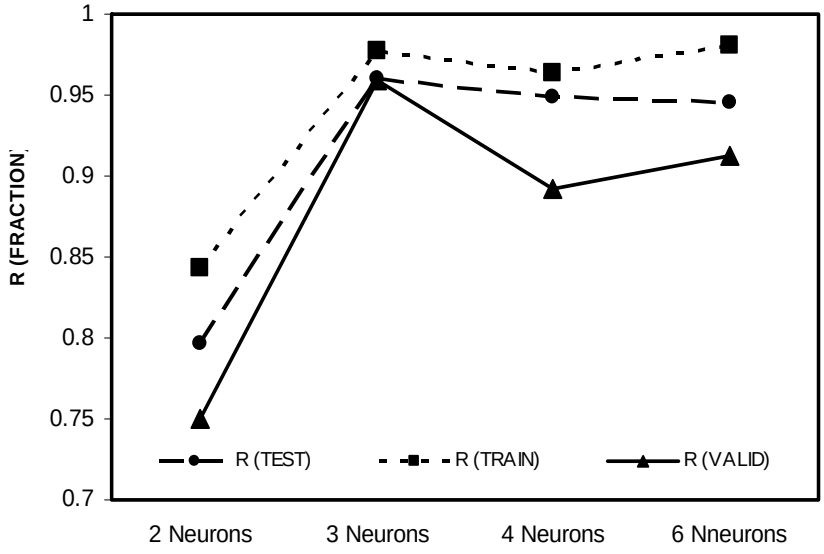

Figure 5.3: Effect of Changing Number of Neurons in the First Hidden Layer on Correlation Coefficient.

A model with three hidden layers is needed to improve the whole performance; especially in validation set (increasing the correlation coefficient and lowering the average absolute percent error). Table 5.4 show the effect of changing number of neurons in the third hidden layer with resepect to average absolute percent error and correlation coefficient (after maintaining six neurons in the first hidden layer and three hidden neurons in the second hidden layer). Three neurons in the third hidden layer are selected (Figures 5.6 and 5.7), which provides the highest correlation coefficient for the test set and the lowest average absolute percent error for the validation set. This final selection of model topology is further assessed through conducting a trend analysis.

5.3.5 Objective Function

To train a network and measure how well it performs, an *objective function* (or c*ost function*) must be defined to provide an explicit numerical rating of system performance. Selection of an objective function is very important because it represents the design goals and decides what training algorithm can be taken. A few basic functions are commonly used. One of them, used in this study, is the sum of the squares of the errors.

$$Error = \frac{1}{NP}\sum_{p=1}^{P}\sum_{k=1}^{N}(y_{pk} - o_{pk})^2 \quad \text{.....(5.1)}$$

Where, p refers to patterns in the training set, *k* refers to output nodes, and o_{pk} and y_{pk} are the target and predicted network output for the *k*th output unit on the *p*th pattern, respectively.

Table 5.2: Effect of Changing Number of Neurons in the First Hidden Layer with Resepect to Average Absolute Percent Error and Correlation Coefficient.

No of Neurons	AAPE (TEST)	AAPE (TRAIN)	AAPE (VALID)	R (TEST)	R (TRAIN)	R (VALID)
2	5.8079	5.2881	6.3708	0.79714	0.84343	0.75019
3	2.5378	2.048	2.9144	0.96057	0.97672	0.95937
4	2.7299	2.5421	3.4781	0.94874	0.9636	0.89206
6	2.7648	1.9733	3.8247	0.94586	0.98097	0.91255

Table 5.3: Effect of Changing Number of Neurons in the Second Hidden Layer with Resepect to Average Absolute Percent Error and Correlation Coefficient.

No of Neurons	AAPE (TEST)	AAPE (TRAIN)	AAPE (VALID)	R (TEST)	R (TRAIN)	R (VALID)
2	2.7576	1.2457	3.5384	0.94973	0.99167	0.92141
3	2.8539	0.61236	4.0736	0.94817	0.99749	0.90096
4	3.3088	2.2675	3.8332	0.9282	0.974	0.90242
6	3.0141	2.0547	3.5613	0.94907	0.97851	0.90973

Table 5.4: Effect of Changing Number of Neurons in the Third Hidden Layer with Resepect to Average Absolute Percent Error and Correlation Coefficient.

No of Neurons	AAPE (TEST)	AAPE (TRAIN)	AAPE (VALID)	R (TEST)	R (TRAIN)	R (VALID)
2	2.9799	1.5469	3.2156	0.94636	0.98593	0.94494
3	2.1598	1.7544	2.9275	0.97348	0.98461	0.93588
4	2.3929	1.9277	2.9769	0.96237	0.98072	0.95459
6	2.4878	1.1434	3.6175	0.96626	0.99265	0.91104

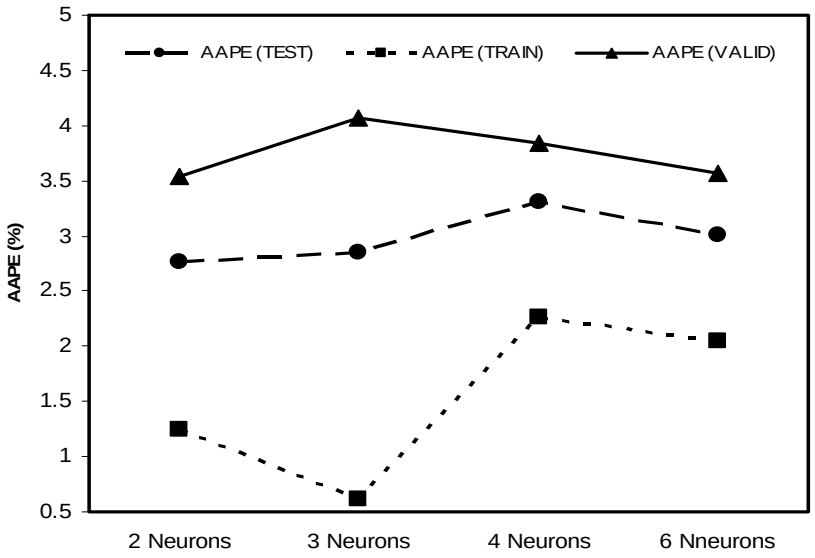

Figure 5.4: Effect of Changing Number of Neurons in the Second Hidden Layer on Average Absolute Percent Error.

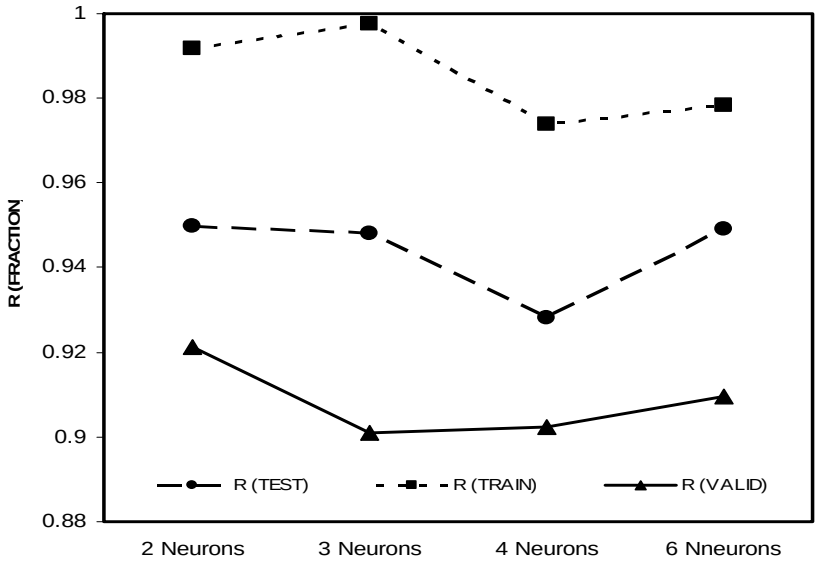

Figure 5.5: Effect of Changing Number of Neurons in the Second Hidden Layer on Correlation Coefficient.

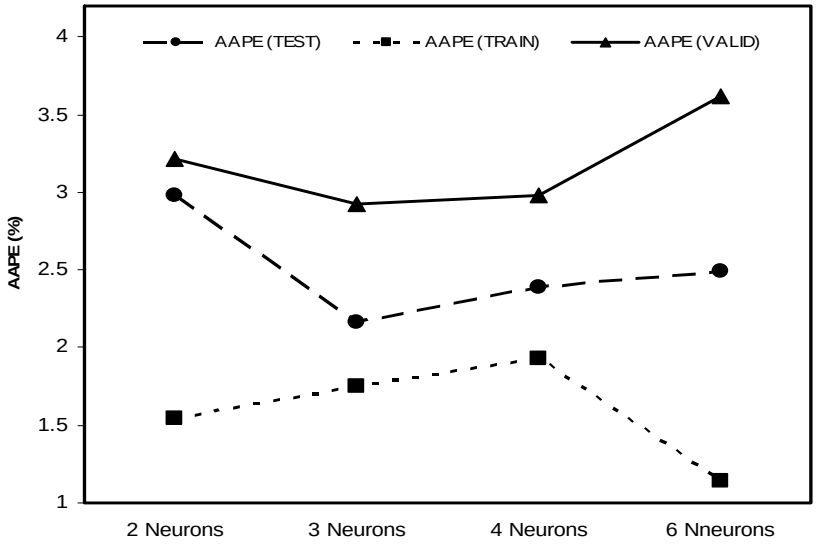

Figure 5.6: Effect of Changing Number of Neurons in the Third Hidden Layer on Average Absolute Percent Error.

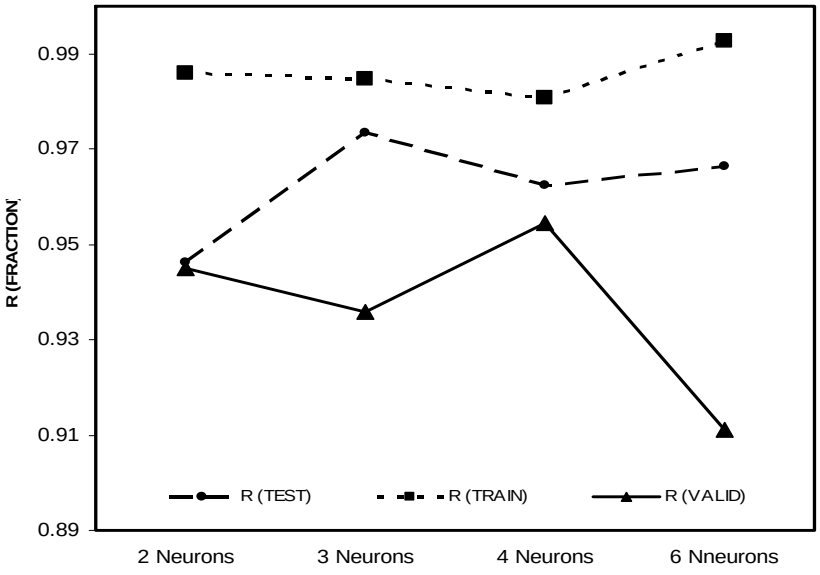

Figure 5.7: Effect of Changing Number of Neurons in the Third Hidden Layer on Correlation Coefficient.

5.4 Software Used

MatLab software[63] (version 6.5) environment was utilized due its high range of flexibility associated with programming and graphs visualization. Moreover, the software offers a good way to monitor the performance of the three set of data (training, validation, and testing) at the same time. A Matlab program is developed and training parameters were modified in order to ensure that these parameters are well optimized. The final model structure is shown in Figure 5.8. The problem encountered during training was the trapping of the model in a local minima several times. The reason behind this problem was found to be the low range of certain variables in the data. The concept of local and global minima was discussed by several mathematicians and ANN researchers[64, 65]. It defines the error gradient surface as if one look at it as a hyperbolic surface where the global minima point lies at the bottom of this surface. Hence, beyond this point the error starts to increase dramatically. The training session should be exactly stopped at this point to assure the generalization of the developed model.

The default of the software is to escape only five local minima. This option has been changed to fifteen in order to allow the network to capture the real behavior between input parameters and output (flowing bottomhole pressure). The problem of underfitting and overfitting (using too few; and too many units in hidden layer, respectively) was avoided through the use of cross-validation data set. Cross-validation data set is presented to the network after each epoch of training to check the generality (model succeeded to capture minor relationships between input set and the desired output when new cases are submitted to it) and stability of the model[62]. Input weight matrix (from input to the hidden

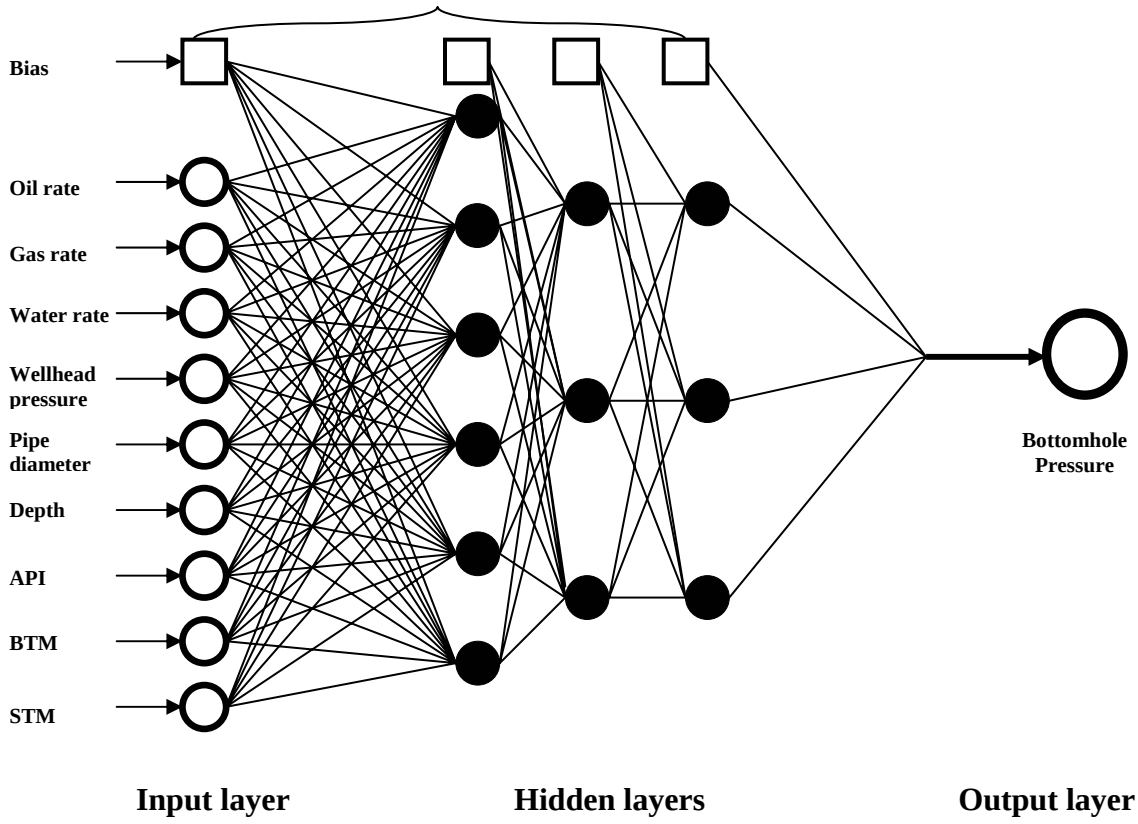

Figure 5.8: Schematic of the Developed Model.

Layers), hidden layer weight matrices, and the layers bias vectors for the retained network, all are extracted from this program and presented in *Appendix B*. These weights and biases were utilized in developing an executable code, which provides an easy way for users to implement in predicting pressure values.

5.5 Trend Analysis

A trend analysis was carried out to check whether the developed model is physically correct or not. For this purpose, synthetic sets were prepared where in each set only one input parameter was changed while other parameters were kept constant. To test the developed model, the effects of gas rate, oil rate, water rate, tubing diameter, and pipe length on flowing bottomhole pressure were determined and plotted on Figures 5.9 through 5.13. Figure 5.9 shows the effect of changing gas rate on bottomhole pressure. As expected, the developed model produced the correct trend where the flowing bottomhole pressure decreases as the gas rate increases.

Hagedorn and Brown[2], Orkiszewski[4], Beggs and Brill[5], and Mukherjee and Brill[7] correlations and Gomez model[20] showed a decrease in bottomhole pressure followed by an increase when gas rate increase. The reason is that when the gas liquid ratio becomes very high, additional increase in gas rate results in an increase in frictional and acceleration pressure drop which is more than the decrease in the hydrostatic head. Figure 5.10 shows the effect of changing oil rate with respect to the empirical correlations, mechanistic model, and the developed neural network model. Although the developed model did not produce the same shape as other correlations and mechanistic model, it did predict the general expected trend of increasing flowing bottomhole pressure with

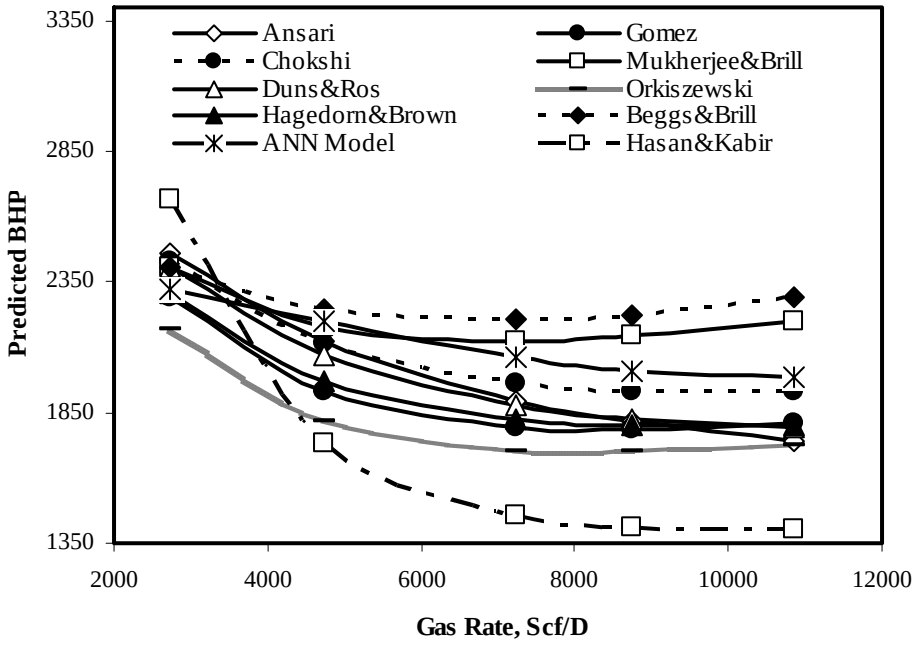

Figure 5.9: Effect of Gas Rate on Bottomhole Pressure at Pipe Diameter = 3.958 Inches.

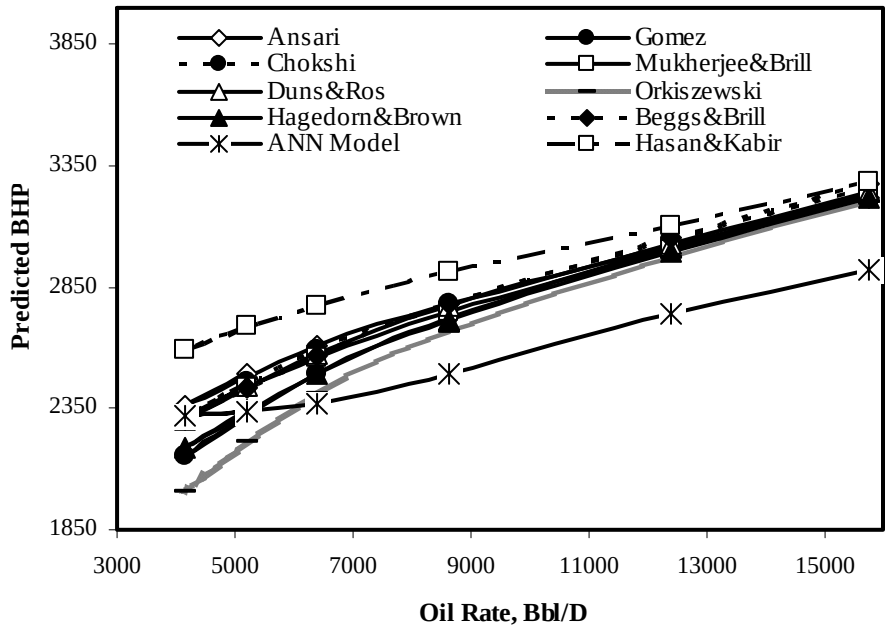

Figure 5.10: Effect of Oil Rate on Bottomhole Pressure at Pipe Diameter = 3.958 inches.

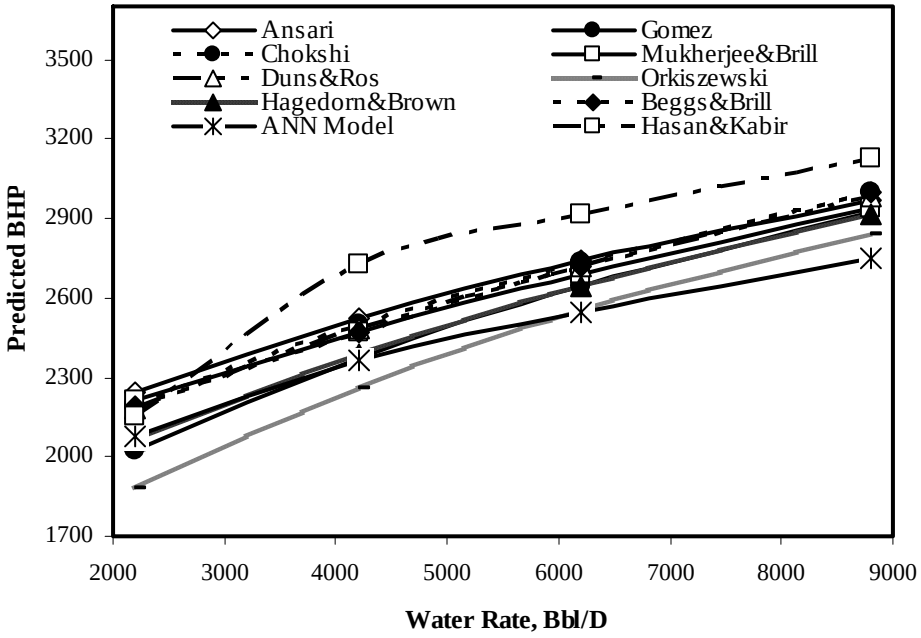

Figure 5.11: Effect of Water Rate on Bottomhole Pressure at Pipe Diameter = 3.958 inches.

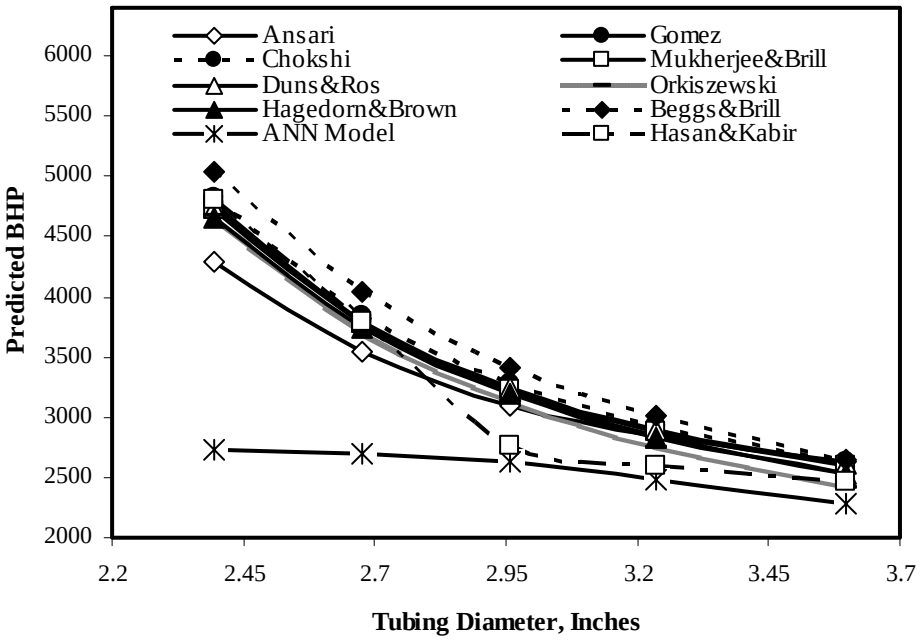

Figure 5.12: Effect of Tubing Diameter on Bottomhole Pressure.

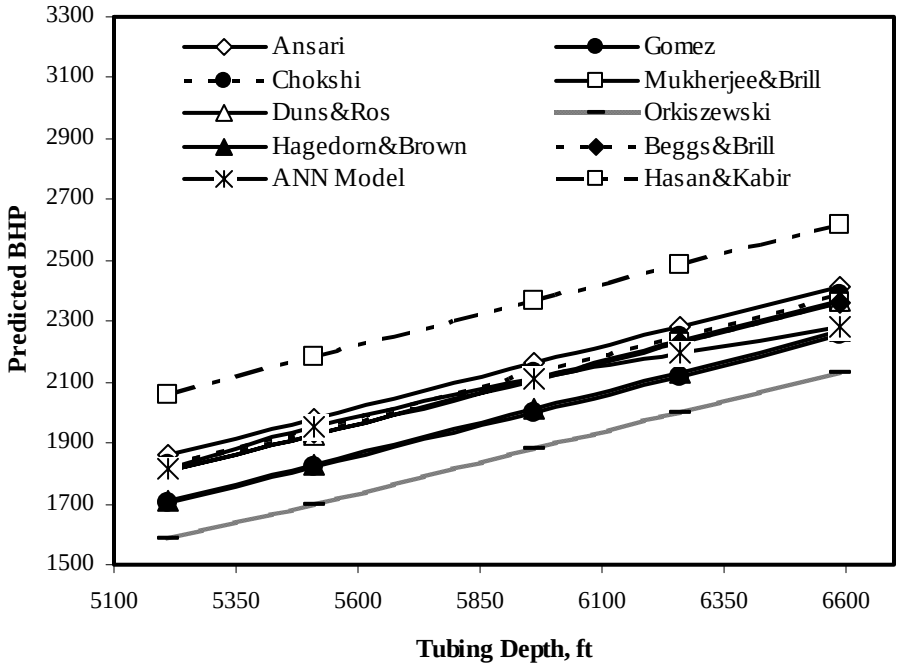

Figure 5.13: Effect of Pipe Length on Bottomhole Pressure at Pipe Diameter = 3.958 inches.

increasing oil rate. Figure 5.11 shows the effect of water rate on flowing bottomhole pressure. Again, the ANN model simulates the actual physical phenomenon; the higher the water rate, the higher the flowing bottomhole pressure. The effect of tubing size is shown in Figure 5.12, where the bottomhole pressure was found to decrease with increasing tubing diameter. The effect of tubing length, where flowing bottomhole pressure increases with tubing length, was also predicted by the neural network model as shown in Figure 5.13. To further examine the validity of the model, the trend analysis is checked at three different tubing sizes. Figures 5.14 to 5.17 show the trend analysis for oil rate, gas rate, water rate, and tubing depth, respectively.

5.6 Group Error Analysis

To demonstrate the robustness of the developed model, other statistical analysis was conducted, which is group error analysis. Average absolute relative error is a good indicator of the accuracy of all empirical correlations, mechanistic model; as well as the new developed model. This effective comparison of all investigated correlations and mechanistic models provides a good means of evaluating models performance. Average absolute relative error is utilized in this analysis by grouping input parameter and hence plotting the corresponding values of average absolute relative error for each set. Figures 5.18 through 5.22 present the statistical accuracy of flowing bottomhole pressure correlations and models under different groups. Figure 5.18 shows the statistical accuracy of bottomhole pressure grouped by oil rate. The ANN model outperforms the best available correlations and mechanistic models by providing the lowest average absolute relative error for the range of tested data.

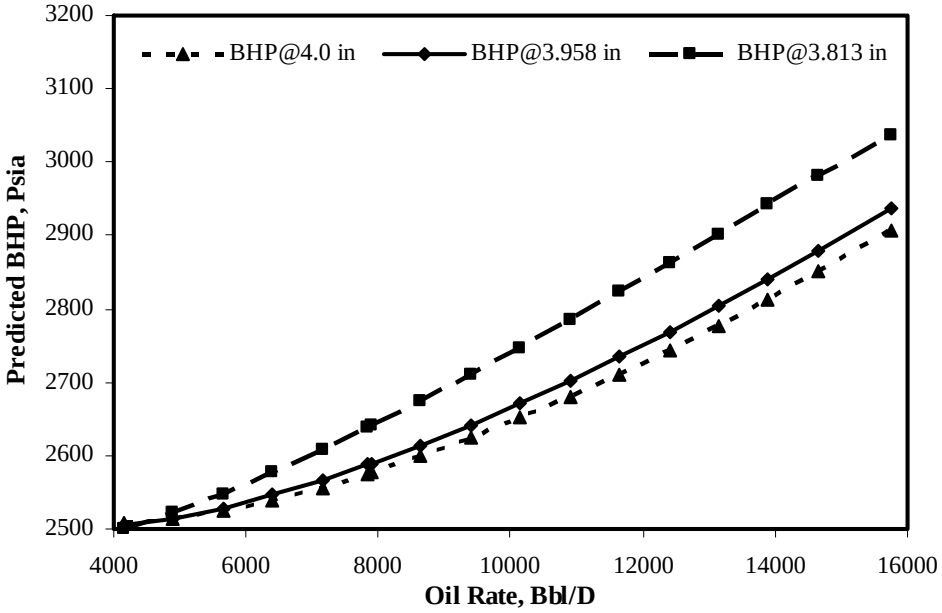

Figure 5.14: Effect of Changing Oil Rate for Three Different Tubing Sizes.

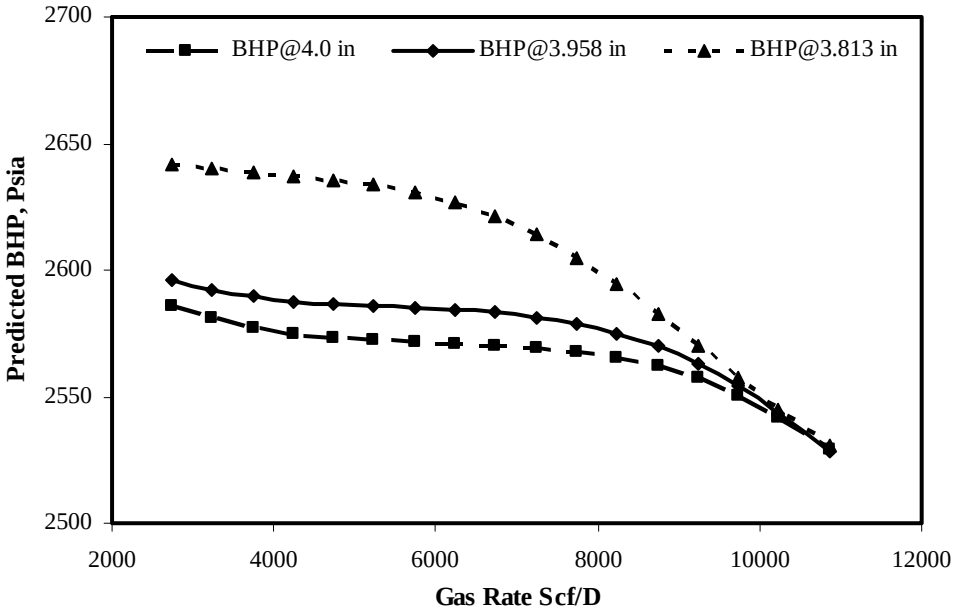

Figure 5.15: Effect of Changing Gas Rate for Three Different Tubing Sizes.

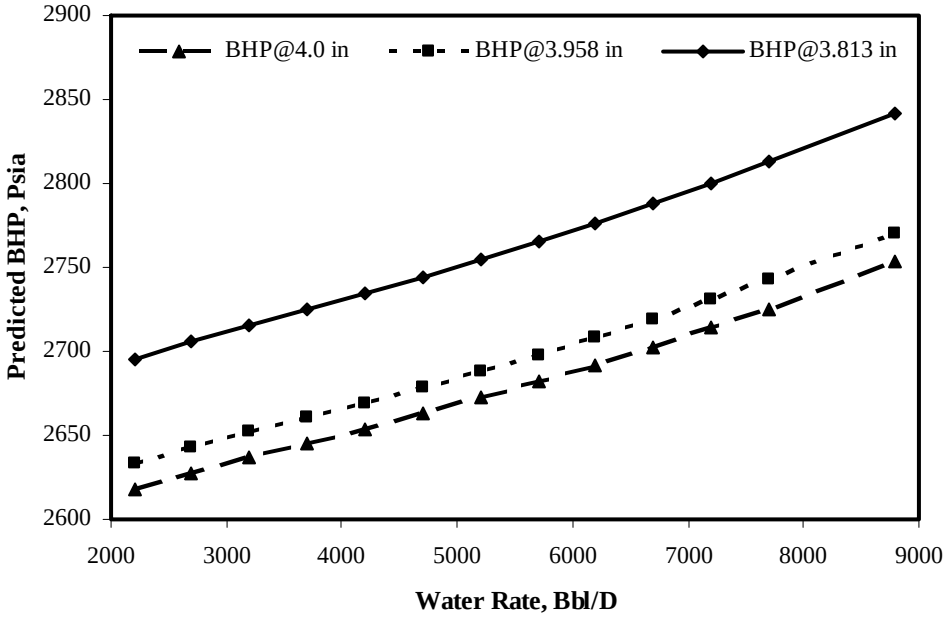

Figure 5.16: Effect of Changing Water Rate for Three Different Tubing Sizes.

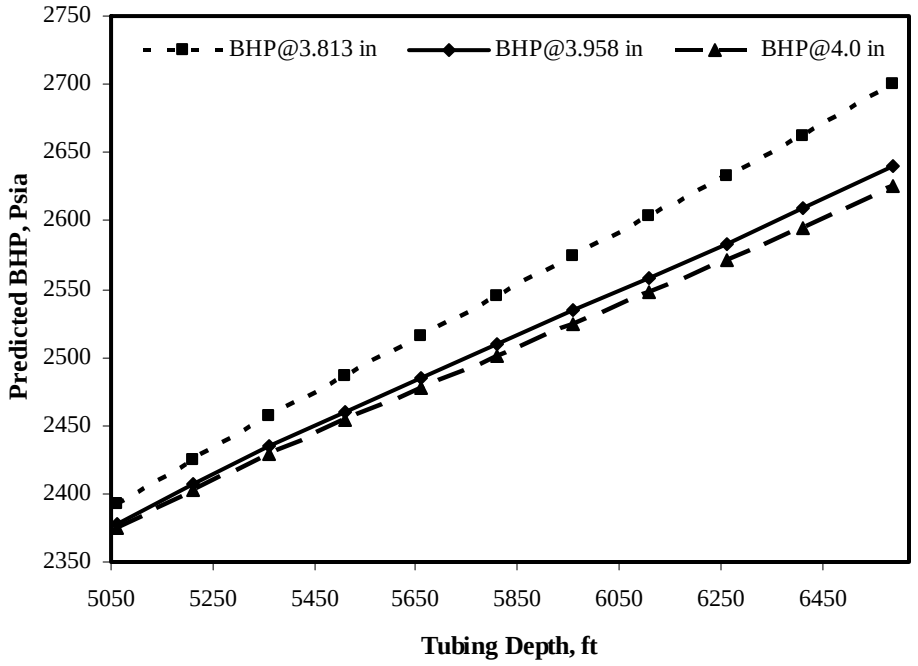

Figure 5.17: Effect of Changing tubing Depth for Three Different Tubing Sizes.

As shown in Figure 5.19, again ANN model provides the best accuracy when the average absolute relative error plotted against different gas rate groups. Figure 5.20 shows the statistical accuracy of predicted flowing bottomhole pressure grouped by water rate. The ANN model outperforms other tested methods especially in the range of water rate greater than 3900 barrel per day. The ANN model showed better results than other tested models when tubing diameter is greater than 3.958 inches is used, as shown in Figure 5.21. Additionally, the statistical accuracy of flowing bottomhole pressure is also grouped by the depth interval as shown in Figure 5.22. The model also provides the lowest average absolute relative error compared to other tested models.

5.7 Statistical and Graphical Comparisons

5.7.1 Statistical Error Analysis

This error analysis is utilized to check the accuracy of the models. The statistical parameters used in the present work are: average percent relative error, average absolute percent relative error, minimum and maximum absolute percent error, root mean square error, standard deviation of error, and the correlation coefficient. Equations for those parameters are given below. Summary of statistical comparisons between models and correlations is presented in Table 5.5.

1. Average Percent Relative Error (APE):

It is the measure of relative deviation from the experimental data, defined by:

$$E_r = \frac{1}{n}\sum_{i=1}^{N} E_i$$

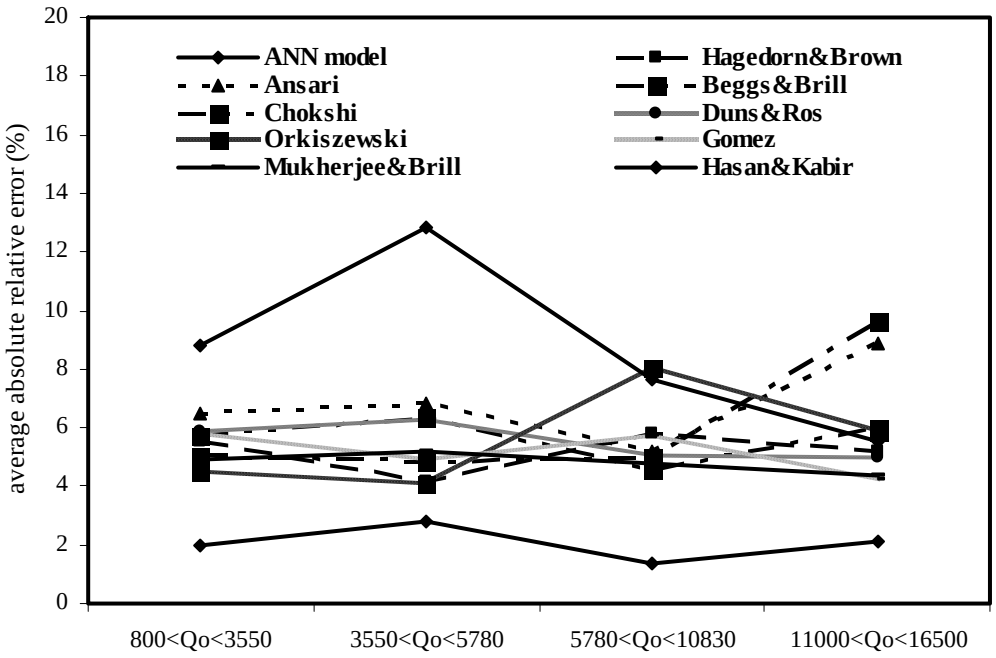

Figure 5.18: Statistical Accuracy of BHP Grouped by Oil Rate (With Corresponding Data Points).

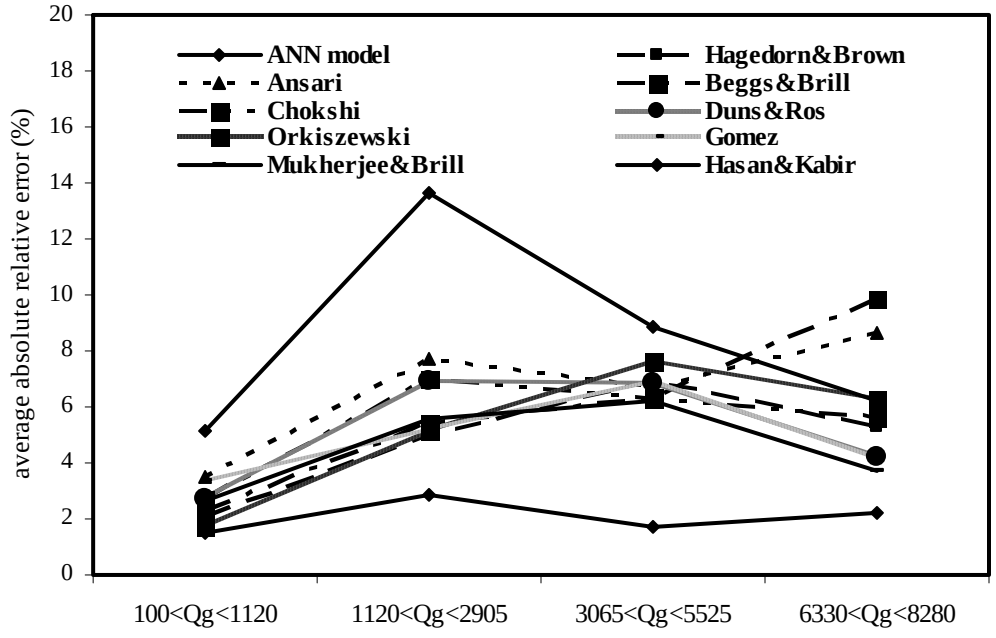

Figure 5.19: Statistical Accuracy of BHP Grouped by Gas Rate (With Corresponding Data Points).

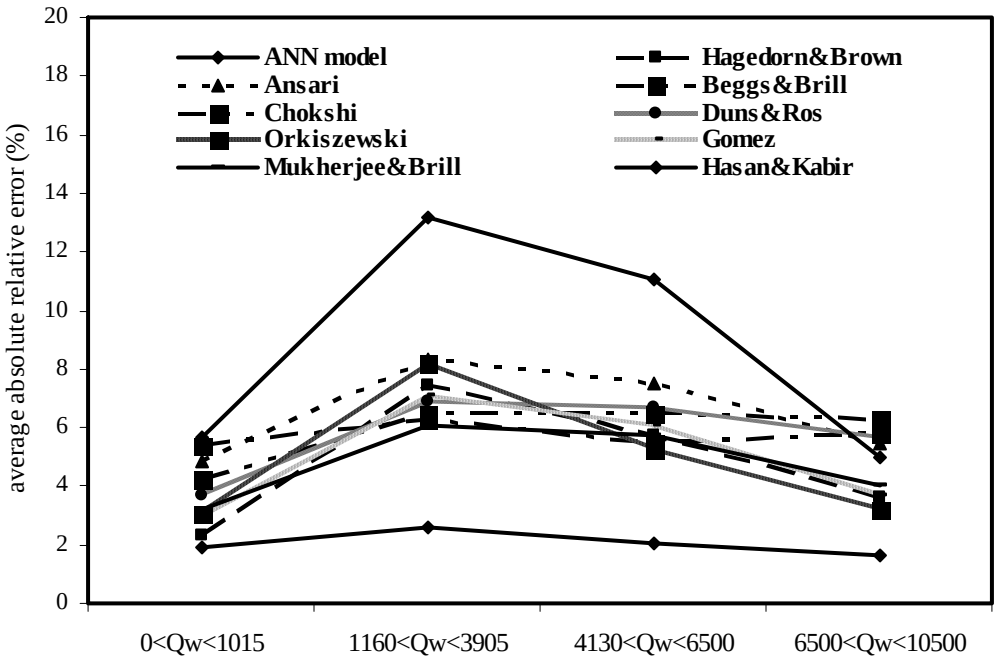

Figure 5.20: Statistical Accuracy of BHP Grouped by Water Rate (With Corresponding Data Points**).**

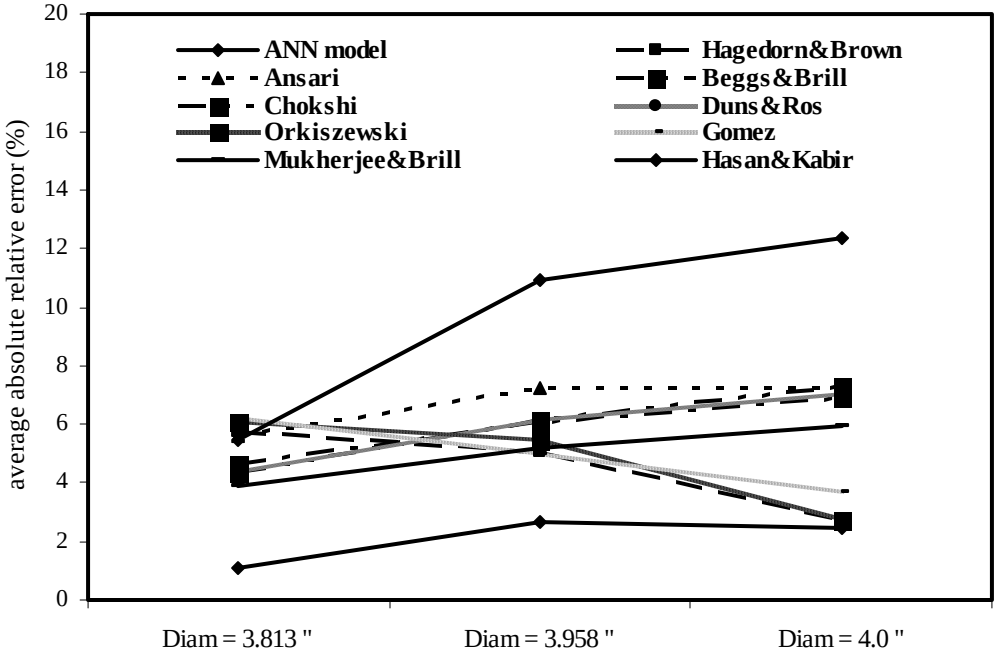

Figure 5.21: Statistical Accuracy of BHP Grouped by Tubing Diameter (With Corresponding Data Points**).**

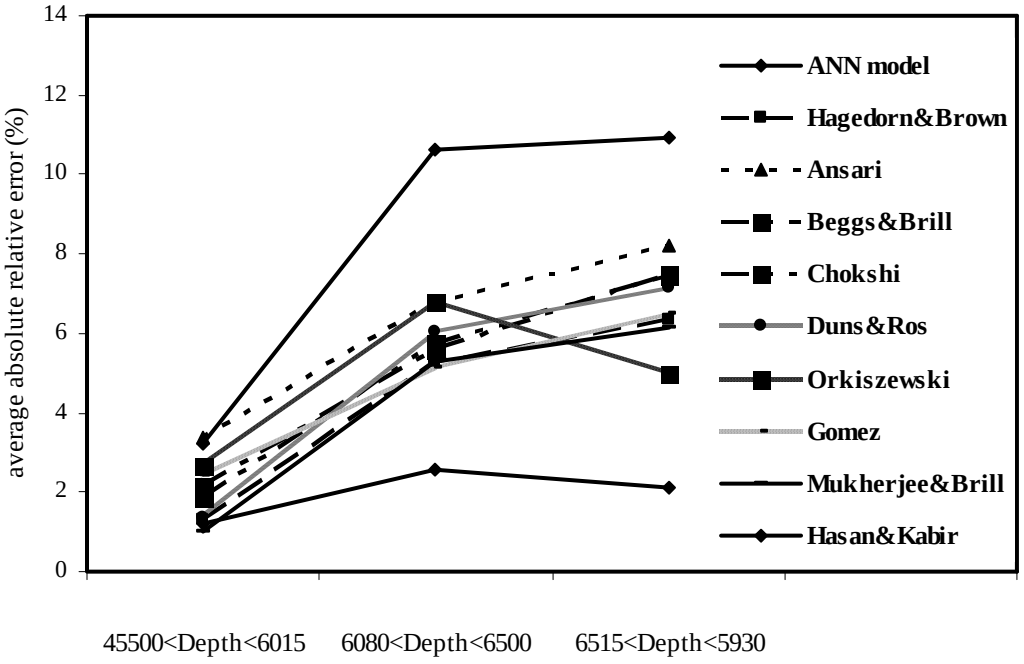

Figure 5.22: Statistical Accuracy of BHP Grouped by Tubing Depth (With Corresponding Data Points**).**

Table 5.5: Statistical Analysis Results of Empirical Correlations and Mechanistic Models**.**

	E_a	E_r	E_{Max}	E_{Min}	RMSE	R	STD
Kabir and Hasan[15]	9.230	-7.190	35.140	0.486	11.944	0.7502	215.644
Ansari *et al.*[18]	6.754	-1.451	16.612	0.025	8.089	0.8178	196.930
Chokshi *et al.*[19]	5.759	-2.852	17.843	0.355	7.009	0.8836	155.684
Gomez *et al.*[20]	5.204	1.212	26.617	0.019	7.643	0.8324	184.069
Hagedorn and Brown[2]	5.029	1.461	26.569	0.141	7.373	0.8508	177.840
Duns and Ros[3]	5.758	-2.834	20.437	0.009	7.564	0.8495	173.083
Orkiszewski[4]	5.376	4.617	20.592	0.042	7.251	0.9015	138.053
Beggs and Brill[5]	5.690	-1.892	19.533	0.326	7.144	0.8647	167.755
Mukherjee and Brill[7]	4.903	-1.164	16.209	0.201	6.217	0.8792	147.572
This Study "ANN"	2.165	-0.419	7.1401	0.066	2.801	0.9735	66.245

Where; E_i is the relative deviation of an estimated value from an experimental value

$$E_i = \left[\frac{(BHP)_{meas} - (BHP)_{est}}{(BHP)_{meas}} \right] \times 100, \quad \text{i} = 1,2,3,...,\text{n}$$

where;

$(BHP)_{meas}$ is the actual value of bottomhole pressure

$(BHP)_{est}$ is the estimated value of bottomhole pressure

2. Average Absolute Percent Relative Error (AAPE):

It measures the relative absolute deviation from the experimental values, defined by:

$$E_a = \frac{1}{n} \sum_{i=1}^{n} |E_i|$$

(This will be considered as the main criterion in statistical error analysis throughout this study).

3. Minimum Absolute Percent Relative Error:

$$E_{\min} = \min_{i+1}^{n} |E_i|$$

4. Maximum Absolute Percent Relative Error:

$$E_{\max} = \max_{i+1}^{n} |E_i|$$

5. Root Mean Square Error:

Measures the data dispersion around zero deviation, defined by:

$$RMSE = \left[\frac{1}{n} \sum_{i=1}^{n} E_i^{\,2} \right]^{0.5}$$

6. Standard Deviation:

It is a measure of dispersion and is expressed as:

$$STD = \sqrt{\left[\left(\frac{1}{(m-n-1)}\right)\right]\sum_{i=1}^{m}\left[\left\{\frac{(BHP_{act} - BHP_{est})}{BHP_{act}}\right\}100\right]^2}$$

Where; (m-n-1) represents the degree of freedom in multiple- regression. A lower value of standard deviation indicates a smaller degree of scatter.

7. The Correlation Coefficient:

It represents the degree of success in reducing the standard deviation by regression analysis, defined by:

$$R = \sqrt{1 - \frac{\sum_{I=1}^{n}\left[(BHP)_{act} - (BHP)_{est}\right]}{\sum_{I=1}^{n}(BHP)_{act} - \overline{\Delta BHP}}}$$

Where

$$\overline{\Delta BHP} = \frac{1}{n}\sum_{I=1}^{n}\left[(\Delta BHP)_{act}\right]_I$$

'R' values range between 0 and 1. The closer value to 1 represents perfect correlation whereas 0 indicates no correlation at all among the independent variables.

5.7.2 Graphical Error Analysis

Graphical tools aid in visualizing the performance and accuracy of a correlation or a model. Three graphical analysis techniques are employed; those are crossplots, error distribution, and residual analysis.

5.7.2.1 Crossplots

In this graphical based technique, all estimated values are plotted against the measured values and thus a crossplot is formed. A 45° straight line between the estimated versus actual data points is drawn on the crossplot, which denotes a perfect correlation line. The tighter the cluster about the unity slope line, the better the agreement between the experimental and the predicted results.

Figures 5.23 through 5.34 present crossplots of predicted bottomhole pressure versus the actual one for the developed model, other empirical correlations and mechanistic models. Investigation of these figures clearly shows that the developed ANN model outperforms all correlations and mechanistic models. Graphical comparison between models is given in Figure 5.35 and 5.36, which show the correlation coefficients and root mean squared errors of all models. The ANN model achieved the highest correlation coefficient (0.9735), while other correlations indicates higher scattering range, where 0.81780 is obtained for Ansari *et al.*[18] model, 0.88360 for Chokshi *et al.*[19] model, 0.83240 for Gomez *et al.*[20]. model, 0.86470 for Duns and Ros[3] correlation, 0.90150 for Orkiszewski[4] correlation, 0.85080 for Hagedorn and Brown[2] correlation, 0.84950 for Beggs and Brill[5] correlation, and 0.87920 for Mukherjee and Brill[7] correlation. Orkiszewski[4] correlation achieved the highest correlation coefficient among the other correlations and mechanistic models. This agrees with the result obtained by Lawson and Brill[11]. Comparison between the performance of mechanistic models and empirical correlations is provided in Table 5.5. Hasan and Kabir[15] model achieved the worst correlation coefficient among other mechanistic models and empirical correlations.

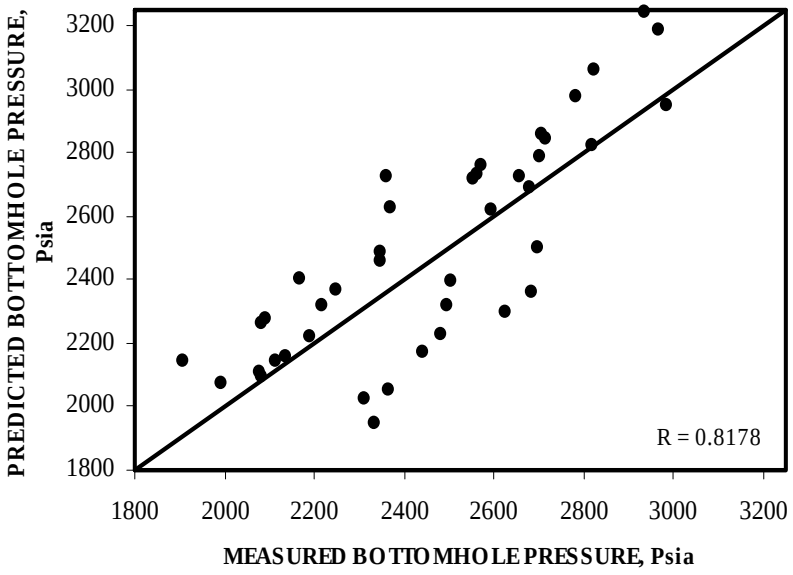

Figure 5.23: Crossplot of Observed vs. Calculated BHP for Ansari *et al.* Model.

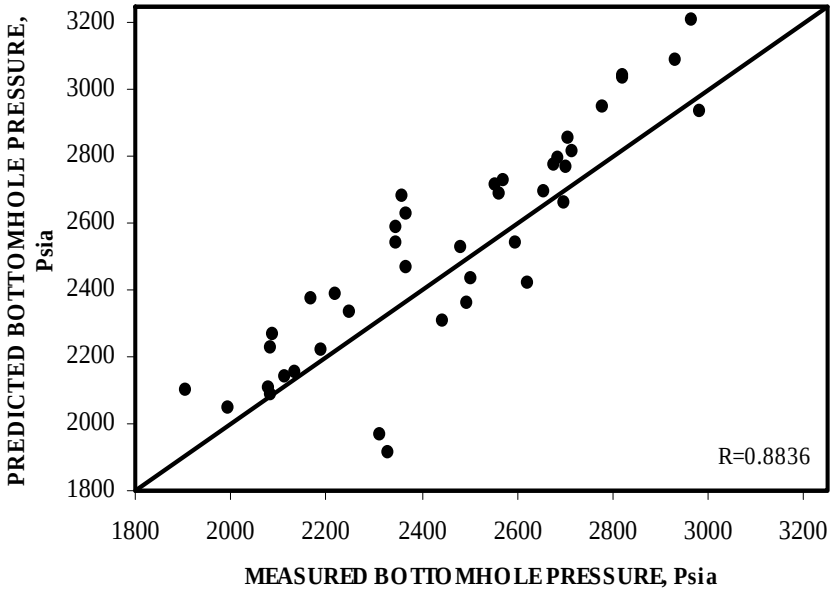

Figure 5.24: Crossplot of Observed vs. Calculated BHP for Chokshi *et al.* Model.

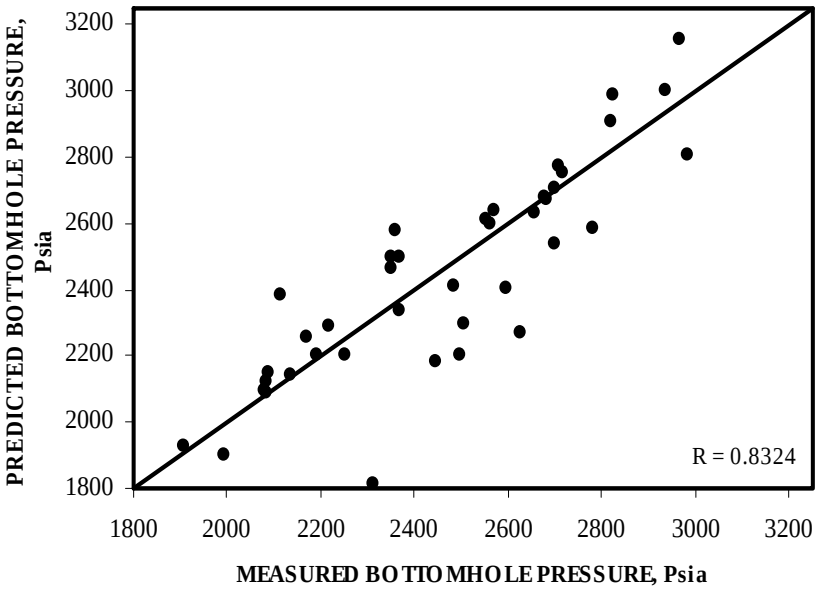

Figure 5.25: Crossplot of Observed vs. Calculated BHP for Gomez *et al.* Model.

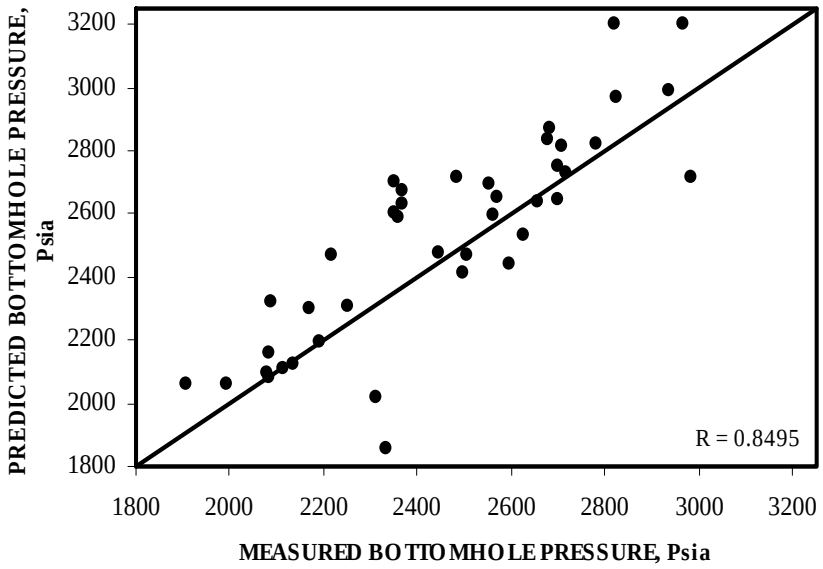

Figure 5.26: Crossplot of Observed vs. Calculated BHP for Beggs and Brill Correlation.

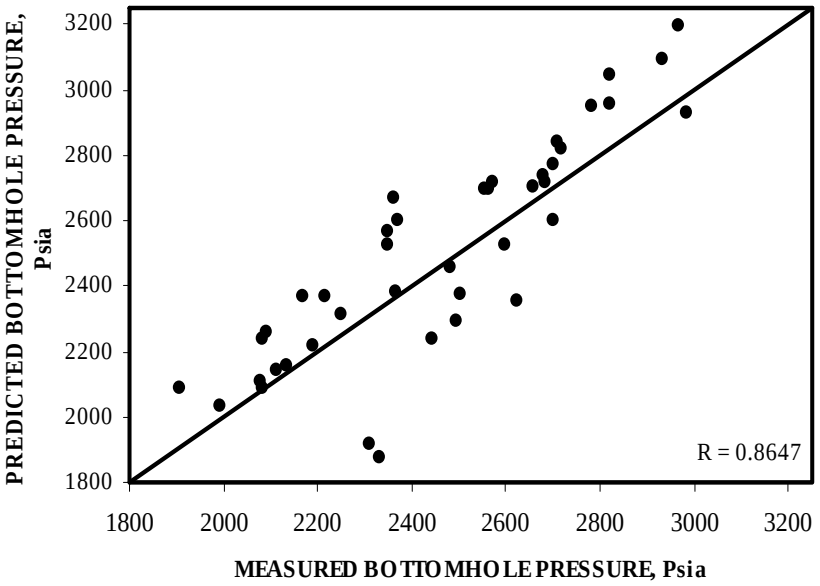

Figure 5.27: Crossplot of Observed vs. Calculated BHP for Duns and Ros Correlation.

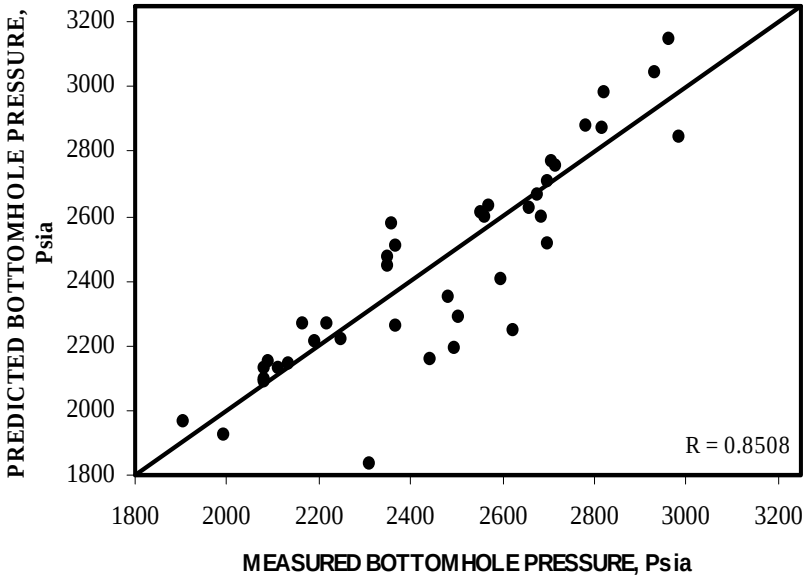

Figure 5.28: Crossplot of Observed vs. Calculated BHP for Hagedorn and Brown Correlation.

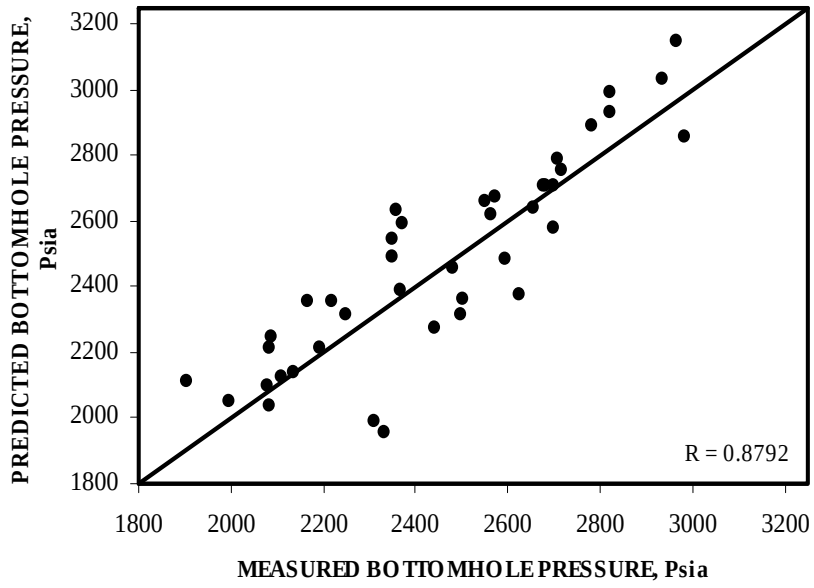

Figure 5.29: Crossplot of Observed vs. Calculated BHP for Mukherjee and Brill Correlation.

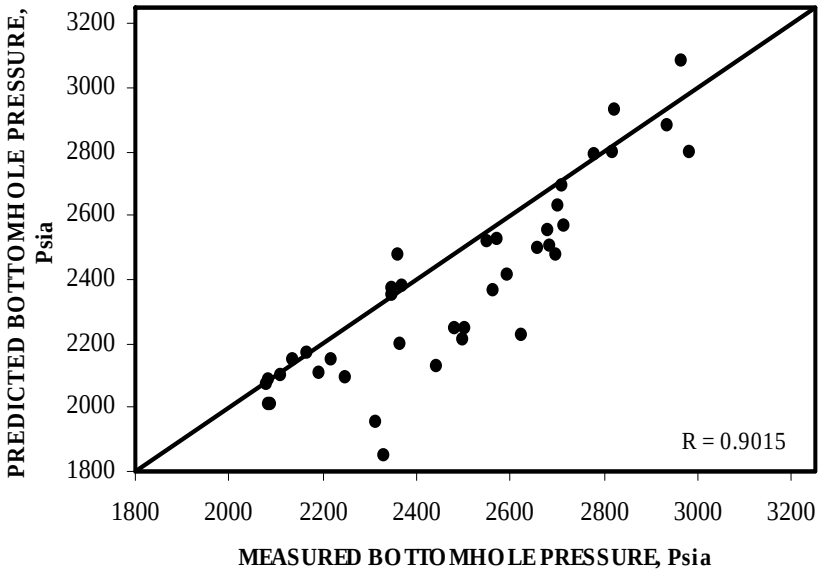

Figure 5.30: Crossplot of Observed vs. Calculated BHP for Orkiszewski Correlation.

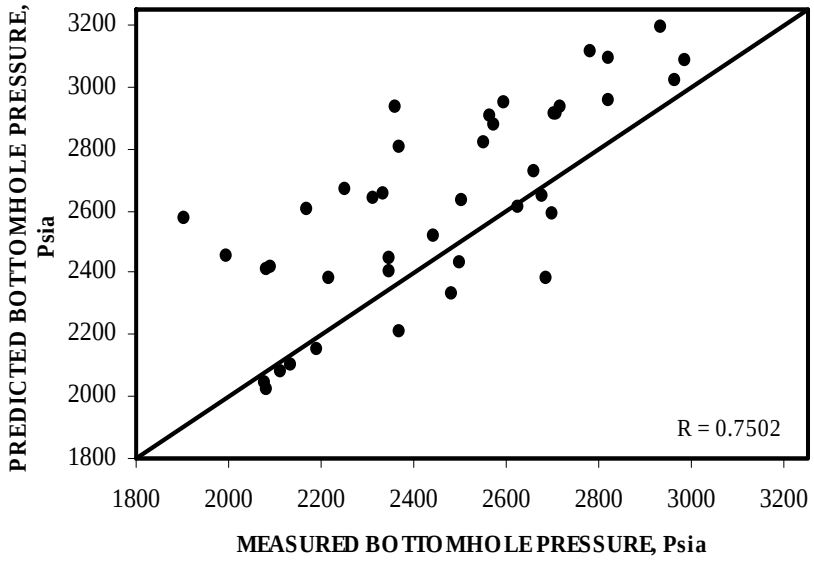

Figure 5.31: Crossplot of Observed vs. Calculated BHP for Hasan and Kabir Model.

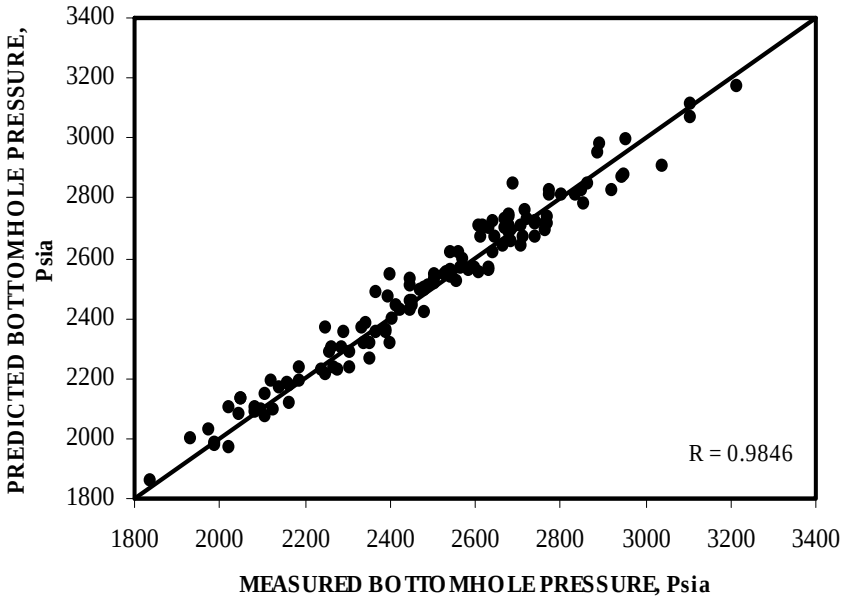

Figure 5.32: Crossplot of Observed vs. Calculated BHP for Training Set (ANN Model).

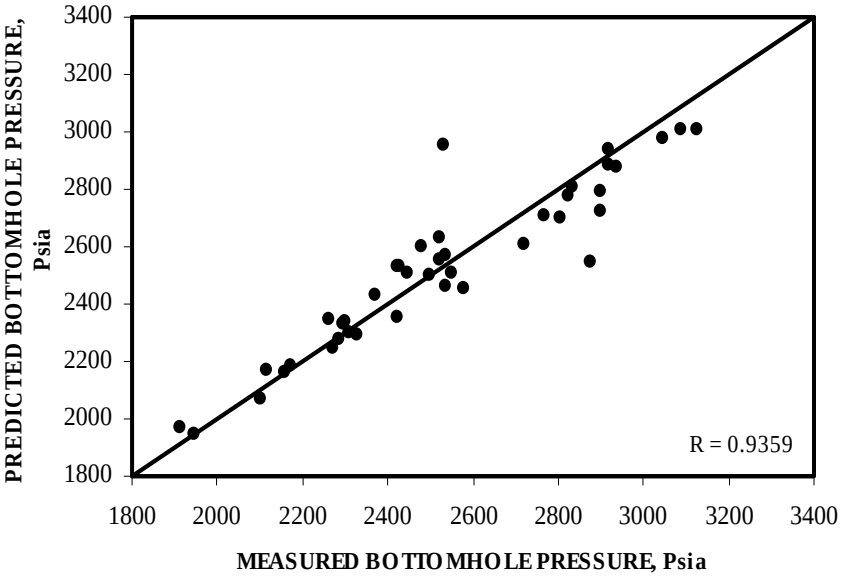

Figure 5.33: Crossplot of Observed vs. Calculated BHP for Validation Set (ANN Model).

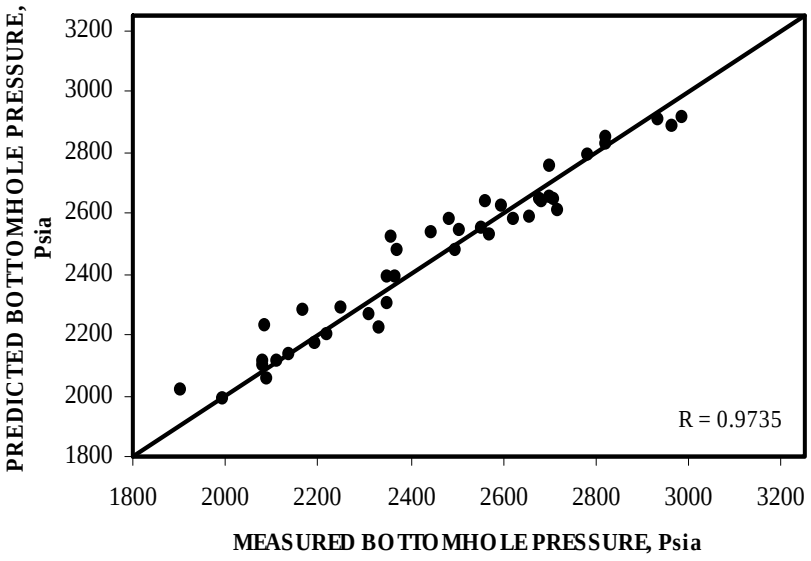

Figure 5.34: Crossplot of Observed vs. Calculated BHP for Testing Set (ANN Model).

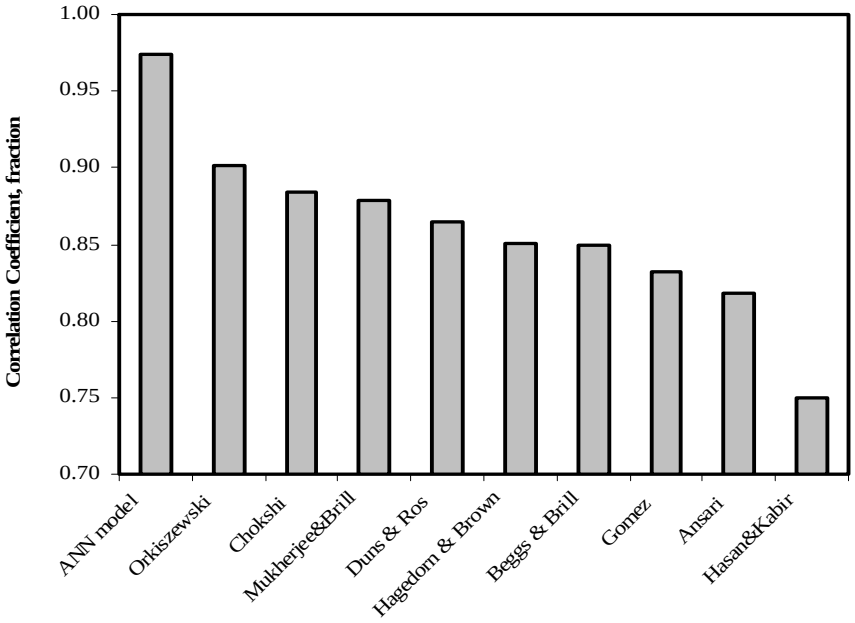

Figure 5.35: Comparison of Correlation Coefficients for the Developed Model, Empirical Correlations, and Mechanistic Models.

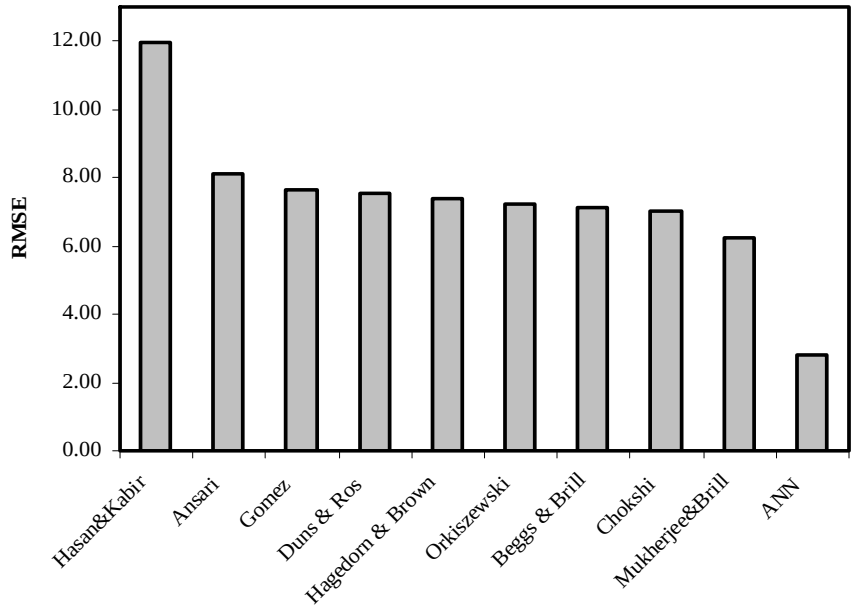

Figure 5.36: Comparison of Root Mean Squared Errors for the Developed Model, Empirical Correlations, and Mechanistic Models.

Comparison between average absolute percent error for all correlations and mechanistic models and the new developed model is provided in Figure 5.37. As seen from Table 5.5, Mukherjee and Brill[7] correlation outperforms other correlations and mechanistic models in terms of lowest average absolute percent error, lesser maximum error, lowest errors standard deviation, lowest average relative error, and the lowest root mean squared error. The developed model accomplished the lowest average absolute percent relative error (2.1654%), lowest maximum error (7.1401%), lowest root mean squared error (2.8013), lowest errors standard deviation (66.2448), lowest average relative percent error among other correlations and mechanistic errors (-0.4186%) and the highest correlation coefficient among other empirical correlations and mechanistic models (97.350%), as shown in Table 5.6.

The average absolute percent relative error is a significant sign of the accuracy of the models. Its value for ANN was 2.11654%, while other correlations indicate high error values of 6.7536% for Ansari *et al.*[18] model, 5.7589% for Chokshi *et al.*[19] model, 5.2044% for Gomez *et al.*[20] model, 5.6903% for Duns and Ros[3] correlation, 5.3763% for Orkiszewski[4] correlation, 5.0286% for Hagedorn and Brown[2] correlation, 5.7585% for Beggs and Brill[5] correlation, and 4.9032% for Mukherjee and Brill[7] correlation.

Table 5.6: Statistical Analysis Results of Developed Neural Network Model.

Statistical Parameter	**Training**	**Validation**	**Testing**
E_a	1.7546	2.9273	2.1654
E_r	-0.3289	0.1843	-0.4186
E_{Max}	6.0866	16.7049	7.1401
E_{Min}	0.0480	0.0823	0.0655
RMSE	2.1841	4.1793	2.8013
R "fraction"	0.98461	0.93589	0.97345
STD	53.333	111.144	66.245

5.7.2.2 Error Distributions

Figures 5.38 through 5.40 show the error distribution histograms for the neural network model. Normal distribution curves are fitted to each one of them. The errors are said to be normally distributed with a mean around the 0%. Hence, most investigated correlations and mechanistic models show either slight negatively skewed error distributed or positively ones.

Figure 5.41 shows the error distribution histogram and the normal distribution curve for Ansari *et al.*[18] model. It shows a slight shift of the mean of the errors towards the negative side of the plot (about two degrees) indicating that the flowing bottomhole pressure is overestimated. Figure 5.42 shows the error distribution histogram and the normal distribution curve for Chokshi *et al.*[19] model. The errors are normally distributed with a mean approximately equals to -3%, indicating the model is overestimating the flowing bottomhole pressure. Figure 5.43 shows the error distribution histogram and the normal distribution curve for Gomez *et al.*[20] model. The model shows good performance with reasonable error distributed (shifted 0.5% to the positive side). Figure 5.44 shows the error distribution histogram and the normal distribution curve for Beggs and Brill[5] correlation. The correlation errors histogram suffered from a pronounced shift towards the left (-3%), indicating that correlation overpredicted the flowing bottomhole pressure. Figure 5.45 shows the error distribution histogram and the normal distribution curve for Duns and Ros[3] correlation. The correlation overestimates the pressure due to the shift of its normal distribution curve towards the left (-2%). On contradictory, Hagedorn and Brown[2] correlation underestimates the pressure (Figure 5.46) due to the shift of the normal distribution curve to the right side (1.5%). It is evident that, from Mukherjee and

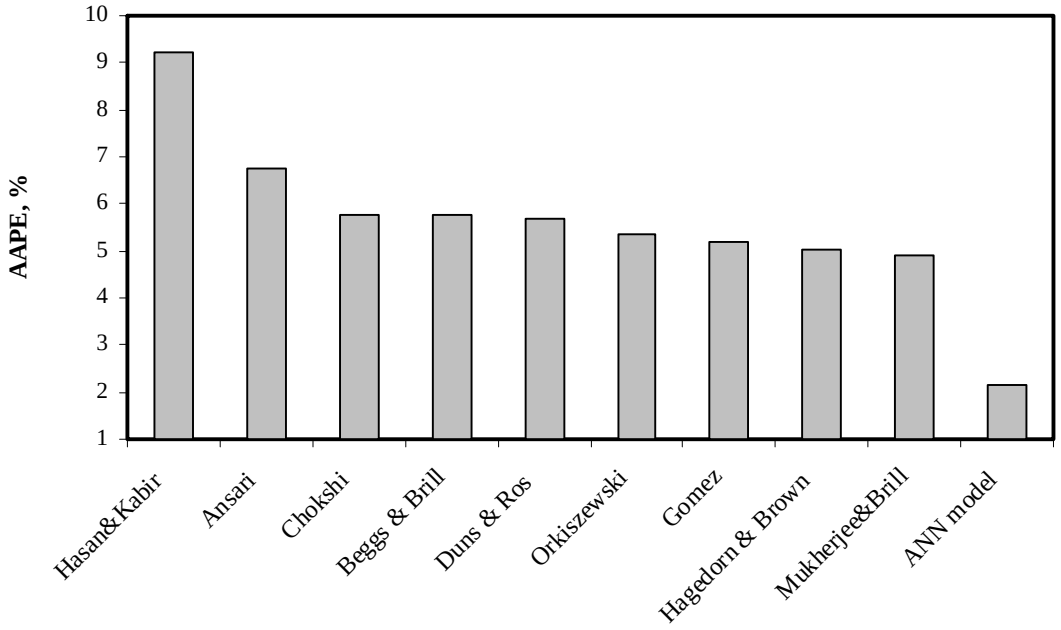

Figure 5.37: Comparison of AAPE for the Developed Model and other Correlations and Mechanistic Models**.**

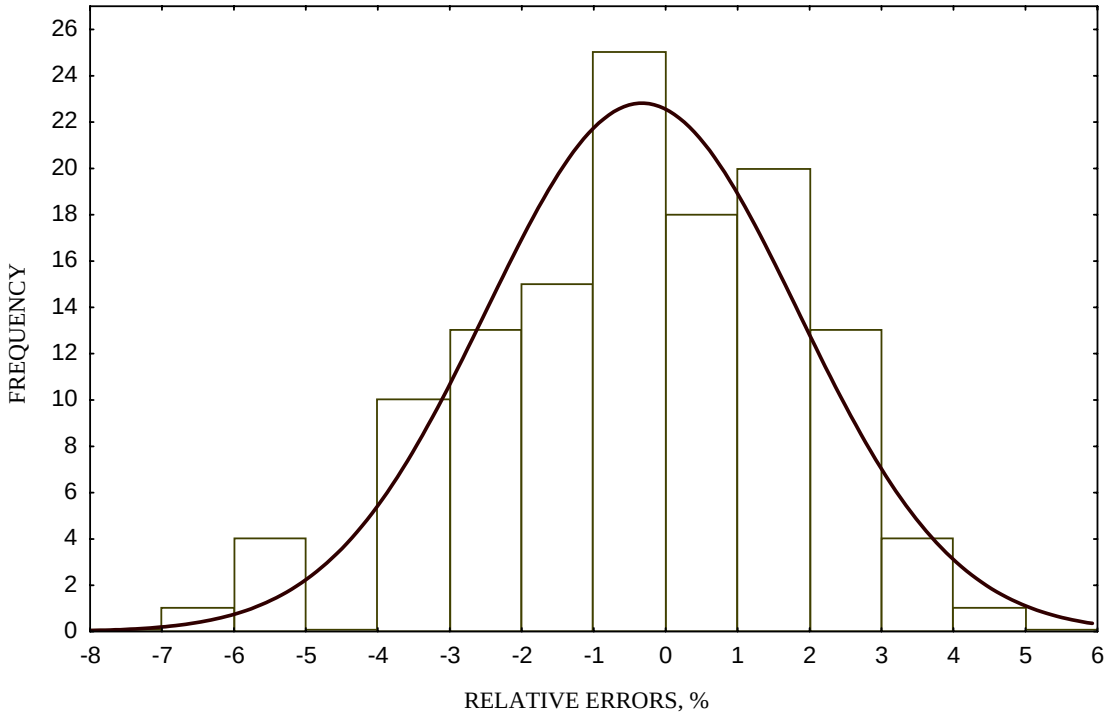

Figure 5.38: Error Distribution for Training Set (ANN Model).

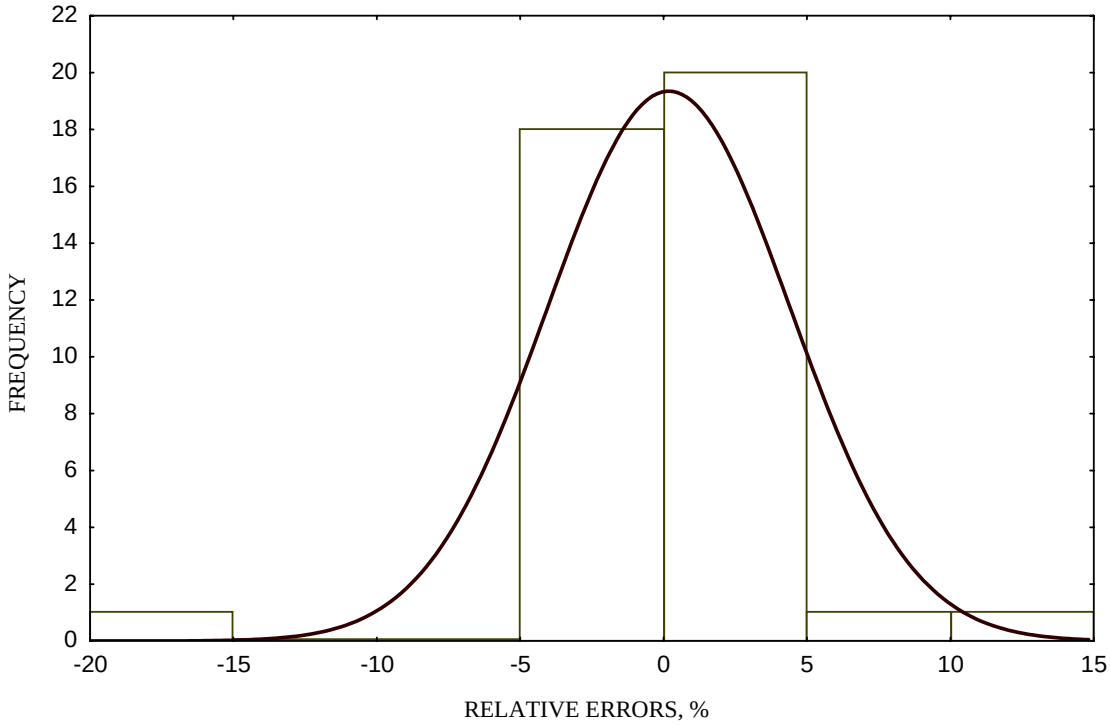

Figure 5.39: Error Distribution for Validation Set (ANN Model).

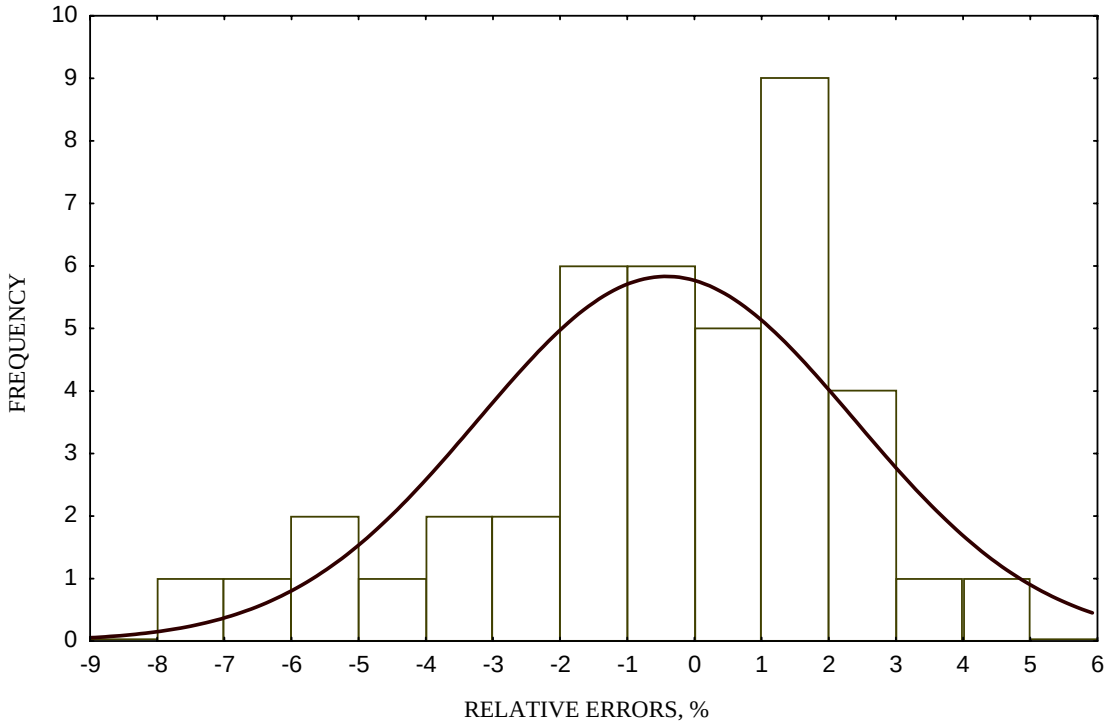

Figure 5.40: Error Distribution for Testing Set (ANN Model).

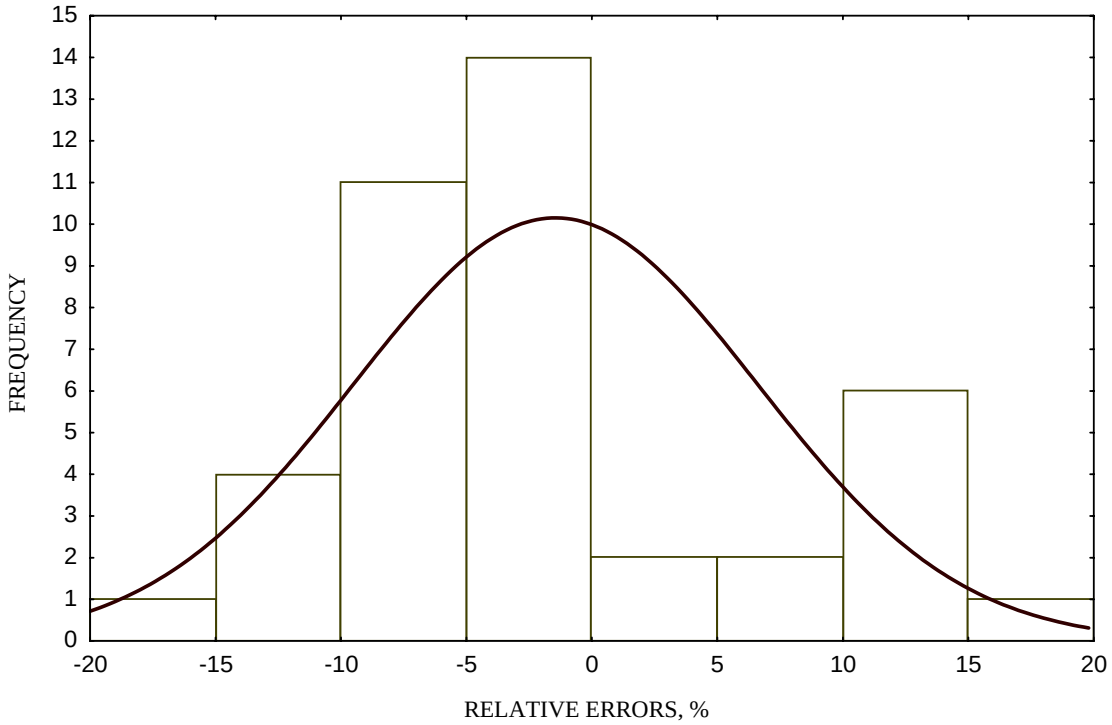

Figure 5.41: Error Distribution for Ansari *et al.* Model.

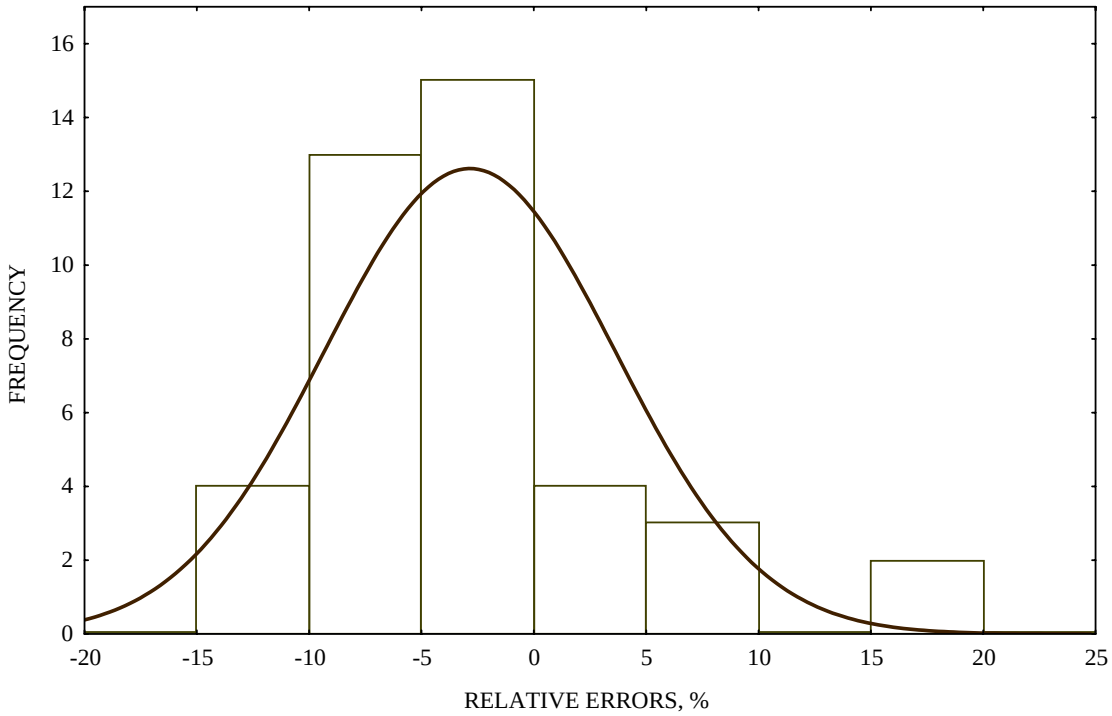

Figure 5.42: Error Distribution for Chokshi *et al.* Model.

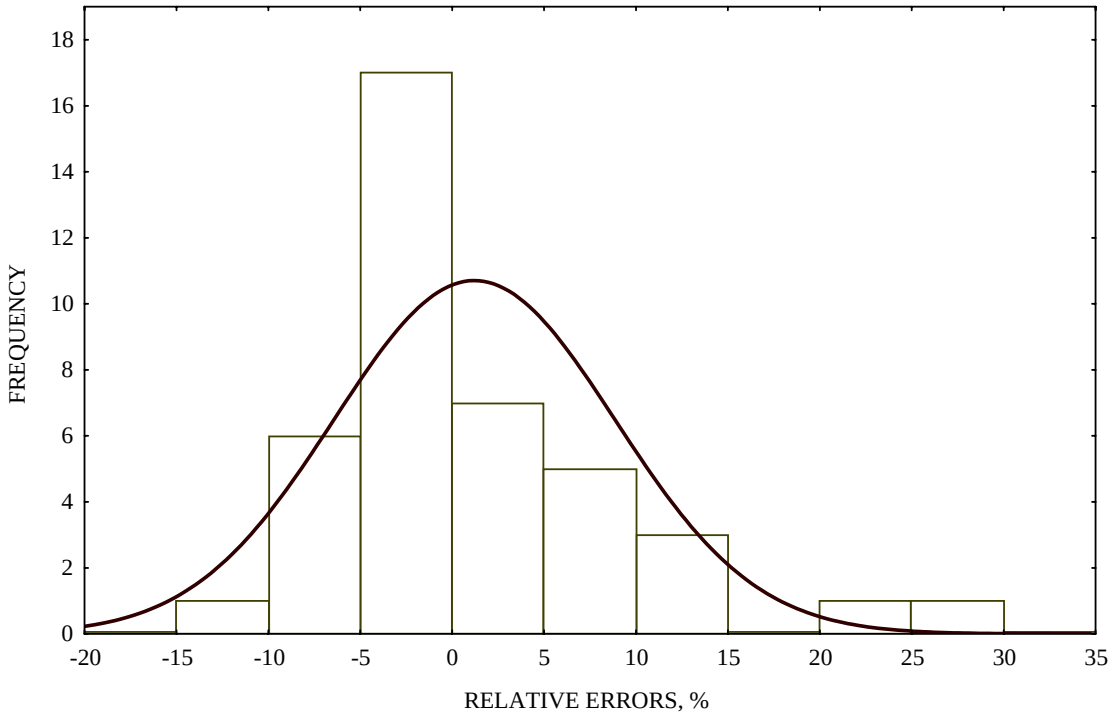

Figure 5.43: Error Distribution for Gomez *et al.* Model.

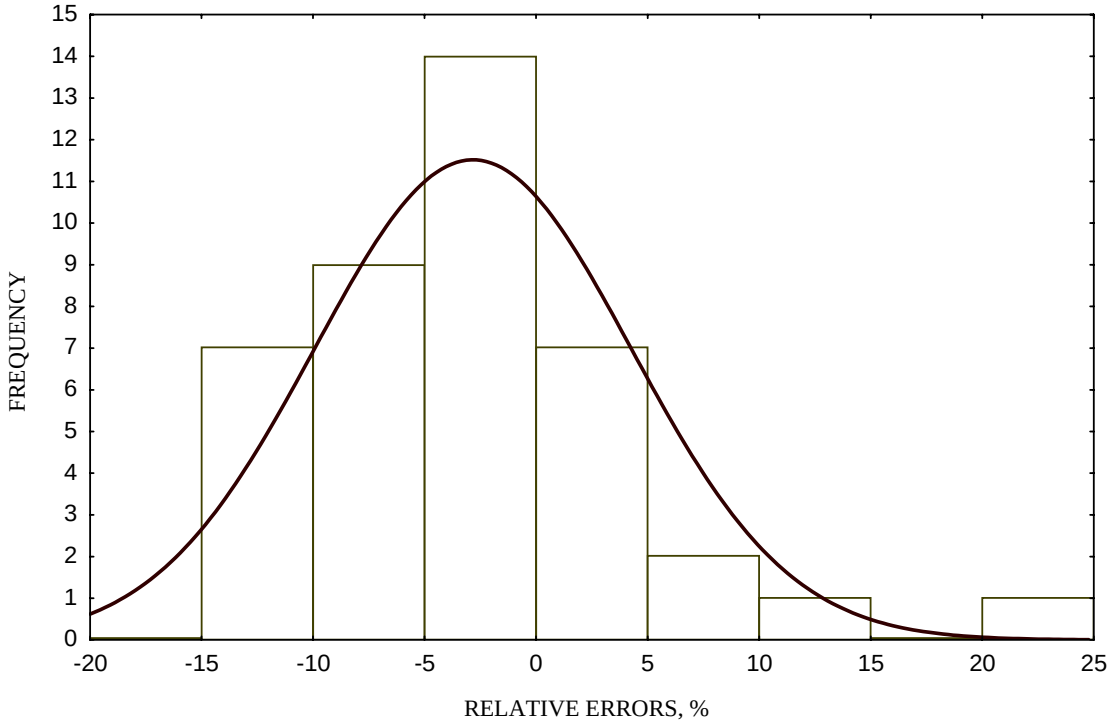

Figure 5.44: Error Distribution for Beggs and Brill Correlation.

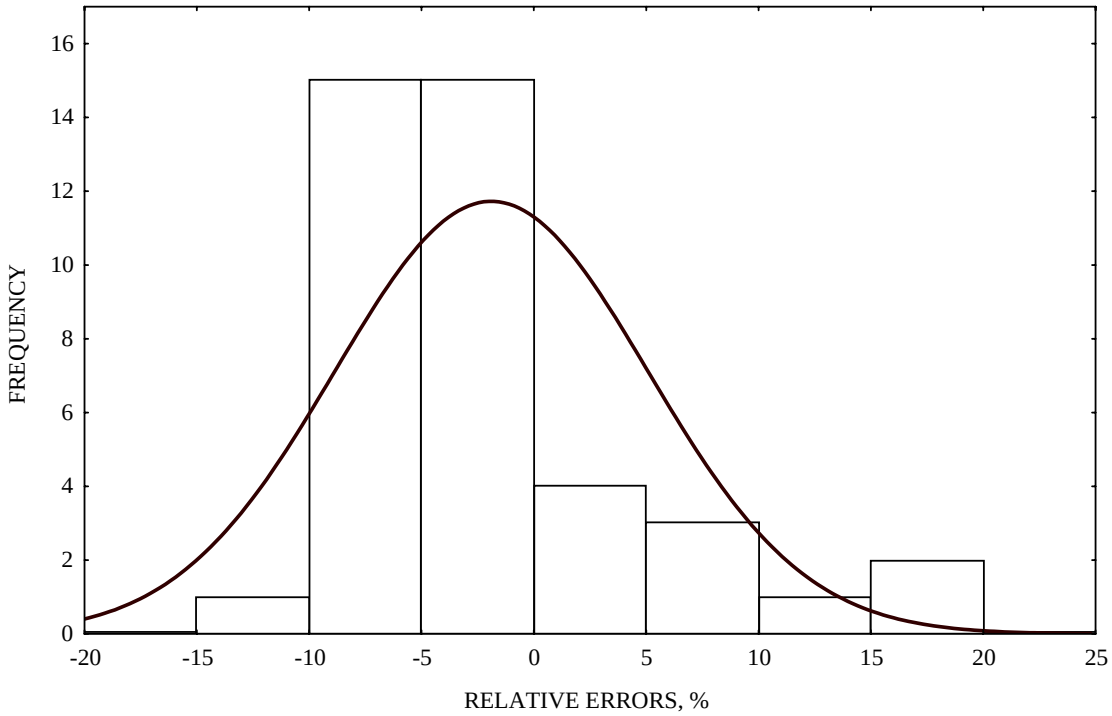

Figure 5.45: Error Distribution for Duns and Ros Correlation.

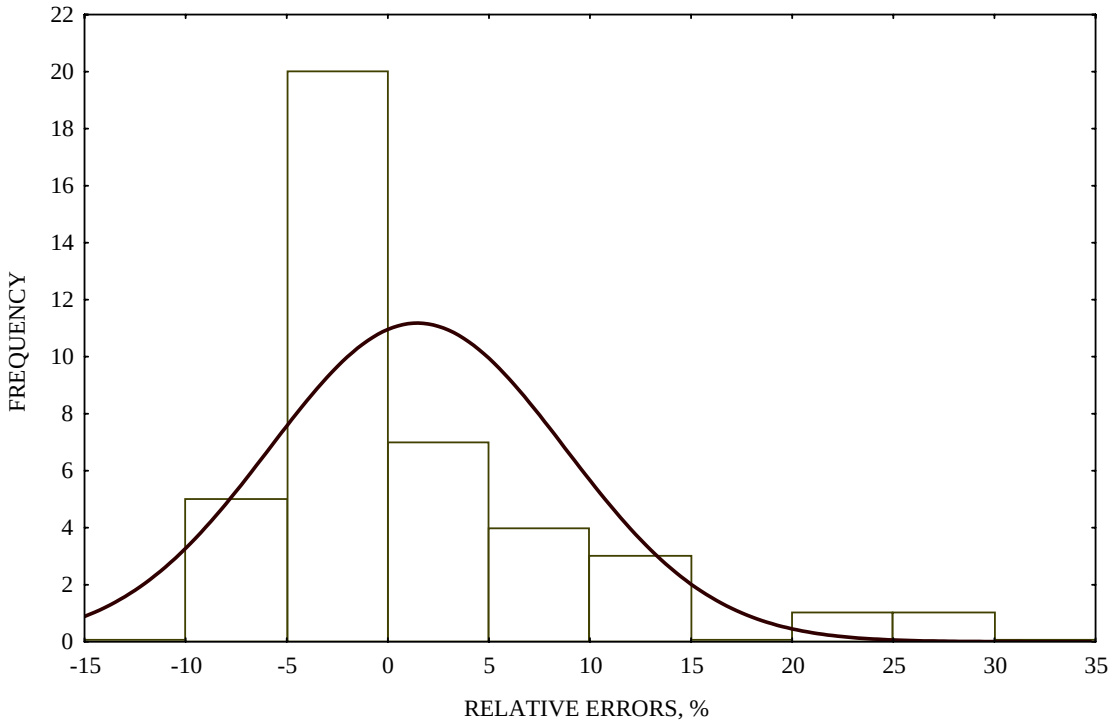

Figure 5.46: Error Distribution for Hagedorn and Brown Correlation.

Brill[7] correlation's histogram (Figure 5.47), the pressure was overpredicted slightly due to the shift of the error distribution mean towards the left (-1.0%). Orkiszewski[4] correlation showed the worst error distribution curve among empirical correlations, where it shifted around 4.5% towards the right side indicating underestimation of flowing bottomhole pressure, as illustrated in Figure 5.48. Figure 5.49 shows the error distribution histogram and the normal distribution curve for Hasan and Kabir[15] model. The model histogram suffered from a very large shift towards the left among all correlations and mechanistic models (-11%), which indicates the inadequacy of the model for predicting flowing bottomhole pressure under the tested range of variables.

The range of errors also is an important parameter for detecting the accuracy of each model. A range of -14% to 18% is used for the best correlation, among other correlations and mechanistic models, (Mukherjee and Brill[7] correlation), whereas an error range of -9% to 6% in bottomhole pressure is achieved for testing set, which indicates the superiority of the new developed model over other correlations and mechanistic models. Figure 5.40 shows the error distribution histogram and the normal distribution curve for the newly developed model. The errors are normally distributed with a mean approximately equals to -0.5%, indicating the model is estimating the bottomhole pressure properly. Figure 5.39 can be used to judge the model consistency where validation histogram achieved an ideal normal distribution with zero deviation. All correlations and mechanistic models demonstrate moderate predictability of bottomhole pressure with errors normally distributed with a negative or positive mean.

The new developed model has not suffered from memorizing the pressure values because it shows satisfactory degree of consistency when compared to the validation

results. If the correlation coefficient is used as a main criterion for selecting the best overall performance, Orkiszewski[4] correlation could be selected based on this feature. Because standard deviation is one of the measures of scattering tendencies, it is included as a measure of how points are distributed and scattered. Based on this criterion, Orkiszewski[4] correlation performs the best (138.053) followed by Mukherjee and Brill[7] correlation (147.572) and Chokshi *et al.*[19] model (155.684).

Mukherjee and Brill[7] correlation showed the lowest average absolute percent error, the lowest RMSE, the lowest maximum error, the lowest average relative percent error, and the second best in standard deviation measurement compared to the other correlations and mechanistic models. Moreover, it is noted that at reasonably low gas-liquid ratios and gas-oil ratios, Mukherjee and Brill[7] correlation performs the best when compared to the rest of correlations and mechanistic models.

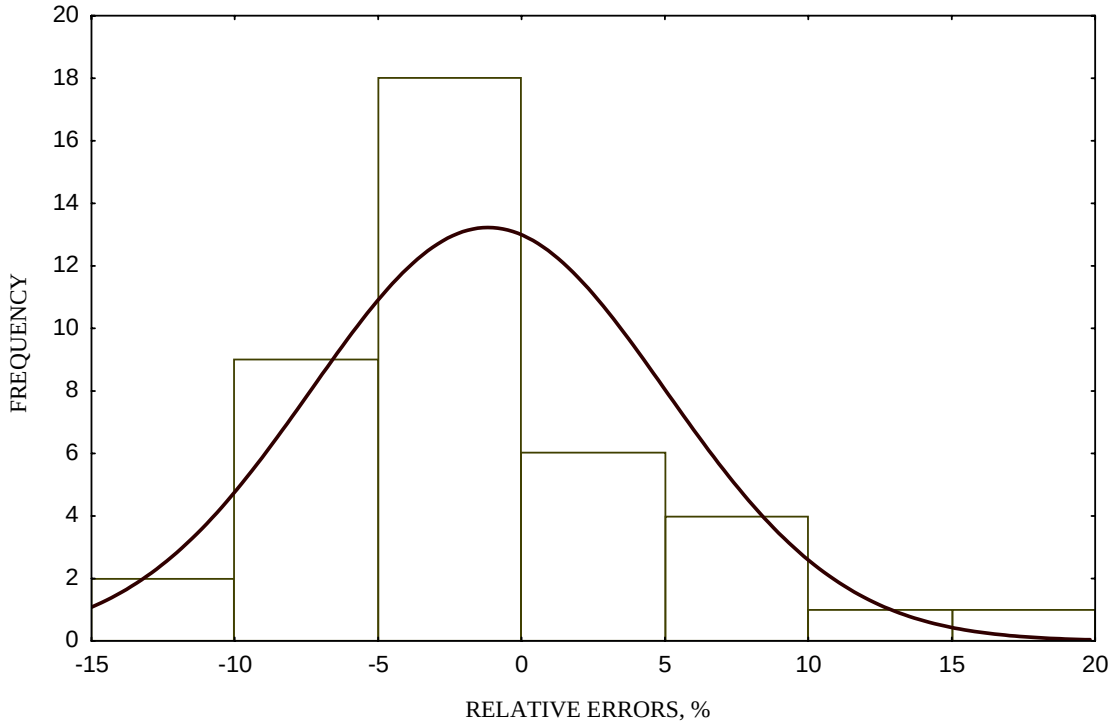

Figure 5.47: Error Distribution for Mukherjee and Brill Correlation.

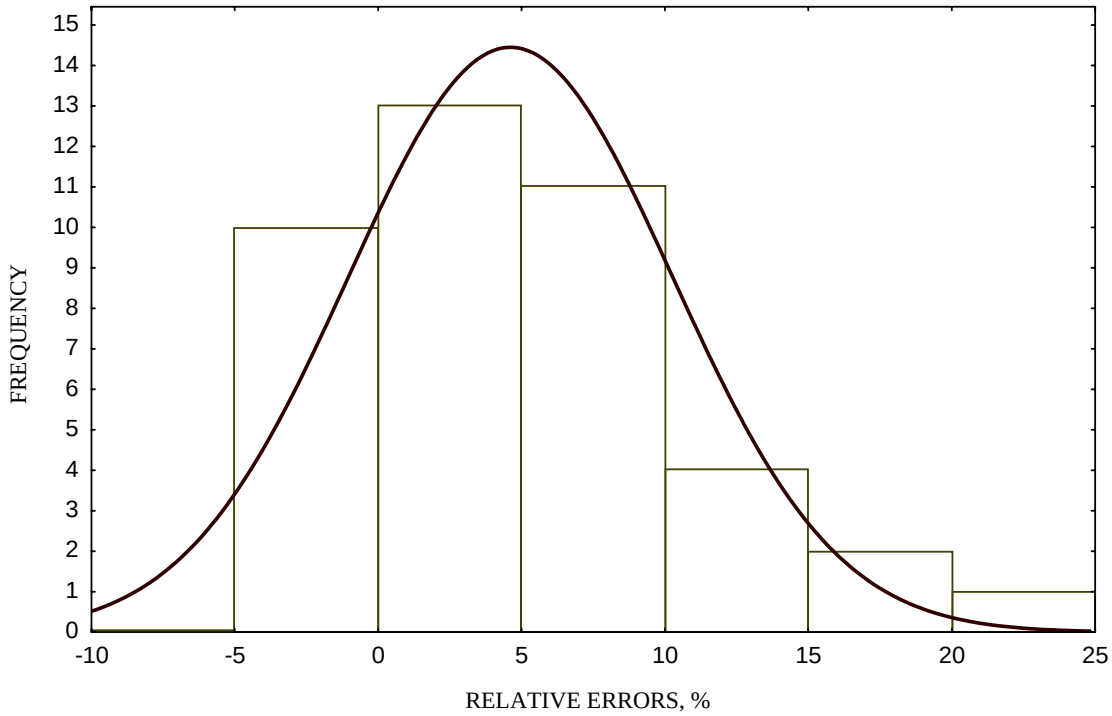

Figure 5.48: Error Distribution for Orkiszewski Correlation**.**

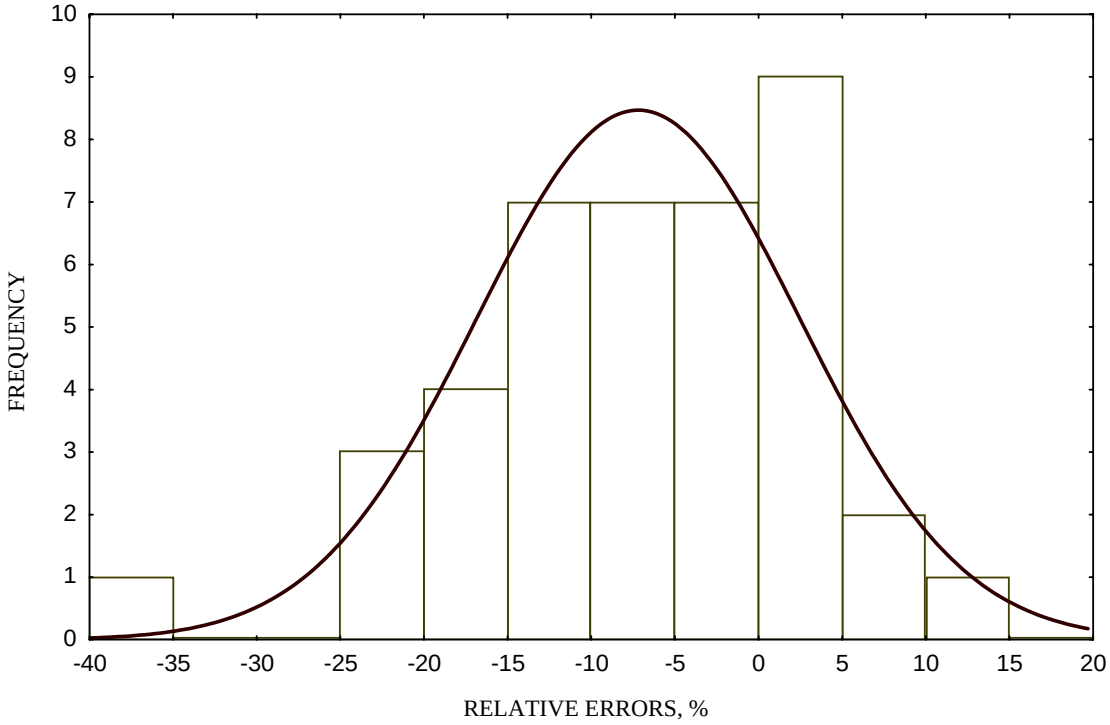

Figure 5.49: Error Distribution for Hasan and Kabir Model.

5.7.2.3 Residual Analysis

According to the data partitioning scheme, the test set contains 41 sets, which were utilized to perform all statistical and graphical tests. The relative frequency of deviations between estimated and actual values is depicted in Figures 5.50 through 5.58 for the tested correlations and mechanistic models. These Figures showed the error distribution around the zero line to verify whether models and correlation have error trends.

Analysis of residual (predicted bottomhole pressure minus the actual bottomhole pressure) is an effective tool to check model deficiencies. Residual limits of each correlation and mechanistic model are shown in Table 5.7. Gomez *et al.*[20] model and Hagedorn and Brown[2] correlation show the worst negative error performance with a maximum value of -620 psia, almost, for both of them. While Hasan and Kabir[15] model showed the worst positive error performance (670 psia). Mukherjee and Brill[7] correlation showed the best error trend around zero (378 to -278) followed by Ansari *et al.*[18] model (367 to -387). Figures 5.59 through 5.61 show the residual plots for the new developed model separately (training, validation, and testing sets). A maximum value of -109 to 159 is found out by testing set. These maximum values are the lowest compared to all investigated correlations and mechanistic models. This is an additional indication that the new developed model outperforms the best available correlations and mechanistic models in a sense of error distribution around the zero line.

Table 5.7: Residual limits of the New ANN Model and Best Available Empirical Correlations and Mechanistic Models.

Model Name	**Minimum**	**Maximum**
ANN Model	-109	159.1
Hasan and Kabir[15] model	-302.46	669.76
Ansari *et al.*[18] model	-387.4	366.6
Chokshi *et al.*[19] model	-416.1	320.3
Gomez *et al.*[20] model	-620.7	271.4
Beggs and Brill[5] correlation	-476.6	382.9
Duns and Ros[3] correlation	-455.5	309.9
Hagedorn and Brown[2] correlation	-619.6	216.5
Mukherjee and Brill[7] correlation	-378	276.3
Orkiszewski[4] correlation	-480.2	117.8

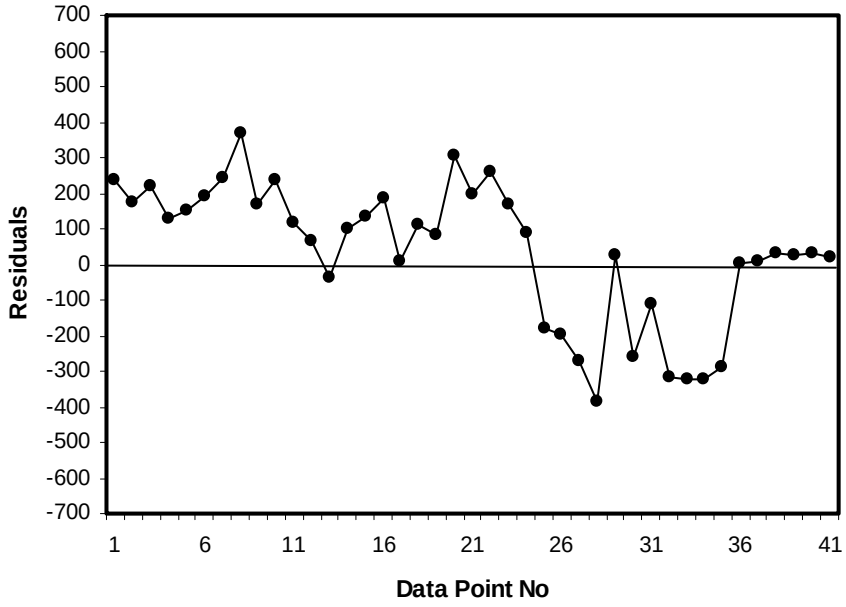

Figure 5.50: Residual Graph for Ansari *et al.* Model.

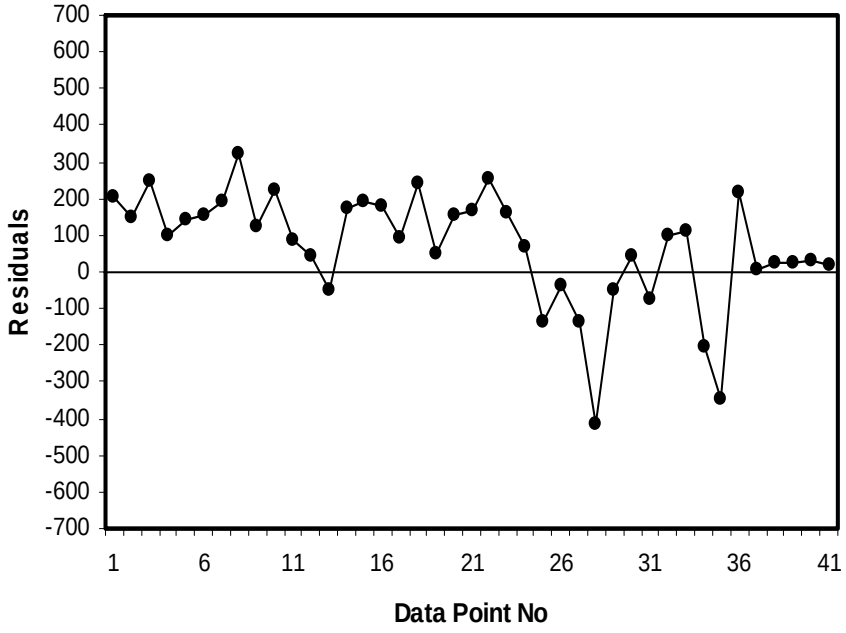

Figure 5.51: Residual Graph for Chokshi *et al.* Model.

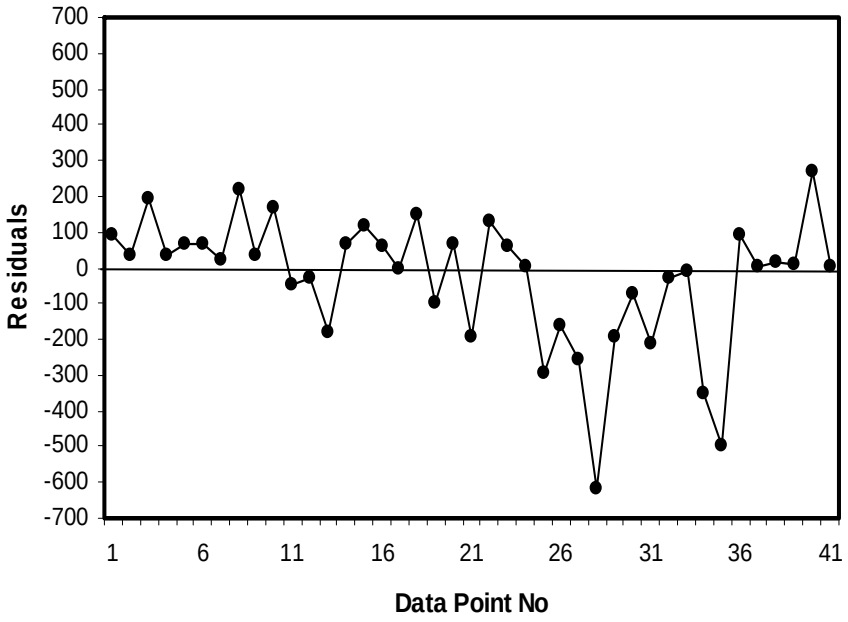

Figure 5.52: Residual Graph for Gomez *et al.* Model.

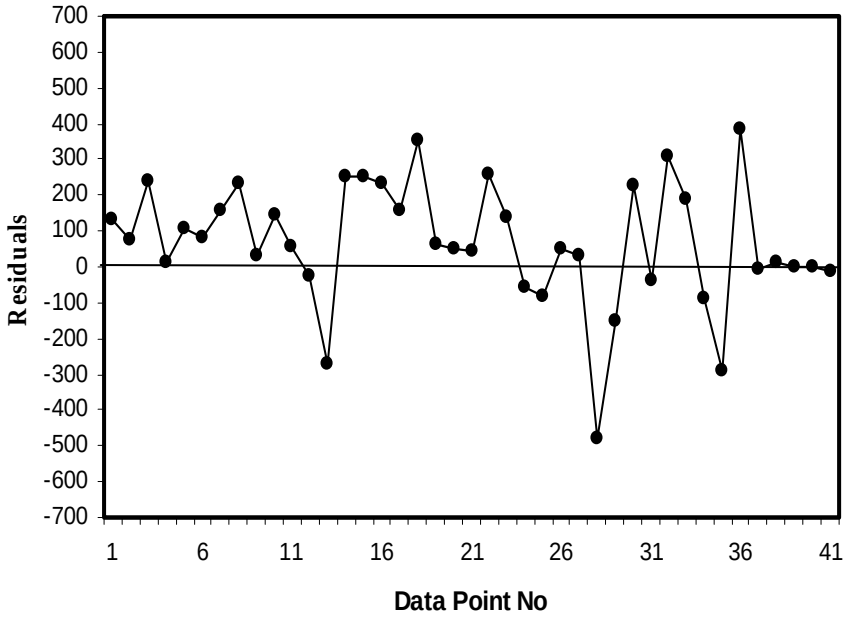

Figure 5.53: Residual Graph for Beggs and Brill Correlation.

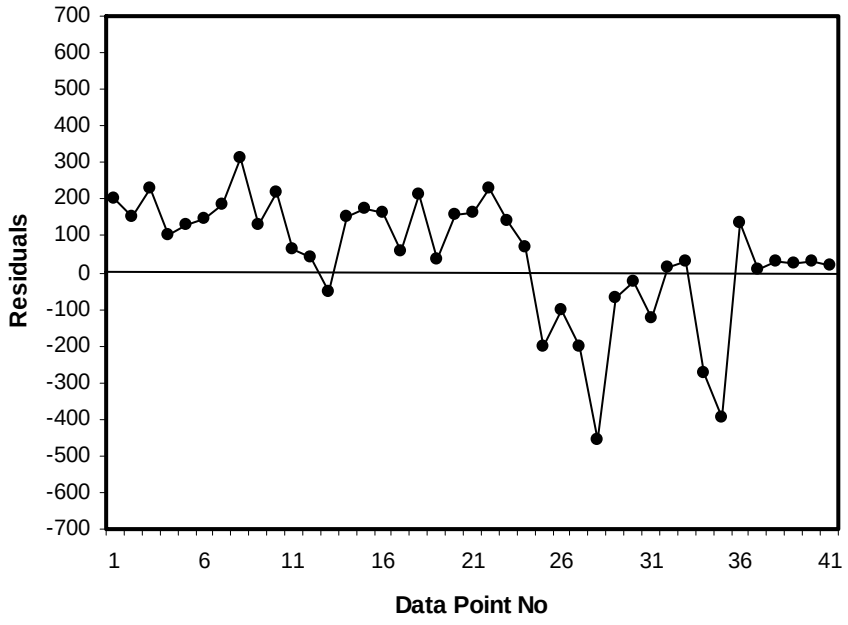

Figure 5.54: Residual Graph for Duns and Ros Correlation.

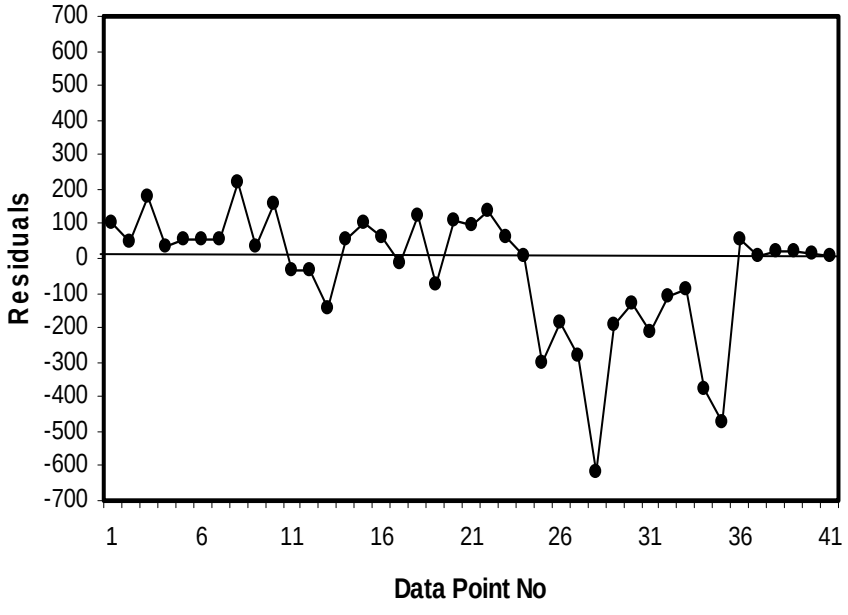

Figure 5.55: Residual Graph for Hagedorn and Brown Correlation.

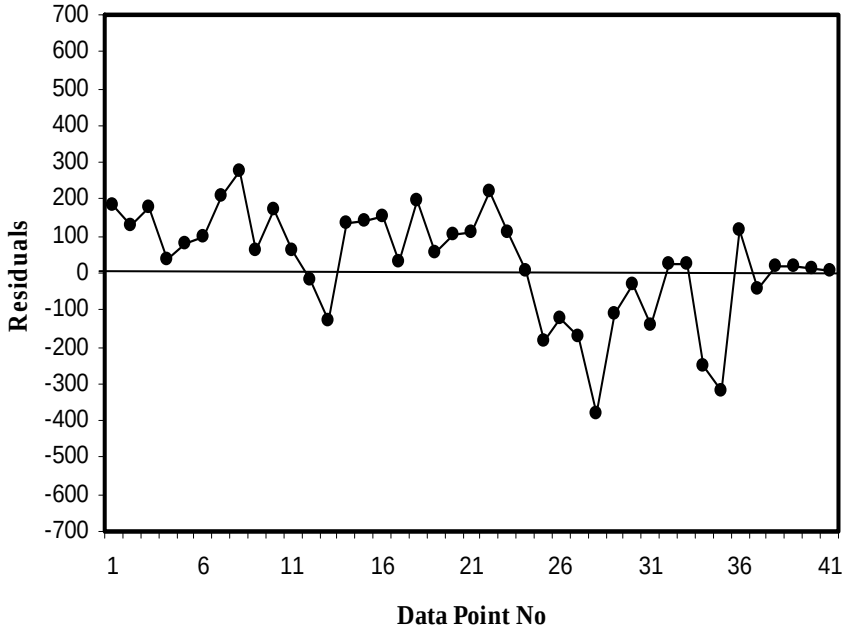

Figure 5.56: Residual Graph for Mukherjee and Brill Correlation.

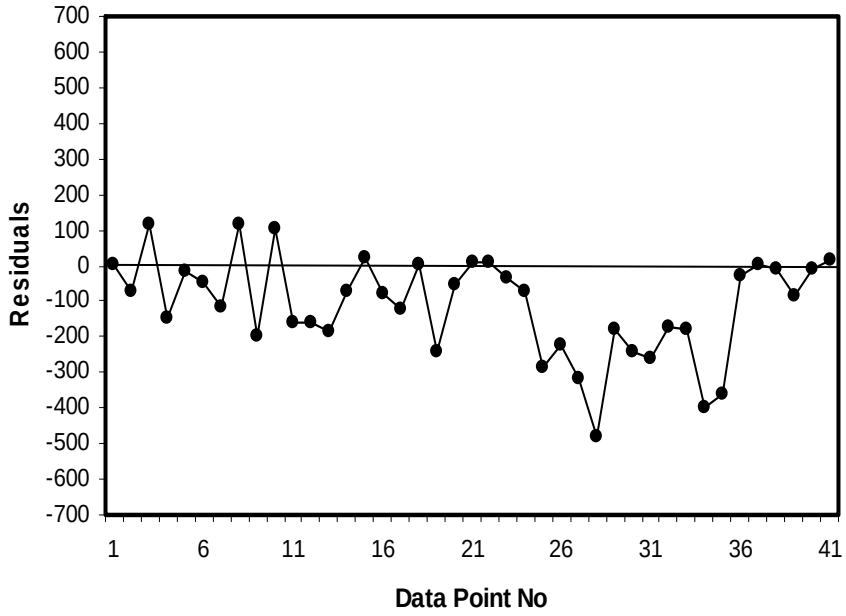

Figure 5.57: Residual Graph for Orkiszewski Correlation.

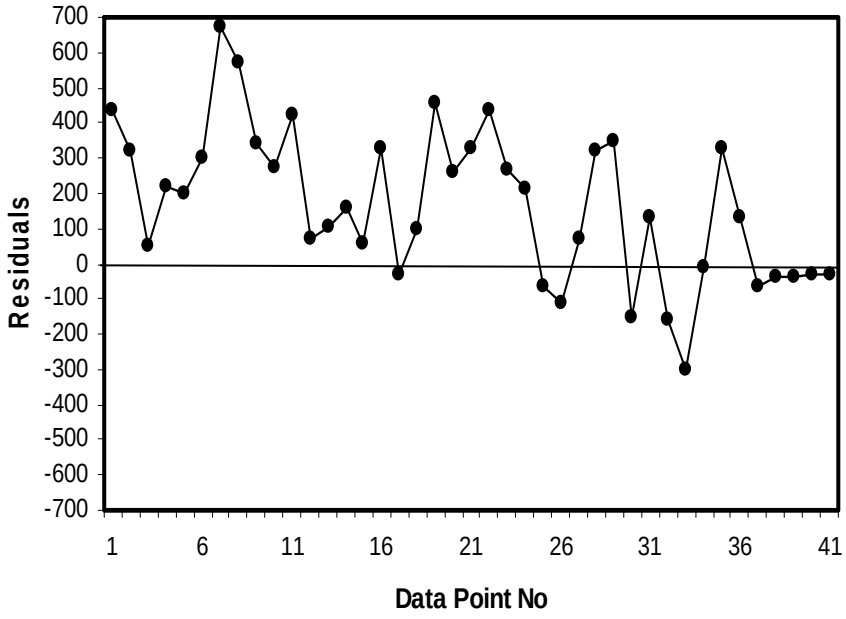

Figure 5.58: Residual Graph for Hasan and Kabir Model.

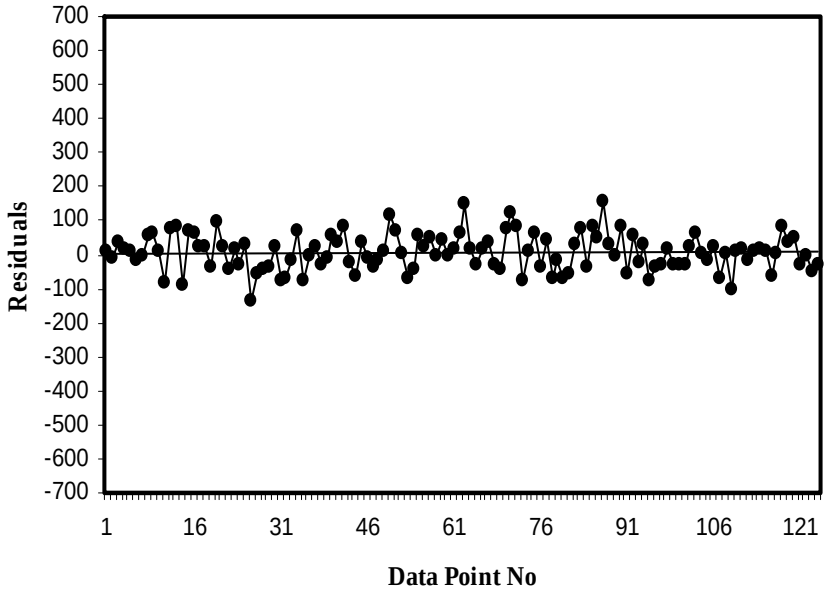

Figure 5.59: Residual Graph for Training Set (ANN Model).

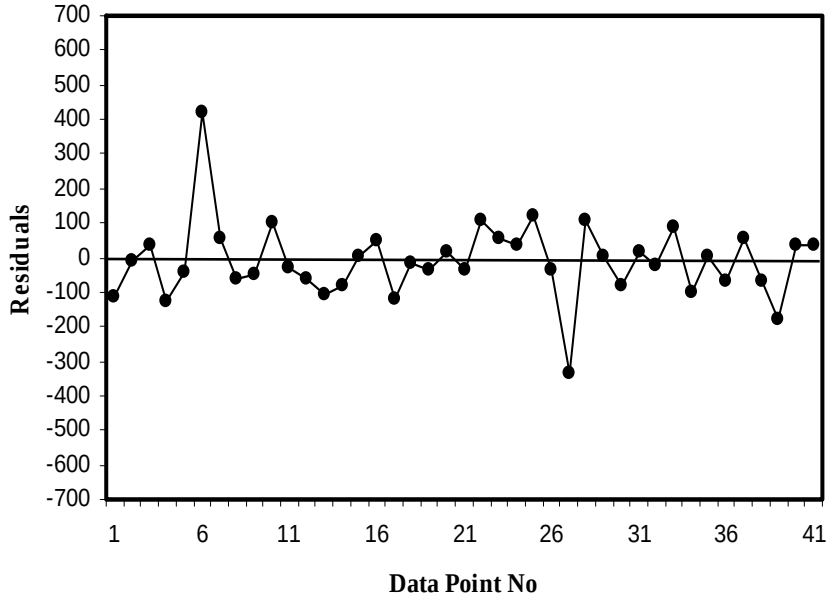

Figure 5.60: Residual Graph for Validation Set (ANN Model).

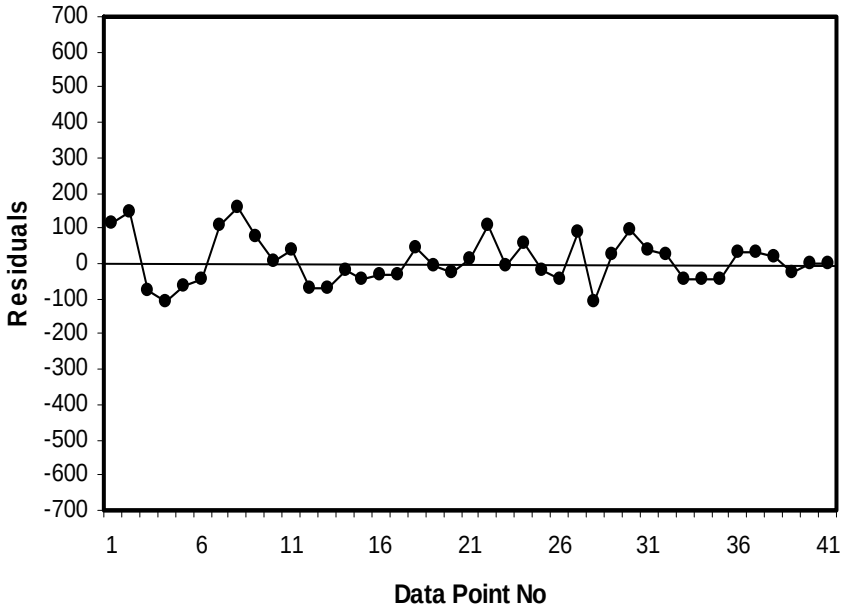

Figure 5.61: Residual Graph for Testing Set (ANN model).

CHAPTRE 6

CONCLUSIONS AND RECOMMENDATIONS

6.1 CONCLUSIONS

Based on the results and discussion presented in this study, the following conclusions can be drawn:

1. Artificial Neural Network technique; specifically back-propagation learning algorithm has been used successfully in developing a model for predicting flowing bottomhole pressure in vertical wells.
2. The developed model outperformed the best available empirical correlations and mechanistic models.
3. The developed model achieved best correlation coefficient (0.9735), the lowest maximum absolute relative error (7.1401%), the lowest root mean squared error (2.8013), the lowest standard error deviation (66.2448), and the lowest average absolute percent error (2.1654%).
4. The model consistency has been checked through using a query data after training and fixing the weights.

5. An executable program has been developed after obtaining the weights from the original program. It can be used for estimating pressure drop in vertical multiphase wells.
6. A trend analysis showed that the developed model accurately predicts the physical process.
7. The developed model could perform better if redundancy in data does not exist.
8. The new developed model results can only be used within the range of used data. Caution should be taken beyond the range of used input variables.

6.2 RECOMMENDATIONS

The following recommendations are made as a possible extension of the present work

1. The model performance can be more improved through using another data set with a wider range of variables.
2. Commingling horizontal, vertical, and inclined multiphase flow data may contribute a lot in developing a universal model.
3. The importance of all input variables can be further investigated in a future work to determine the most important parameters that are involved in estimating bottomhole pressure in vertical wells; this may result in reducing the number of input variables.

REFERENCES

1. Tackacs, G.: “Considerations on the Selection of an Optimum Vertical Multiphase Pressure Drop Prediction Model for Oil Wells,” Paper SPE 68361, Presented at the 2001 Production and Operations Symposium, Oklahoma, 24-24 March.

2. Hagedorn, A.R. and Brown, K.E.: "Experimental Study of Pressure Gradients Occurring During Continuous Two-Phase Flow in Small-Diameter Vertical Conduits," *Journal of Petroleum Technology* (April 1965) 475-84; Trans., AIME, **234**.

3. Duns, H. Jr. and Ros, N.C.J.: "Vertical Flow of Gas and Liquid Mixtures from Boreholes," Proceedings of the Sixth World Petroleum Congress, Frankfurt (19-26 June 1963) Section II, 22-PD6.

4. Orkiszwiski, J.: "Predicting Two-Phase Pressure Drops in Vertical Pipes," SPE 1546, Presented at the 41st Annual Fall Meeting, Dallas, TX, 2-5 October 1966.

5. Beggs, H.D and Brill, J.P.: "A Study of Two-Phase Flow in Inclined Pipes," *Journal of Petroleum Technology* (May 1973) 607-17; Trans., AIME **255**.

6. Aziz, K., Govier, G.W., and Fogarasi, M: "Pressure Drop in Wells Producing Oil and Gas," *Journal of Petroleum Technology* (July-September 1972) 38-48.

7. Mukhrejee, H. and Brill, J.P.: "Pressure Drop Correlations for Inclined Two-Phase Flow," *Journal of Energy Resources Technology* (December 1985) 549-554.

8. Espanol, J. H.: "Comparison of Three Methods for Calculating a Pressure Traverse in Vertical Multiphase Flow," M. S Thesis, university of Tulsa, Tulsa, Oklahoma (1968).

9. Camacho, C. A.: "Comparison of Correlations for Predicting Pressure Losses in High Gas Liquid Ratio Vertical Wells," M. S Thesis, University of Tulsa, Tulsa, Oklahoma (1970).

10. Messulam, S. A. G., "Comparison of Correlations for Predicting Multiphase Flowing Pressure Losses in Vertical Pipes," M. S Thesis, The University Of Tulsa, Tulsa, USA (1970).

11. Lawson, J. D and Brill, J. P.: "A Statistical Evaluation of Methods Used To Predict Pressure Losses for Multiphase Flow in Vertical Oil Well Tubing," *Journal of Petroleum Technology* (August 1974) 903.

12. Vohra, I. R., Marcano, N., and Brill, J.P.: "Comparison of Liquid Holdup Correlations for Gas-Liquid Flow in Horizontal Pipes," Paper SPE 4690, Presented At 48th Annual SPE Fall Meeting, Las Vegas, Nevada, (October 1973).

13. Chierici, G. L., Ciucci, G. M., and Sclocchi, G.: "Two-Phase Flow in Oil Wells – Prediction of Pressure Drop," *Journal of Petroleum Technology* (August 1974) 927-937; Trans., AIME, **257**.

14. Griffith, P., and Wallis, G. B.: "Two-Phase Slug Flow," ASME *Journal of Heat Transfer* (August, 1961) 307.

15. Kabir, C. S. and Hasan, A. R.: "A Study of Multiphase Flow Behavior in Vertical Oil Wells: Part II – Field Application," presented at the 56th California Regional Meeting of the Society of Petroleum Engineers, Held in Oakland. CA, April 2-4, 1986.

16. Aggour, M. A., Al-Yousef, H.Y., and Al-Muraikhi, A. J.: " Vertical Multiphase Flow Correlations for High Production Rates and Large Tubulars," Paper SPE 28465, Presented at the 1994 SPE Annual Technical Conference & Exhibition, New Orleans , LA, 25-28 September.

17. Rao, B.: "Multiphase Flow Models Range of Applicability," *CTES* (Coiled Tubing Engineering Services) Publication (May1998)18.

18. Ansari, A. M., Sylvester, N. D., Sarica, C., Shoham, O., and Brill, J. P.: "A Comprehensive Mechanistic Model for Upward Two-Phase Flow in Wellbores," *SPEPF Journal* (May 1994) 217-226.

19. Chokshi, R. N., Schmidt, Z., and Doty, D. R.: "Experimental Study and the Development of a Mechanistic Model for Two-Phase Flow Through Vertical Tubing," Paper SPE 35676 Presented at the Western Regional Meeting, Anchorage, Alaska, 22-24 May 996.

20. Gomez, L. E., Shoham, O., Schmidt, Z., Chokshi, R. N., Brown, A., and Northug, T.: "A Unified Mechanistic Model for Steady-State Two-Phase Flow in Wellbores and Pipelines," Paper SPE 56520 Presented at the 1999 SPE Annual Technical Conferences and Exhibition, Houston, Texas, 3-6 October.

21. Pucknell, J. K., Mason, J. N. E., and Vervest, E.G.: "An Evaluation Of Recent Mechanistic Models Of Multiphase Flow For Predicting Pressure Drops In Oil And Gas Wells," Paper SPE 26682, Presented at the 1993 Offshore European Conference, Aberdeen, 7-10 September.

22. Kaya, A. S., Sarica, C., and Brill, J. P.: "Comprehensive Mechanistic Modeling of Two-Phase Flow in Deviated Well," Paper SPE 56522, Presented at the 1999 SPE Annual Technical Conference & Exhibition, Houston, Texas, 3-6 October.

23. Tengesdal, J. ϕ., Sarica, C., Schmidt, Z., and Doty, D.: "A Mechanistic Model for Predicting Pressure Drop in Vertical Upward Two-Phase Flow," *Journal of Energy Resources Technology* (March 1999) 121/1.

24. Mohaghegh, S. and Ameri.: "Artificial Neural Network as A Valuable Tool for Petroleum Engineers," Paper SPE 29220, Prepared as an Unsolicited Paper for Society of Petroleum Engineers (1995).

25. Bilgesu, H. I., Altmis, U., Ameri, Mohaghegh, S., and Aminian, S, K.: "A new Approach to Predict Bit Life Based on Tooth or Bearing Failures," Paper SPE 51082 Presented at the 1998 SPE East Regional Conference, Pittsburgh, 9-11 November.

26. Dashevskiy, D., Dubinsky, V., and Macpherson D., "Application of Neural Networks for Predictive Control in Drilling Dynamics," Paper SPE 56442 Presented at the Annual Technical Conference and Exhibition, Houston, 3-6 October.

27. Bilgesu, H. I., Tetrick, T., Altmis, U., Ameri, S. Mohaghegh., and Ameri, S.: "A New Approach for the Prediction of Rate of Penetration (ROP) Values," Paper SPE 39231 Presented at the 1997 SPE East Regional Conference, Lexington, KY, 22-24 October.

28. Oyeneyin, M. B. and Faga, A. T., "Formation-Grain-Size Prediction Whilst Drilling: A Key Factor in Intelligent Sand Control Completion," Paper SPE 56626 Presented at the 1999 SPE Annual Technical Conference & Exhibition, Huston, Texas, 3-6 October.

29. Holditch, S.A., Xiong, Hongjie, Rueda, Jose, and Rahim, Zillur.: "Using an Expert System To Select the Optimal Fracturing Fluid and Treatment Volume," Paper SPE 26188 presented at the 1993 SPE Gas Technology Symposium, Calgary, Alberta, Canada, 28-30 June.

30. Mohaghegh, S., Arefi, R., Belgesu, L., Ameri, S, and Rose, D.: "Design and Development of Artificial Neural Network for Estimation of Formation Permeability," Paper SPE 28237, Presented at the SPE Production Computer Conference, Dallas, 31 July to 3rd August.

31. Hu, Z. and Zhao, B., "A New Method for Discrimination of Automatic Parameters in Horizontal Well Test Analysis," presented at *Natural Gas Industry* (25 March 1997)17, No. 2, 7A, 59-62.

32. Sultan, M. A., and Al-Kaabi, A. U.: "Application of Neural Network to the Determination of Well-Test Interpretation for Horizontal Wells," Paper SPE 77878 presented at the 2002 SPE Asia Pacific Oil and Gas Conference and Exhibition, Melbourne, Australia, 8-10 October.

33. Al-Kaabi, A., and Lee, W. J.: "Using Artificial Neural Nets to Identify the Well Test Interpretation Model," *SPE Formation Evaluation Journal* (September 1993) 233-240.

34. Elmo, R. O. and Jabbar Elmatalab.: "A Practical Artificial Neural Network Model for Estimating Tight Gas Sand Permeability," Paper SPE 39703 Presented at the 1998 Asia Pacific Conference, Kuala Lampur, Malaysia, 23-24 March.

35. Osman, E. A., O. A. Abdel-Wahab, and Al-Marhoun, M. A.: "Prediction of Oil PVT Properties Using Neural Networks," Paper SPE 68233, Presented at the12th MEOS (Middle East Oil and Gas Show and Conference), 17-20 March 2001.

36. Varotsis, N., Nighswander, J., Guieze, P., and Gaganis, V.: "A Novel Non-Iterative Method for the Prediction of The PVT Behavior of Reservoir Fluids," Paper SPE 56745 Presented at the 1999 SPE Annual Technical Conference & Exhibition, Houston, Texas, 3-6 October.

37. Boukadi, F., Al-Alawi, S., Al-Bemani, A., and Al-Qassabi, S.: "Establishing PVT Correlations for Omani Oils," *Petroleum Science Technology* (June-July 1999)17, No. 5-6, 637-662.

38. Garrouch, A. and Smaoui, N. H.: "An Artificial Neural Network Model for Estimating Tight Gas Sand Permeability," Paper SPE 39703 Presented at the 1998 Integrated Modeling for Asset Manage Asia Pacific Conference, Kuala Lampur, Malaysia, 23-24 March.

39. Ali, J. K.: "Neural Networks: A New Tool for the Petroleum Industry?," Paper SPE 27561, presented at the 1994 European Petroleum Computer Conference, Aberdeen, K. U., 15-17 March.

40. Arirachakaran, S., Jefferson, L. L., Brill, J. P., and Shoham, O.: “Intelligent Utilization of a Unified Flow Pattern Prediction Model in Production System Optimization,” Paper SPE 22869 Presented at 66th Annual Technical Conference and Exhibition of the Society of Petroleum Engineers, Dallas, Texas, 6-9 October 1991.

41. Ternyik, J., Bilgesu, H.1., and Mohaghegh, S.: “Virtual Measurements in Pipes: Part 2-liquid Holdup and Flow Pattern Correlations," Paper SPE 30976 Presented at the 1995 SPE Eastern Regional Conference and Exhibition, Morgantown, WV-USA, 17-21 September.

42. Mukherjee, H.: "An Experimental Study of Inclined Two-Phase Flow," PhD Dissertation, University of Tulsa, Oklahoma, (1979).

43. Osman, S. A.: "Artificial Neural Networks Models for Identifying Flow Regimes and Predicting Liquid Holdup in Horizontal Multiphase Flow," Paper SPE 68219, Presented at the 2001 SPE Middle East Oil and Gas Show and Conference, Bahrain, 17-20 March.

44. Osman, S. A. and Aggour, M. A.: "Artificial Neural Network Model for Accurate Prediction of Pressure Drop in Horizontal-Multiphase Flow," *Petroleum Science and Technology* (2002) 20 No.1 and 2, 1-15.

45. Shippen, M. E. and Scott, L. S.: "A Neural Network Model for Prediction of Liquid Holdup in Two-Phase Horizontal Flow," Paper SPE 77499, Presented at the 2002 SPE Annual Technical Conference and Exhibition, San Antonio, Texas, 29 September – 2nd October.

46. Sage, A. P, Ed.: "Concise Encyclopedia of Information Processing in Systems and Organizations," New York, Pergamon, (1990).

47. Memmi, D.: "Connectionism and Artificial Intelligence," *Neuro-Nimes, International Workshop on Neural Network and Their Application*, Nimes, France, (1989) 17-34.

48. McCulloch, W. S. and Pitts, W.: "A Logical Calculus of the Ideas Immanent in Nervous Activity," *Bulletin of Mathematical Biophysics* 5, 115-133, (1943).

49. Hebb, D. O.: "The Organization of Behavior: A Neuropsychological Theory," New York, Wiley, (1949).

50. Ashby, W. R: "Design for A Brain," New York, Wiley, (1952).

51. Gabor, D.: "Communication Theory and Cybernetics," *IRE* Transaction on Circuit Theory CT-1, 19-31, (1954).

52. Rosenblatt, F.: "The Preceptron: A Probabilistic Model for Information Storage and Organization in the Brain," *Psychological Review* 65, 386-408, (1958).

53. Minsky, M. L. and Papert, S. A.: "Preceptrons," Cambridge, MA. MT Press, (1969).

54. Rumelhart, D. E., Hinton, G. E., and Williams, R. J.: "Learning Representations by Back-Propagation Errors," *Nature*, London, 323 (1986) 533-536.

55. Haykin, S.: "Neural Network: A Comprehensive Foundation," Macmillan Publishing Company, NJ, Lehigh Press, (1994).

56. Aleksander. I. and Morton, H.: "An Introduction to Neural Computing," London, Chapman & Hall, (1990).

57. Shepherd, G. M. and Koch, C.: "Introduction to Synaptic Circuits," in the Synaptic Organization of the Brain. New York, Oxford University Press, (1990) 3-31.

58. James, A. Freeman and David, M. Skapura.: "Neural Networks: Algorithms, Applications, and Programming Techniques," Addison-Wesley Publishing Company, (1991).

59. Elman, J.L.: "Finding Structure in Time," *Cognitive Science*, (1990) 14,179-211.

60. Kramer, A. H. and Sangiovanni, V. A.: "Efficient Parallel Learning Algorithms for Neural Networks," in Advances in Neural Information Processing Systems 1 (D. S. Touretzky, Edition), San Mateo, CA, Morgan Kaufmann. (1989) 40-78.

61. Rai, R., Singh, I., and Srini-Vasan, S.: "Comparison of Multiphase Flow Correlations with Measured Field Data of Vertical and Deviated Oil Wells in India," *SPE PE* (August 1989) 341-8.

62. Simon Haykin.: "Neural Network: A Comprehensive Foundation," Upper Saddle River, NJ, Prentice Hall (1999).

63. "MATLAB," Mathwork, Neural Network Toolbox Tutorial, (http://www.mathtools.net/MATLAB/Neural_Networks/index.html).

64. Minsky, M. L. and Papert, S. A.: "Preceptrons," Expanded Edition. Cambridge, MA. MT Press, (1988).

65. Gori, M. and Tesi, A.: "On the Problem of Local Minima in Back-Propagation," *IEEE* Transactions on Pattern Analysis and Machine Intelligence (1992)**14**, 76-86.

66. Taitel, Y. and Duckler, A. E.: "A Model for Predicting Flow Regime Transitions in Horizontal and Near Horizontal Gas-Liquid Flow," *AIChE Journal* (1976) 22, No. 1, 47-55.

67. Barnea, D.: "A Unified Model for Predicting Flow Pattern Transitions for the Whole Range of Pipe Inclinations," *International Journal of Multiphase Flow* (1987)13, No. 1,1-12.

68. Taitel, Y. and Barnea, D.: "Two-Phase Slug Flow," Academic Press Inc. (1990).

69. Scott, S. L., Shoham, O., and Brill, J. P.: "Prediction of Slug Length in Horizontal Large-Diameter Pipes," *SPE Production Engineering* (August 1989) 335-340.

70. Alves, I., N., Caetano, E. F., Minami, K., and Shoham, O.: "Modeling Annular Flow Behavior for Gas Wells," *SPE Production Engineering* (November 1991) 435-440.

APPENDIX A

EMPIRICAL CORRELATIONS AND

MECHANISTIC MODELS

APPENDIX A

EMPIRICAL CORRELATIONS AND MECHANISTIC MODELS

This appendix is divided into two sections. A detailed review of the most commonly used vertical multiphase flow empirical correlations is presented in section A.1 whereas a detailed discussion of the three evaluated mechanistic models is presented in section A.2.

A.1 *Vertical Multiphase Flow Empirical Correlations*

Some of the most used vertical multiphase empirical correlations will be discussed thoroughly in the next section. Those are; modified Hagedorn & Brown[2], Duns & Ros[3], Orkiszweski[4], Beggs & Brill[5], Aziz & Govier[6], and Mukhrejee & Brill[7]

A.1.1 Generalized Correlation of Hagedorn and Brown (1965):

Hagedorn and Brown[2] correlation is a semi empirical method based on the original work of Hagedorn and Brown in 1964 with the addition of a correlation for liquid hold up. It incorporated general energy equation and 1500 ft test well data. General energy equation defined summation of three terms to be equal to the total pressure gradient in pipes, which includes hydrostatic gradient, friction gradient, and acceleration gradient. These terms can be stated in Equation (1) below.

$$\left(\frac{dP}{dh}\right)_{total} = \left(\frac{dP}{dh}\right)_{elevation} + \left(\frac{dP}{dh}\right)_{friction} + \left(\frac{dP}{dh}\right)_{acceleration}$$

The previous equation can be written in a detailed form as;

$$144\left(\frac{\Delta P}{\Delta h}\right) = \rho_{avm} + \frac{fw^2}{2.9652\times10^{11} d^5 \rho_m} + \rho_{avm}\frac{\Delta\left(\frac{V_m^2}{2g_c}\right)}{\Delta h}$$

Where;

$$\rho_{avm} = \rho_{avL} H_L + \rho_{avG}\left(1 - H_L\right)$$

Where;

ΔP = pressure drop in psi, through a vertical distance Δh in ft

d =tubing diameter, ft

f = friction factor

w = mass flow rate, lbm/D

V_m = velocity of mixture, ft/sec

ρ_{avm} = average mixture density, lbm/ft^3

ρ_{avL} = average liquid density, lbm/ft^3

ρ_{avG} = average gas density, lbm/ft^3

H_L = hold up

The pressure drop calculation depends on the determination of hold up first (part of pipe that occupied by the denser fluid). The author collected wide range of data in order to provide generality for his correlation. The correlation was developed using pipes with 1 to 2.5 in., 5 different fluids, namely: water and four types of oil with viscosities ranging between 10 and 110 cp at 80°F. The two phase viscosity was presented by the Arrhenius viscosity correlation. Thus, the Reynolds number for two phase flow can be stated as;

$$\left(N_{\mathrm{Re}}\right)_{T.P} = 2.2\times10^{-2}\frac{w}{d\mu_L^{H_L}\mu_g^{1-H_L}}$$

Where;

$(N_{\mathrm{Re}})_{T.P}$ = Reynolds number for two phase flow

μ_L = liquid viscosity, Cp, and

μ_g = gas viscosity, Cp

The developed correlation does not recognize flow regimes. However, assuming one flow pattern for the whole pipe weakened the correlation where different flow patterns are observed along the length of the pipe and the pressure losses vary accordingly. In other words, the correlation ignored the variation of flow patterns, which significantly affect the pressure loss calculations. The calculation of the liquid holdup depends on four dimensionless numbers which are the liquid velocity number, the gas velocity number, the pipe diameter number and the liquid viscosity number listed below:

$$N_{LV} = V_{sL}\left(\frac{\rho_L}{g\sigma}\right)^{1/4}$$

$$N_{gV} = V_{sg}\left(\frac{\rho_L}{g\sigma}\right)^{1/4}$$

$$N_D = d\left(\frac{\rho_L g}{\sigma}\right)^{1/2}$$

$$N_L = \mu_L\left(\frac{g}{\rho_L \sigma^3}\right)^{1/4}$$

Where;

N_{LV} = liquid-velocity number

N_{gV} = gas-velocity number

N_D = pipe-diameter number

N_L = liquid-viscosity number

V_{sL} = superficial liquid velocity, ft/sec

V_{sg} = superficial gas velocity, ft/sec

ρ_L = liquid density, lb_m/ft^3

σ = surface tension, lb_m/sec^2

The hold up is actually treated as a pseudo holdup that could be calculated by taking into consideration the total pressure drop and friction factor that are calculated a step before. Some modifications have been made to account for these shortcomings by different investigators later on. Hagedorn and Brill made other adjustment including calculation of mixture density using hold up correlation and comparing it with the mixture density for no-slippage. The largest of these two values is then used.

A.1.2 Duns and Ros Correlation (1963):

The *Duns & Ros*[3] *correlation* was developed using data from a large-scale, carefully controlled laboratory facilities. The correlation was suitably modified using field data for vertical flow of gas and liquid mixtures in wells. This correlation is valid for a wide range of oil and gas mixtures and flow regimes. Based on the inlet superficial gas and liquid velocities, the authors developed a chart to identify the various flow regimes. The different flow regimes like single phase, bubble, plug, froth, slug, transition and mist flow are grouped into three broad flow regions; these are; bubble flow, slug flow, and mist flow. The different nature of these three main regions necessitates separate correlations for friction and liquid holdup for each region. These flow patterns could be defined using dimensionless groups described in the previous

section. Slippage effect and friction factor have been incorporated in the total pressure gradient calculation for each flow pattern.

The following equations were used for each flow region:

Bubble Flow Region

Slip factor, $s = F_1 + F_2 N_{LV} + F_3^{/}\left(\frac{N_{gV}}{1 - N_{LV}}\right)^2$

$$F_3^{/} = F_3 - \frac{F_4}{N_d}$$

Slip velocity, $V_s = \frac{s}{1.938\left(\frac{\rho_L}{\sigma_L}\right)^{0.5}}$

Where; $F_1, F_2, F_3, F_4, F_5, F_6, F_7$ are dimensionless groups

$$H_L = \frac{V_s - V_{sg} - V_{sL} + \left[\left(V_s - V_{sg} - V_{sL}\right)^2 + \left(4V_s V_{sL}\right)\right]^{0.5}}{2V_s}$$

Duns and Ros suggested the following limit for bubble flow region:

$$0 \le N_{gV} \le \left(L_1 + L_2 N_{LV}\right)$$

Slug Flow Region

Slip factor, $s = \left(1 + F_5\right)\frac{\left(N_{gV}\right)^{0.982} + F_6^{\backslash}}{\left(1 + F_7 N_{LV}\right)^2}$

where

$F_6^{\backslash} = 0.029 N_d + F_6$

These dimensionless groups can be obtained from Figures A1 & A2

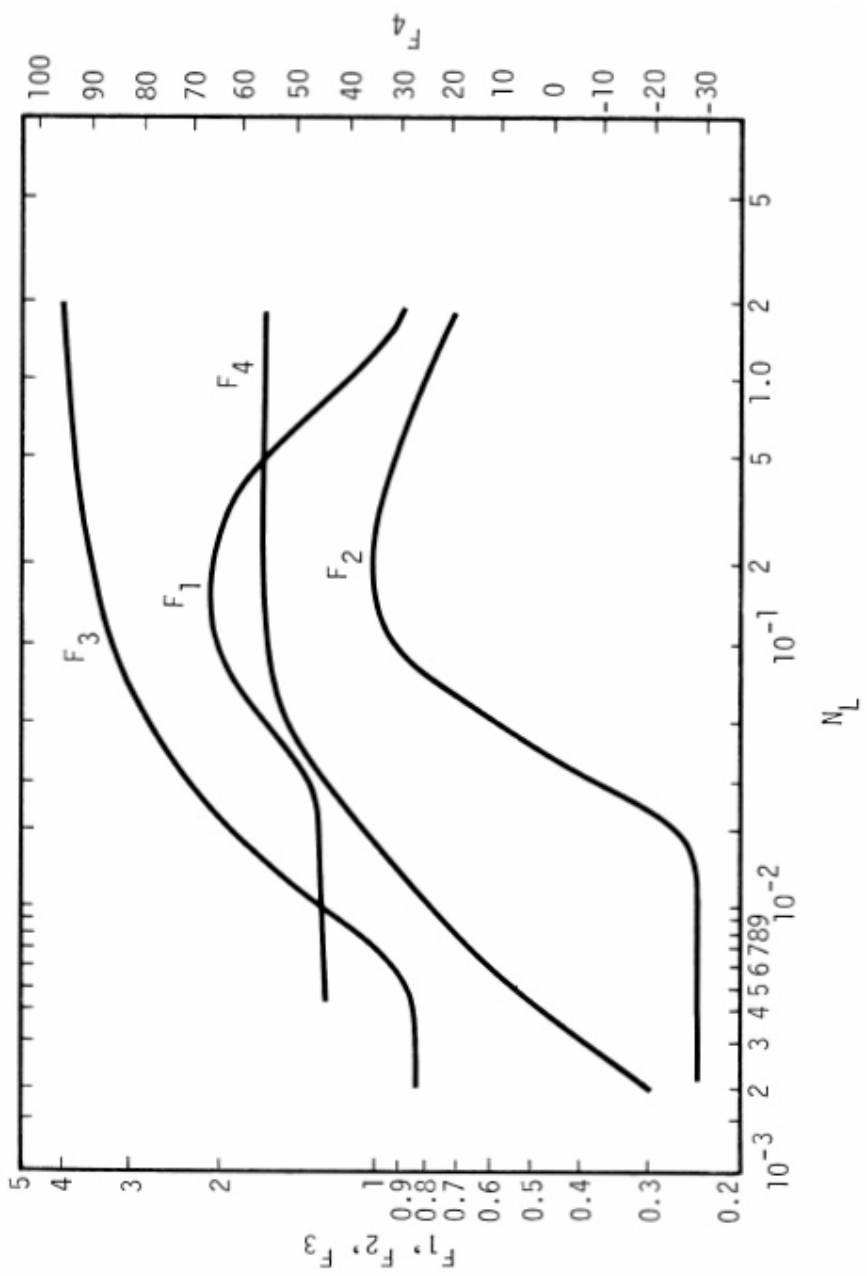

Figure A1: F_1, F_2, F_3, and F_4 against Viscosity number N_L

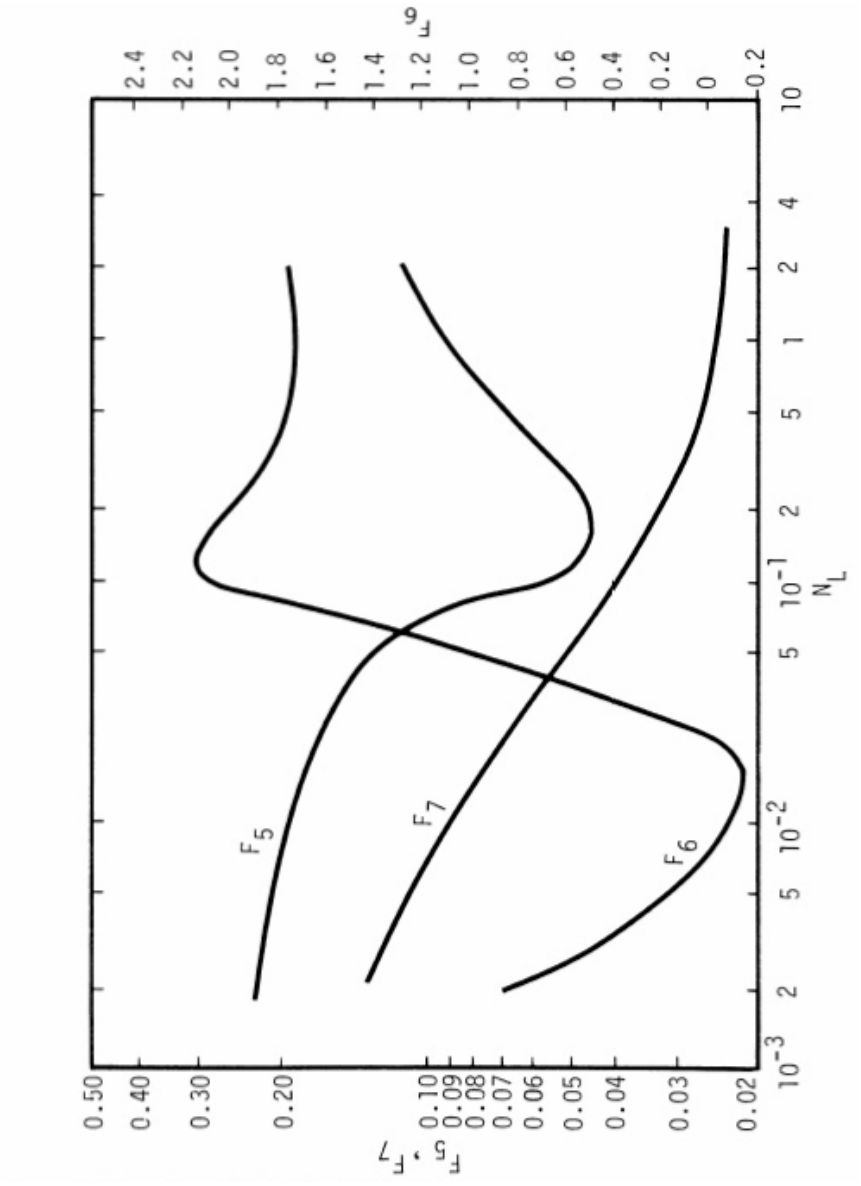

Figure A2: F_5, F_6, and F_7 against Viscosity number N_L

The slip velocity and the holdup are similarly calculated using the bubble flow regions corresponding equations.

Duns and Ros suggested the following limit for slug flow region:

$$L_1 + L_2 N_{LV} < N_{gV} < (50 + 36 N_{LV})$$

Mist Flow Region:

Slip factor, *s = zero*

$$H_L = \frac{1}{\left(1 + \frac{V_{sg}}{V_{sL}}\right)}$$

The static gradient due to mixture flowing density is given by:

$$G_{st} = H_L + (1 - H_L)\frac{\rho_g}{\rho_L}$$

Duns and Ros suggested the following limit for slug flow region:

$$N_{gV} > (75 + 84 N_{LV}^{0.75})$$

L_1, L_2 are function of $\mathrm{N_d}$, and can be obtained from Figure A3

Each flow regime has its own friction factor correlation. For the bubble and slug regimes, the friction gradient is calculated using the following equations:

$$\left(\frac{dP}{dz}\right)_f = \frac{4 f_w \rho_L V_{sL}^2}{2d}\left(1 + \frac{V_{sg}}{V_{sL}}\right)$$

f_w was formulated from the experimental data as follows:

$$f_w = \frac{f_1 f_2}{f_3}$$

f_1, f_2 can be obtained from Figures A4 & A5

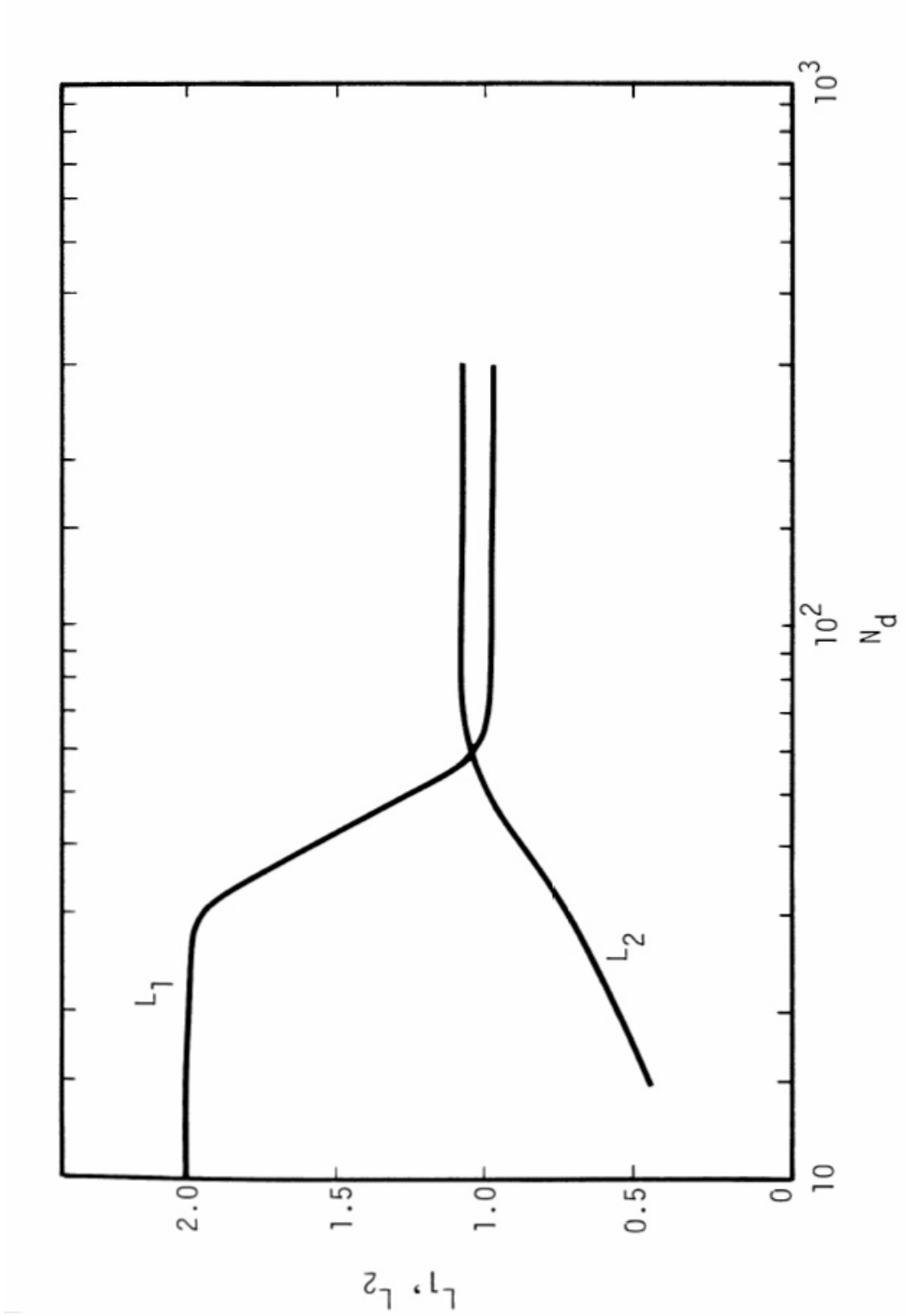

Figure A3: L-Factors against Diameter Number N_d

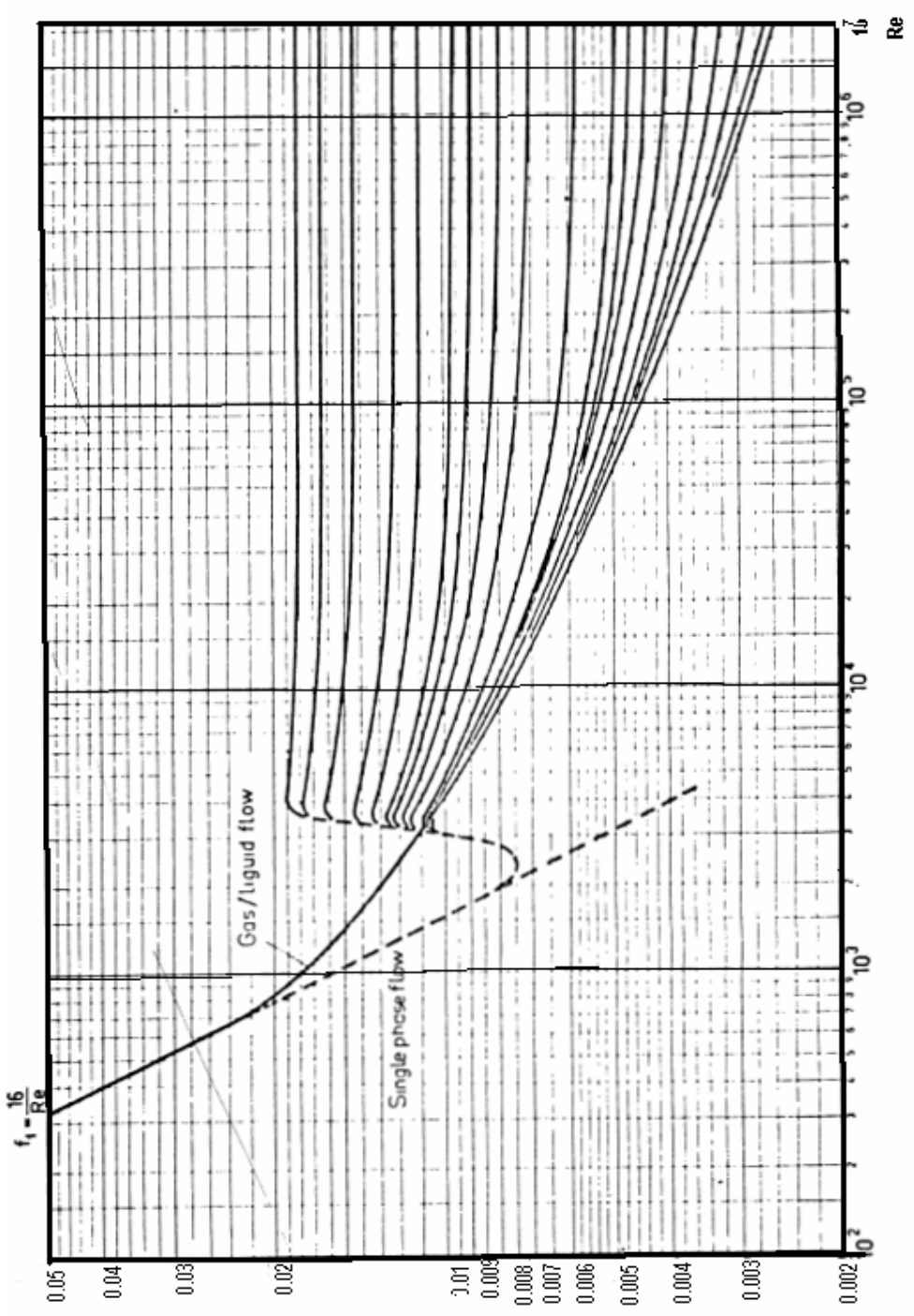

Figure A4: Ros Friction Factor Curves

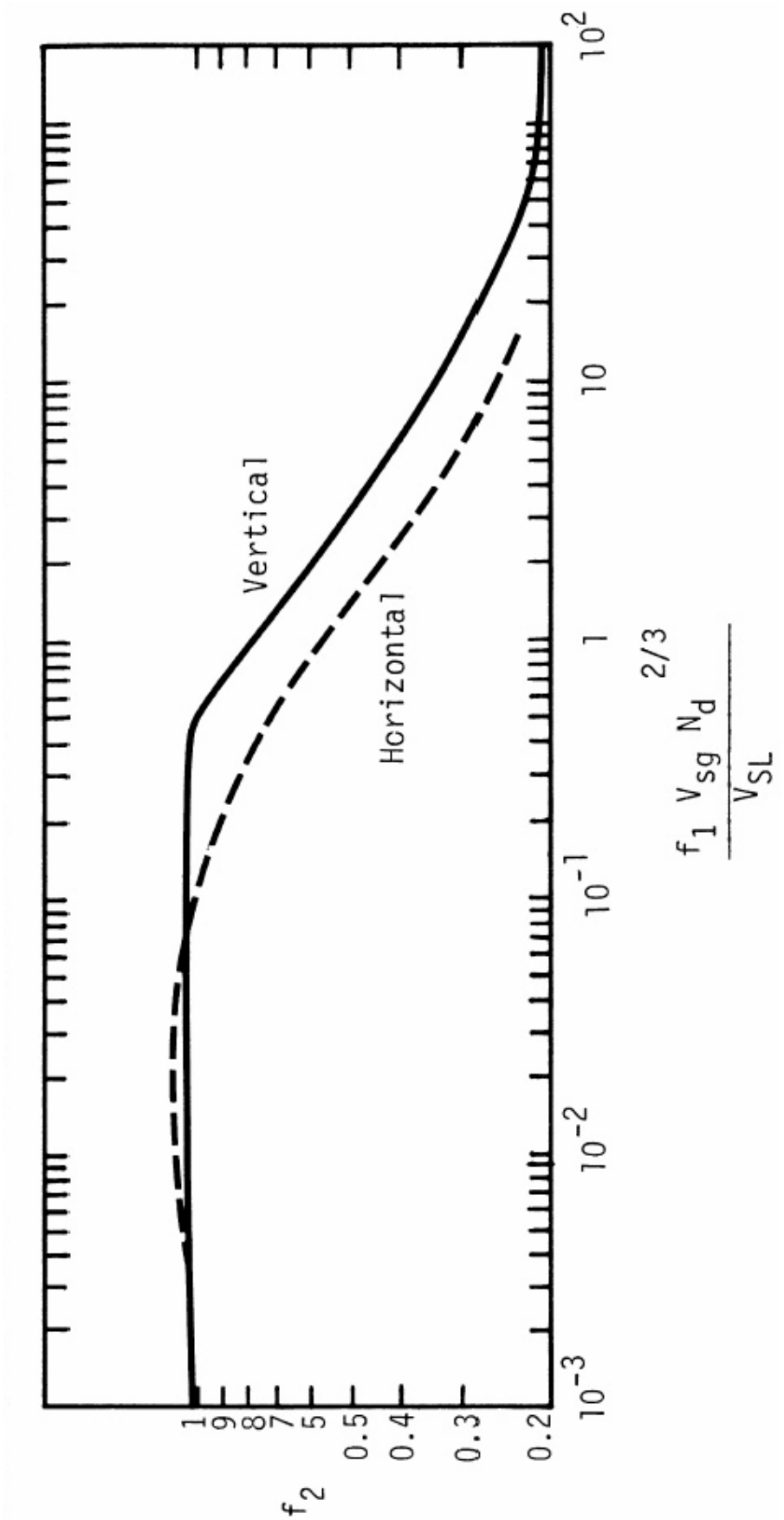

Figure A5: Bubble Friction Factor

f_3 is an additional correction to the liquid viscosity and the in situ gas liquid ratio equals to:

$$f_3 = 1 + 0.02 f_1 \left(\frac{V_{sg}}{V_{sL}} \right)$$

The Reynolds number is expressed as follows:

$$(R_e)_L = \rho_L \frac{V_{sL}}{\mu_L} d$$

In the mist flow, the friction gradient is calculated as:

$$\left(\frac{dP}{dz} \right)_f = \frac{4 f_w V_{sg}^2 \rho_g}{2d}$$

Where f_w is taken to be equal to f_1, which is obtained from Figure A4

The Reynolds number is calculated using the gas velocity and density as follows:

$$(R_e)_g = \rho_g \frac{V_{sg}}{\mu_g} d$$

The pressure gradient due to friction equals to:

$$G_f = \frac{144 \times \left(\frac{dP}{dz} \right)_f}{\rho_L}$$

The pressure gradient due to acceleration is obtained by the formula:

$$G_{acc} = \frac{\rho_L V_{sL} + \rho_g V_{sg}}{\rho_L} P$$

The total pressure gradient is then the sum of the three terms

$$G_{TOT} = G_{st} + G_f + G_{acc}$$

Although the correlation is intended for use with “dry” oil/gas mixtures, it can also be applicable to wet mixtures with a suitable correction (hold up factor). The

method depends on assigning the flow region in order to better apply and obtain high accuracy of flow profiles (pressure traverse). For water contents less than 10%, the Duns-Ros correlation (with a correction factor) has been reported to work well in the bubble, plug, and froth regions.

Pressure gradient was found to be independent of the gas flow rates at low liquid flow rates but it varies considerably at higher liquid flow rates. Three types of correction factors were proposed by Duns and Ros, which accounted for Reynolds number, high gas-liquid ratios, and liquid viscosity. The pressure drop is over predicted at gas-liquid ratios greater than 5000 scf/bbl.

A.1.3 Orkiszweski Correlation (1966):

In a detailed study of two-phase correlations, Orkiszweski[4] compared the pressure behavior predicted from various correlations using actual field data. He concluded that no correlation worked sufficiently well for all flow regimes. He did, however, identify several correlations that work well for specific flow regimes. He developed a correlation which is basically an extension of Griffith & Wallis work. By using variations of existing methods, he presented with an equation for pressure gradient calculation that covered all four flow regimes (bubble, slug, annular-slug and mist). His method is versatile and was validated using 148 measured pressure drops in actual wells.

Because slug flow is present in 95% of the studied cases, the author recommended Griffith and Wallis for this flow pattern. It should be noted that the liquid distribution coefficient (hold-up) is evaluated using the data from the Hagedorn & Brown model. Duns and Ros correlation was used for transition and annular mist flow, whenever it exists.

The pressure drop was expressed by Orkiszweski as:

$$\frac{\Delta P}{\Delta Z} = \frac{1}{144}\left[\frac{\rho + \tau_f}{1 - \frac{W_t q_g}{4637 A_p^2 p}}\right]$$

The flow regime limits are:

For bubble flow regime, $\frac{q_g}{q_t} < (L_b)$

For slug flow regime, $\frac{q_g}{q_t} > (L_b), V_{gd} < (L_s)$

For transition flow regime, $(L_m) > V_{gd} > (L_s)$

For mist flow regime, $V_{gd} > (L_m)$

Where;

$$V_{gd} = q_g \frac{\left(\rho_L / g\sigma_L\right)^{1/4}}{A_p}$$

$$L_b = 1.071 - \frac{\left(0.2218 V_m^2\right)}{\mathrm{d}} \text{ for } (L_b) > 0.13$$

$$L_{slug} = 50 + 36 V_{gd} \frac{q_L}{q_g}$$

$$L_{mist} = 75 + 84\left(V_{gd} \frac{q_L}{q_g}\right)^{0.75}$$

Where:

L_b, L_s and L_m = bubble-slug, slug-transition, transition-mist boundaries, respectively, dimensionless

ρ_{slug} = fluid density in the slug regime, lb_m/ft^3

ρ_{mist} = fluid density in the mist regime, lb_m/ft^3

ρ = fluid density, lb/ft^3

V_{gd} = dimensionless gas velocity

τ_f = friction loss gradient, psi/ft

W_t = total mass flow rate, lb/sec

q_L , q_g and q_t = volumetric flow rate of liquid, gas and total flow rate, respectively, ft^3/sec

A_p = pipe cross-sectional area ft^2

d = inside pipe diameter, ft

p = average pressure, psi

σ_L =liquid interfacial tension, lb_m/sec^2

g = gravitational acceleration, ft/sec^2

ρ_L = liquid density, lb_m/ft^3

V_m = mixture velocity, ft/sec

For slug flow, the average density is calculated as follows;

$$\rho = \frac{W_t + \rho_L V_{sb} A_p}{q_t + V_{sb} A_p} + \delta \rho_L$$

Where V_{sb} is the bubble rise velocity, ft/sec, and δ is the liquid distribution coefficient which may be determined by the equation which meets the following equation:

For water cut 75% or more and V_m<10:

$$\delta = \left(\frac{0.013 \log \mu_L}{d^{1.38}} \right) - 0.681 + 0.232 \log V_m - 0.428 \log \mathrm{d}$$

For water cut 75% or more and V_m>10:

$$\delta = \left(\frac{0.045 \log \mu_L}{d^{0.799}} \right) - 0.709 + 0.162 \log V_m - 0.888 \log \mathrm{d}$$

For water cut less than 75% or more and V_m<10:

$$\delta = 0.0127\log\left(\frac{\mu_L + 1}{d^{1.415}}\right) - 0.284 + 0.167\log V_m + 0.113\log \mathrm{d}$$

For water cut less than 75% or more and V_m>10:

$$\delta = 0.0274\log\left(\frac{\mu_L + 1}{d^{1.371}}\right) + 0.161 + 0.569\log \mathrm{d}$$
$$-\log V_m\left(\frac{0.01\log(\mu_L + 1)}{d^{1.571}}\right) + 0.397 + 0.63\log \mathrm{d}$$

$$V_{sb} = C_1 C_2 (gd)^{1/2}$$

C_1 is obtained from Figure A6 as a function of bubble Reynolds Number, which is given as:

$$R_e = \frac{1488 V_{sb} d\rho_L}{\mu_L}$$

C_2 is obtained from Figure A7 as a function of both N_b and liquid Reynolds Number:

$$R_e = \frac{1488 V_m d\rho_L}{\mu_L}$$

When C_2 cannot be read from Figure A8, the extrapolated values of V_s may be calculated by the following equations:

For $N_b \le 3000$

$$V_{sb} = 0.546 + 8.74\times10^{-6} R_e (gd)^{0.5} \quad 3000 < N_b < 8000$$

$$V_{si} = \left(0.251 + 8.74\times10^{-6} R_e\right)(gd)^{0.5}$$

$$V_{sb} = 0.5\left[V_{si} + \left(V_{si}^2 + \frac{13.59\mu_L}{\rho_L (d)^{0.5}}\right)^{0.5}\right] \quad \text{For } N_b \ge 8000$$

$$V_{sb} = \left(0.35 + 8.74\times10^{-6} R_e\right)(gd)^{0.5}$$

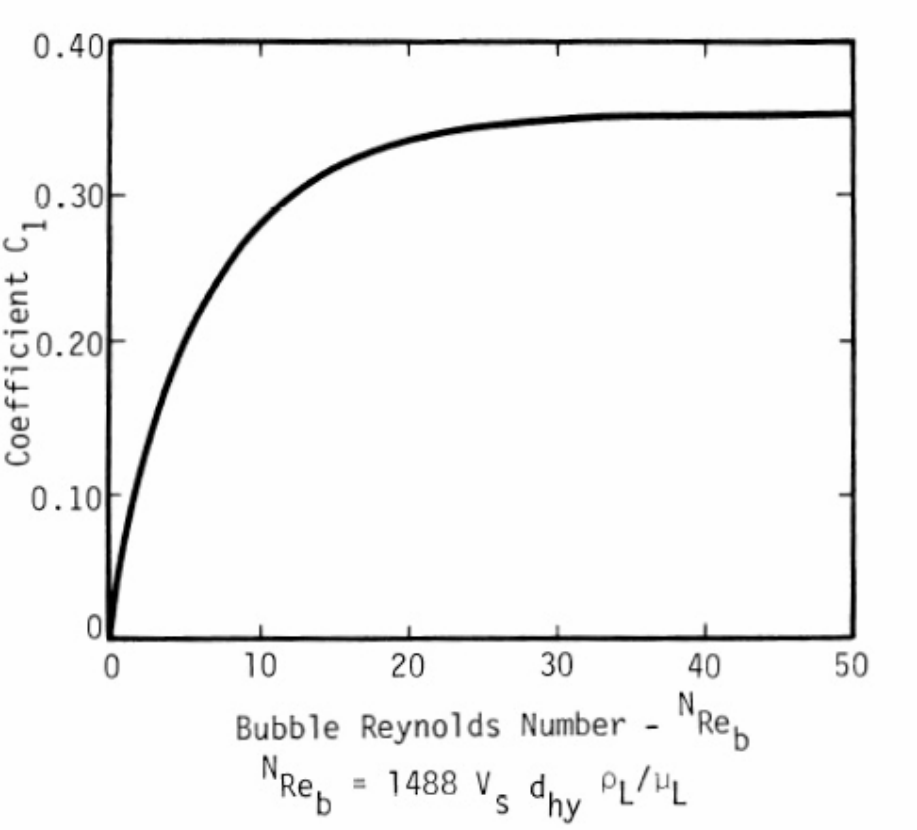

Figure A6: Griffith and Wallis' C_1 vs. Bubble Reynolds Number

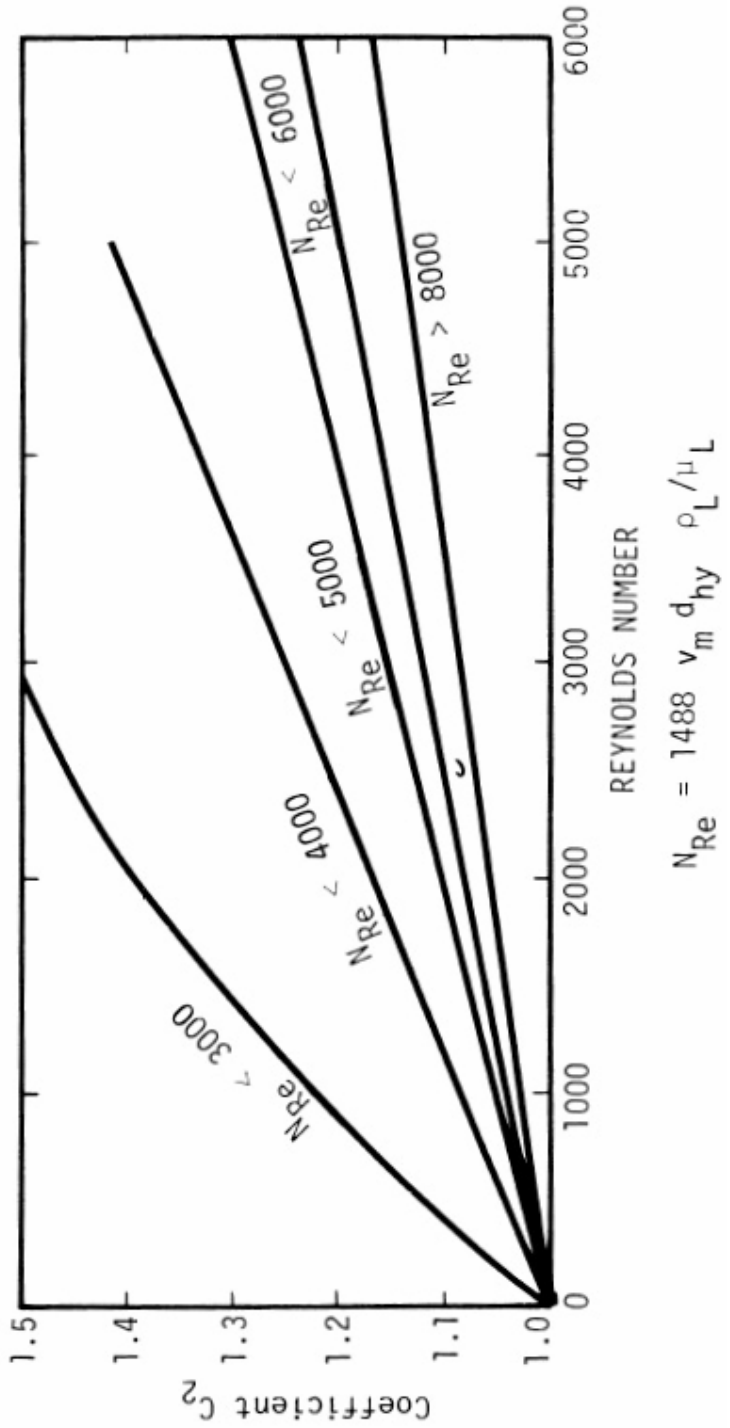

Figure A7: Griffith and Wallis' C_2 vs. Bubble Reynolds Number

The wall friction loss term is expressed as:

$$\tau_f = \frac{f\rho_L V_m^2}{2g_c d}\left[\frac{q_L + V_{sb}A_p}{q_t + V_{sb}A_p} + \delta\right]$$

The friction factor f is obtained from Moody Chart Figure A8

The Reynolds Number equation is as follows

$$R_e = \frac{1488\, V_m d\rho_L}{\mu_L}$$

For mist flow regime, the wall friction loss term is expressed as:

$$\tau_f = \frac{f\rho_g V_g^2}{2g_c d}$$

In the bubble flow:

$$\tau_f = \frac{f\rho_L V_L^2}{2g_c d}$$

Where g_c is the dimensionless conversion factor = 32.2 lb_m/ft^3

Griffith & Wallis[14] and Duns and Ros[4] correlations were found to be more accurate than other tested methods. A combination of both methods was tested against the 148 data set. Griffith & Wallis[14] was shown more reliable in the lower flow rate range of slug flow. However, Duns and Ros correlation gave the same result and failed in higher viscosity oils in the low flow-rate range. Orkiszewski extended Griffith & Wallis work to higher velocity ranges.

A.1.4 Aziz -Govier and Fogarasi Correlation (1972)

In this work, the authors conducted an extensive review of the best available flow regimes formulae. Four flow patterns were recognized; those are bubble, slug,

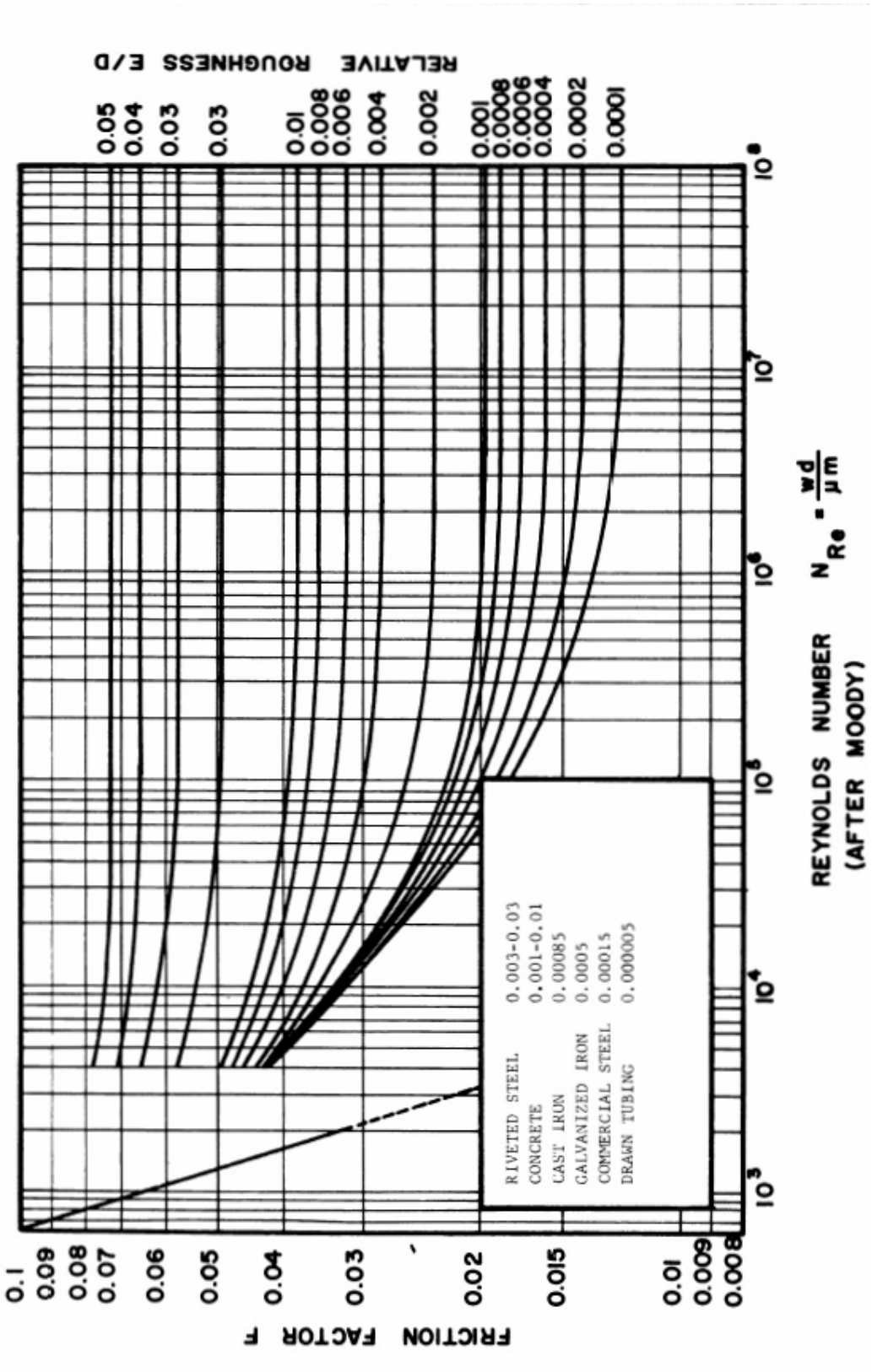

Figure A8: Moody Friction Factor Curves

transition, and mist. A flow pattern map was proposed as a result. The flow patterns were identified based on dimensionless groups as follows:

$$N_x = V_{sg}\left(\frac{\rho_g}{0.0764}\right)^{1/3}\left(\frac{72\rho_L}{62.4\sigma_L}\right)^{1/4}$$

$$N_y = V_{sL}\left(\frac{72\rho_L}{62.4\sigma_L}\right)^{1/4}$$

$$N_1 = 0.51\left(100N_y\right)^{0.172}$$

$$N_2 = 8.60 + 3.8N_y$$

$$N_3 = 70\left(100N_y\right)^{-0.152}$$

Where;

N_x, N_y are dimensionless group

N_1, N_2, N_3 are dimensionless boundary limits

Each flow regime had its own limit as follows:

Bubble Flow:

$$N_y < N_1$$

Slug Flow:

$$N_1 < N_x < N_2 \quad \text{for } N_y < 4.0$$

$$N_1 < N_x < 26.5 \quad \text{for } N_y \geq 4.0$$

Transition Flow:

$$N_2 < N_x < N_3 \quad \text{for } N_y < 4.0$$

Mist Flow:

$$N_x > N_3 \quad \text{for } N_y < 4.0$$

$$N_y > 26.5 \quad \text{for } N_y > 4.0$$

The two phase density for the bubble and slug flows was given by the following equation:

$$\Delta P_s = \left(\frac{dP}{dZ}\right)\rho_m \Delta Z$$

$$\rho_m = \rho_L H_L + \rho_g \left(1 - H_L\right)$$

$$H_L = \left[1 - \frac{V_{sg}}{V_{bf}}\right]$$

Where:

V_{bf} is the bubble rise velocity under flowing condition, ft/sec

Various methods were used to obtain the rise velocity of the bubbles under stagnant, V_{bs} , and flowing, V_{bf} , conditions

The acceleration was considered to be negligible in the bubble and slug flow regimes.

To calculate the pressure gradient for the transition region, the pressure gradients must be calculated using both the slug and mist flow equations; linear interpolation is then performed as follows:

$$\Delta P_s = \left(\frac{dP}{dZ}\right) = A\left(\frac{dP}{dZ}\right)_{slug} + B\left(\frac{dP}{dZ}\right)_{mist}$$

Where:

$$A = \frac{N_3 - N_x}{N_3 - N_2} \quad \& \mathrm{B} = \frac{N_x - N_2}{N_3 - N_2}$$

The Colebrook friction factor equation was used to calculate the pressure drop due to frictions:

$$\frac{1}{\sqrt{f}} = 4\log\frac{d}{2}\varepsilon + 3.48 - 4\log\left(1 + 9.35\frac{d}{2\varepsilon R_e\sqrt{f}}\right)$$

Where ε is the wall roughness factor = 0.00015

To calculate the friction factor for the bubble flow, the friction gradient is given by the following equation:

$$\left(\frac{dP}{dZ}\right)_f = \frac{f\rho_m V_m^2}{2g_c d}$$

The Reynolds number is given as;

$$(R_e) = \rho_L \frac{V_m d}{\mu_L}$$

For the slug flow:

$$\left(\frac{dP}{dZ}\right)_s = \frac{f\rho_L H_L V_m^2}{2g_c d}$$

The total pressure drop gradient is then can be expressed as:

$$\left(\frac{dP}{dZ}\right)_{TOT} = \left(\frac{dP}{dZ}\right)_f + \left(\frac{dP}{dZ}\right)_s$$

A.1.5 Beggs & Brill Correlation (1973)

This method is probably the most widely used method because it can be applied in vertical, horizontal, and inclined pipes. It was developed using experimental data in a small scale experimental, test facility using 1 inch and 1.5 inches diameter pipes. This correlation resulted from experiments using air and water as test fluids over a wide range of parameters. The factors used for correlating are gas flow rate, liquid flow rate, pipe diameter, inclination angle, liquid holdup, pressure gradient and horizontal flow regime. The flow regime is determined based on the limits set for "no-slip" holdup and a dimensionless number called the Froude number. A unique modification of the three horizontal flow regime, as illustrated in Figure A9 was done. Further, different correlations for liquid holdup are presented for each of the three horizontal flow regimes

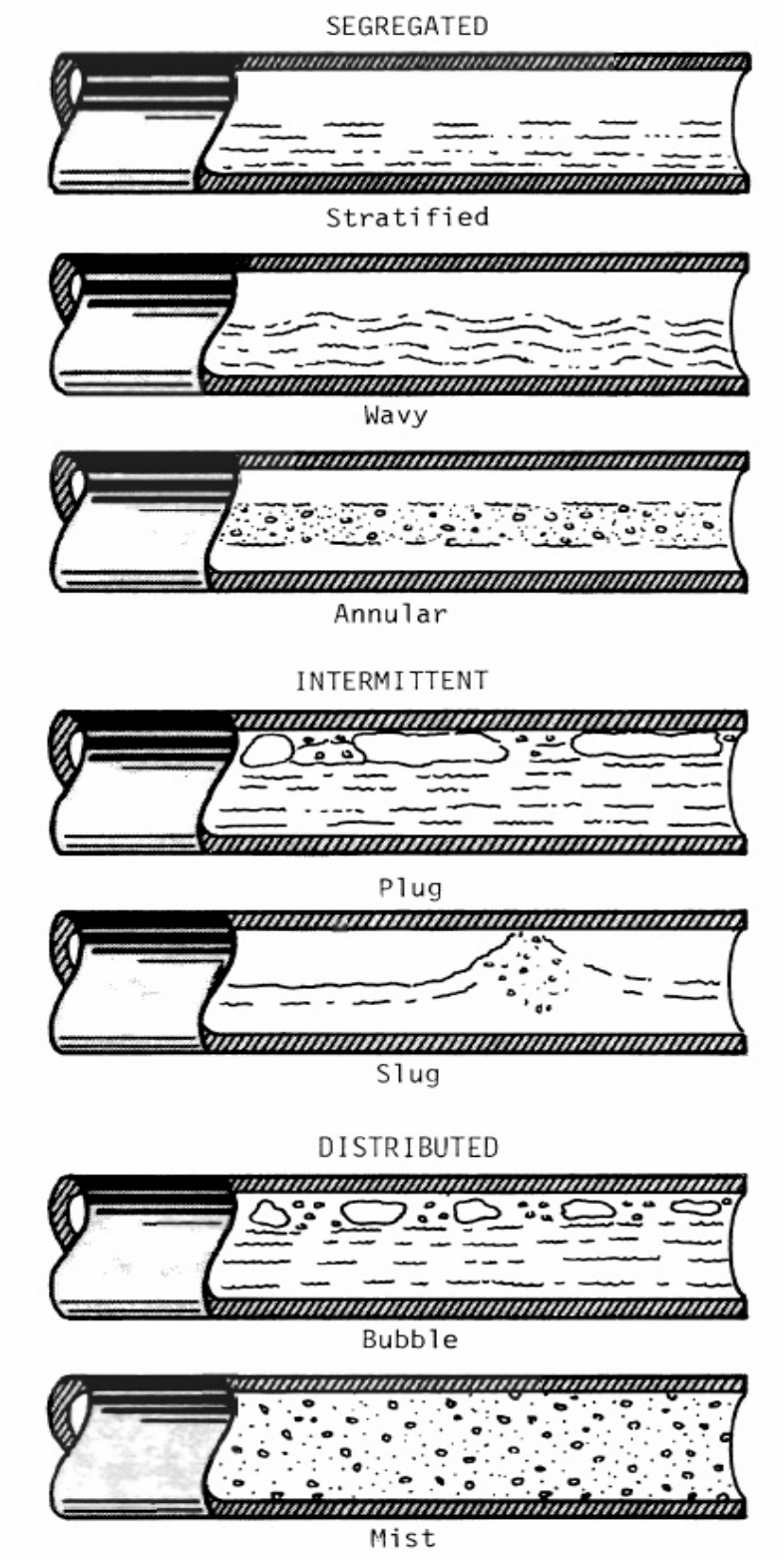

Figure A9: Beggs and Brill Horizontal Flow Patterns

(segregated, intermittent and distributed) with a correction for inclination angle of pipe. A two-phase friction factor is calculated independent of flow regime but depends on liquid holdup. Hold up factor is calculated as a function of horizontal hold up. Flow patterns also were determined using dimensionless groups.

Figure C10 shows a normalized friction factor as a function of liquid holdup and input liquid content.

$$H_{L(0)} = \frac{a\lambda_L^b}{N_{FR}^c}$$

Where: $H_{L(0)}$ is the holdup, which would exist at the same conditions in a horizontal pipe. a, b, and c are determined for each flow pattern from Table A1**,** with the restriction that

$$H_{L(0)} \geq \lambda_L \quad .$$

No slip holdup:

$$\lambda_L = \frac{V_{sL}}{V_m}$$

Froude number can be obtained by the equation

$$N_{FR} = \frac{V_m^2}{gd}$$

The dimensionless group of Beggs and Brill correlation can be stated as;

$$L_1 = 316\lambda_L^{0.302}$$

$$L_2 = 0.0009252\lambda_L^{-2.4684}$$

$$L_3 = 0.10\lambda_L^{-1.4516}$$

$$L_4 = 0.50\lambda_L^{-6.738}$$

In order to correct the holdup for the effect of pipe inclination(ϕ); the following equation is used

Table A1: Relationship between a, b, and c & flow patterns.

Flow Pattern	a	b	c
Segregated	0.980	0.4846	0.0868
Intermittent	0.845	0.5351	0.0173
distributed	1.065	0.5824	0.0609

Table A2: Relationship between d, e, and f & flow patterns.

Flow Pattern	d	e	f	g
Segregated	0.011	-3.768	3.539	-1.614
Intermittent	2.960	0.305	-0.4473	0.0978
distributed	No correction C = 0		$\psi = 1 \quad H_L \neq f(\phi)$	
All flow patterns downhill	4.7	-0.3692	0.1244	-0.5056

$$\psi = 1 + C\left[\sin(1.8\phi) - 0.333\sin^3(1.8\phi)\right]$$

For vertical upward flow $\phi = 90^0$ and ψ becomes;

$$\psi = 1 + 0.3C$$

Where;

$$C = (1 - \lambda_L)\ln\left(d\lambda_L^e N_{LV}^f N_{FR}^g\right)$$

Where d, e, f and g are determined for each flow pattern from the Table A2**:**

With the restriction that $C \geq 0$.

$$\left(\frac{dP}{dZ}\right)_f = \frac{f_{t.p}\rho_n H_L V_m^2}{2g_c d}$$

Where: $\rho_n = \rho_L\lambda_L + \rho_g\lambda_g$ $f_{t.p} = f_n \dfrac{f_{t.p}}{f_n}$ is the two - phase friction factor.

The friction factor is calculated as follows:

The no-slip friction factor is determined from the smooth pipe curve on a moody diagram or from the following equation;

$$f_n = 1\Big/\left[2\log\left(\frac{R_e}{4.5223\log R_e - 3.8215}\right)\right]^2$$

Using the following Reynolds number

$$(R_e) = \frac{\rho_n V_m d}{\mu_n}$$

$$\mu_n = \mu_L\lambda_L + \mu_g(1 - \lambda_g)$$

The ratio of the two-phase to no-slip friction is calculated from:

$$\frac{f_{t.p}}{f_n} = \mathrm{e}^{\mathrm{s}}$$

Where:

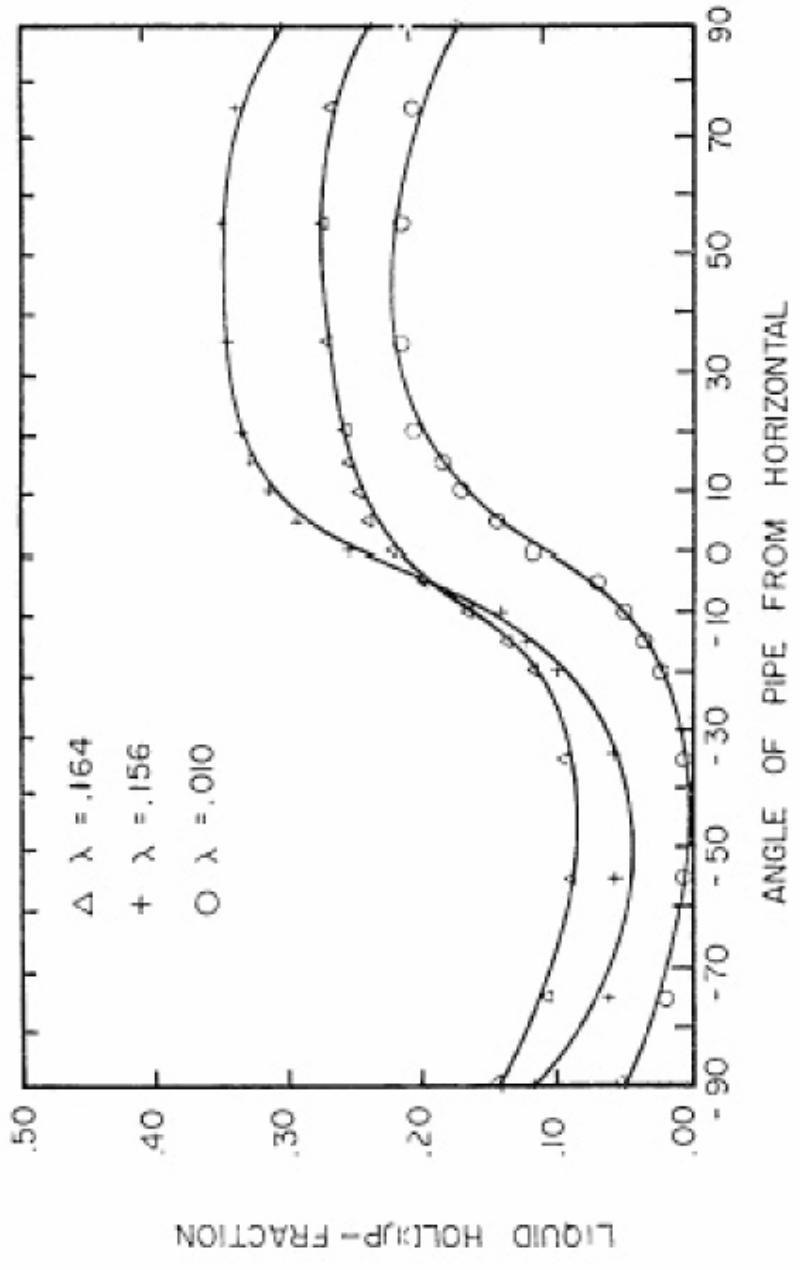

Figure A10: Liquid Holdup vs. Angle

$$s = \left[\frac{\ln(y)}{-0.0523 + 3.182\ln(y) - 0.8725[\ln(y)]^2 + 0.01853[\ln(y)]^4} \right]$$

$$y = \frac{\lambda_L}{\left[H_{L(\phi)}\right]^2}$$

The value of s becomes unbounded at a point in the interval 1< y <1.2, then the function s can be calculated as;

$$s = \ln(2.2y - 1.2)$$

The acceleration pressure drop gradient is given by:

$$\left(\frac{dP}{dZ}\right)_{acc} = \frac{\rho_s V_m V_{sg}}{g_c P}\frac{dP}{dZ}$$

If an acceleration term is defined as;

$$E_K = \frac{\rho_s V_m V_{sg}}{g_c P}$$

Then, the total pressure gradient can be calculated as:

$$\left(\frac{dP}{dZ}\right)_{TOT} = \frac{\left(\frac{dP}{dZ}\right)_{elv} + \left(\frac{dP}{dZ}\right)_f}{1 - E_K}$$

$$where \left(\frac{dP}{dZ}\right)_{elv} = \frac{g}{g_c}\rho_s$$

With a range of conducted experimental investigation, the pressure losses are accurately estimated. Any further increase in tubing size tends to result in an over prediction in the pressure loss.

A.1.6 *Mukhrejee and Brill (1985)*

Mukhrejee and Brill developed a correlation, which was based on experimental work using a U-tube section with the closed end able to incline at any angle from the

horizontal. The correlation developed from their work was tested, with good results, on data from the Prudhoe Bay and North Sea. This method is applicable to both surface pipelines and sub-surface tubing, as well. The two-phase fluid flow was divided into four possible regimes - bubble, slug, stratified and annular-mist.

For the bubble and slug flow regimes, a no-slip friction factor calculated from the Moody chart is accurate enough. For stratified flow, the friction pressure gradient is calculated based on a momentum balance equation for either phase assuming a smooth gas-liquid interface. For annular-mist flow, the friction factor is a function of both the holdup ratio and the no-slip Moody friction factor. The mixture density is used for elevation gradient calculation except for the stratified flow where gas density is used. The acceleration gradient is neglected for the stratified flow.

A.2 *Mechanistic Models*

The first attempt of generating a mechanistic model was done by Aziz *et al.*[6] who developed a model to calculate multiphase flow parameters and ended up with a generation of flow pattern map. Rashid Hasan *et al.*[15] addressed multiphase flow from physical behavior point of view. He nominated four different flow patterns and how to identify transition between these phases. Besides, void fraction and pressure drop prediction were estimated in his study. Therefore, he concluded that 90 to 99% of pressure gradient occurs due to hydrostatic head that is why the need of accurate estimation of in-situ gas void fraction is much important

A.2.1 Kabir and Hasan (1986)

Kabir and Hasan[15] developed a correlation that was based on theoretical models to predict pressure drop. The hydrodynamic condition was studied carefully

and different flow pattern transitions were, hence, determined. Pressure drop for each flow regime is estimated based on the contribution of each term in the general energy equation. Laboratory data (115 data points) were used in developing the correlation. Four flow patterns were identified (bubble, slug, churn and annular) with three flow transitions (bubble-slug flow transition, slug-churn flow transition, and churn-annular flow transition).

Bubble flow transition

$$V_{sg} < \left[0.429V_{sL} + 0.357V_t\right] \;\&\; V_t < VtT$$

Or $E_g < 0.52$

and $$V_m^{1.12} > 4.68(d)^{0.48}\left[g\left(\rho_L - \rho_g\right)/\sigma\right]^{0.5}\left(\sigma/\rho_L\right)^{0.6}\left(\frac{\rho_m}{\mu_L}\right)^{0.08}$$

Where;

$$E_g = \frac{V_{sg}}{\left(C_o V_m + V_t\right)} \quad \& \; C_o = 1.2$$

$$V_t = 1.5\left[\frac{g\sigma\left(\rho_L - \rho_g\right)}{\rho_L^2}\right]^{0.25}$$

Flowing mixture density is calculated as follows

$$\rho_m = \left[1 - E_g\right]\rho_L + E_g\rho_g$$

$$\left(\frac{\Delta P}{\Delta Z}\right)_{st} = \frac{\rho_m}{g_c}g$$

The friction pressure drop is calculated the following correlation:

$$\left(\frac{dP}{dZ}\right)_f = \frac{2fV_m^2\rho_m}{g_c d}$$

$$\frac{1}{f^{0.5}} = 4\log\left\{\frac{\frac{\varepsilon}{d}}{3.7065} - \frac{5.0452\log A}{\mathrm{Re}}\right\}$$

Where;

$$A = \frac{\left(\frac{\varepsilon}{d}\right)^{1.1098}}{2.8257} + \left(\frac{7.149}{\mathrm{Re}}\right)^{0.8981}$$

$$\mathrm{Re} = \frac{1488 D V \rho_m}{\mu}$$

Slug flow transition

$$V_{sg} > \left(0.429 V_{sL} + 0.357 V_t\right) \quad \&$$

$$V_{sg}^2 \rho_g < \left[17.1 \log\left(\rho_L V_{sL}^2\right) - 23.2\right] \quad \text{for} \quad \rho_L V_{sL}^2 > 50$$

Flowing mixture density is calculated as in the bubble flow transition regime

$$\rho_m = \left[1 - E_g\right]\rho_L + E_g \rho_g$$

$$E_g = \frac{V_{sg}}{\left(C_1 V_m + V_{tT}\right)} \quad \& \; C_1 = 1.2$$

$$V_{tT} = 0.345\left[\frac{g d\left(\rho_L - \rho_g\right)}{\rho_L}\right]^{0.5}$$

$$\left(\frac{\Delta P}{\Delta Z}\right)_{st} = \frac{\rho_m}{g_c} g$$

The friction pressure drop is calculated as follows

$$\left(\frac{dP}{dZ}\right)_f = \frac{2 f V_m^2 \rho_L \left(1 - E_g\right)}{g_c d}$$

Churn flow transition

$$V_{sg} < 3.1\left[\sigma g \left(\rho_L - \rho_g\right) \Big/ \rho_g^2\right]^{0.25}$$

and $V_{sg}^2 \rho_g > \left[17.1 \log\left(\rho_L V_{sL}^2\right) - 23.2\right]$ for $\rho_L V_{sL}^2 > 50$

The flowing mixture density is calculated as in the slug flow except that the constant C_1 will be used as 1.0 instead of 1.2. Besides, the frictional pressure drop will be treated as in the slug flow.

Annular flow transition

$$V_{sg} > 3.1\left[\sigma g\left(\rho_L - \rho_g\right)/\rho_g^2\right]^{0.25}$$

Flowing mixture density is calculated as

$$E_g = \frac{V_{sg}}{\left(V_{sg} + EV_{sL}\right)}$$

Where;

$$E = 0.0055\left[\left(V_{sg}\right)_c \times 10^4\right]^{2.86} \quad \text{for } \left(V_{sg}\right)_c \times 10^4 \le 4$$

$$E = 0.857\log\left[\left(V_{sg}\right)_c \times 10^4\right] - 0.2 \quad \text{for } \left(V_{sg}\right)_c \times 10^4 > 4$$

Where;

$$\left(V_{sg}\right)_c = \frac{V_{sg}\mu_g\left(\frac{\rho_g}{\rho_L}\right)^{0.5}}{\sigma}$$

The friction pressure drop is calculated as

$$\left(\frac{\Delta P}{\Delta Z}\right)_f = \frac{2 f_c \rho_c \left(V_{sg}/E_g\right)^2}{g_c d}$$

Where;

$$f_c = 0.079\frac{\left[1 + 75\left(1 - E_g\right)\right]}{\mathrm{Re}^{0.25}}$$

$$E_g = \left(1 + X^{0.8}\right)^{0.378} \quad \& \; \mathrm{X} = \left(\frac{1-x}{x}\right)^{0.9}\left(\frac{\rho_g}{\rho_L}\right)^{0.5}\left(\frac{\mu_L}{\mu_g}\right)^{0.1}$$

$$\rho_c = \left(\frac{V_{sg}\rho_g + EV_{sL}\rho_L}{V_{sg} + EV_{sL}} \right)$$

The acceleration pressure gradient equation is

$$\left(\frac{\Delta P}{\Delta Z} \right)_{acc} = \frac{1}{g_c} \frac{\left[g\rho_c + \left(2 f_c \rho_c V_g^2 / d \right) \right]}{\left[1 - \rho_c V_g^2 / P g_c \right]}$$

The total pressure gradient equation is

$$\left(\frac{dP}{dz} \right)_{TOT} = \left(\frac{dP}{dz} \right)_{st} + \left(\frac{dP}{dz} \right)_{f} + \left(\frac{dP}{dz} \right)_{acc}$$

A.2.2 Ansari *et al.* Model (1994)

They built a comprehensive mechanistic model that dealt with flow pattern identification, liquid holdup, and pressure drop in each flow pattern. Their model was superior for dispersed bubble and annular flows when tested against some cases. The basic work on mechanistic modeling of flow pattern-transitions for upward two-phase flow was presented by Taitel *et al.*[66]**.** Four different flow patterns were identified; those are: bubble, slug, churn, and annular flow. Based on the work done by Taitel *et al.*[66]**,** flow boundaries could be estimated. A unified model was created by Barnea[67] who extended the applicability of the model to include inclined pipes with addition of transitions boundaries determination

Bubble/Slug Transitions

$$d_{\min} = 19.01 \left[\frac{\left(\rho_L - \rho_g \right) \sigma_L}{\rho_L^2 g} \right]^{0.5}$$

For pipes larger than this, the basic transition mechanism is the form of Taylor bubbles.

$$V_{sg} = 0.25 V_s + 0.333 V_{sL}$$

Where V_s is the slip velocity that given by:

$$V_s = 1.53\left[\sigma_L g \left(\rho_L - \rho_g\right) \Big/ \rho_L^2\right]^{0.25}$$

Dispersed Bubble Transition

$$2\left[\frac{0.4\sigma_L}{\left(\rho_L - \rho_g\right)g}\right]^{0.5}\left(\frac{\rho_L}{\sigma_L}\right)^{3/5}\left[\frac{f}{2d}\right]^{2/5}\left(V_{sL} + V_{sg}\right)^{1.2} = 0.725 + 4.15\left(\frac{V_{sg}}{V_{sg} + V_{sL}}\right)^{0.5}$$

The transition for no-slip dispersed bubble flow occurs at a void fraction of 0.76

$$V_{sg} = 3.17V_{sL}$$

Transition to annular flow

This is based on the gas phase velocity required to prevent the entrained liquid droplets from falling back into the gas stream

$$V_{sg} = 3.1\left[\frac{g\sigma_L\left(\rho_L - \rho_g\right)}{\rho_g^2}\right]^{1/4}$$

Flow Behavior Prediction

This step comes after the flow patterns prediction. Now the flow behavior of each pattern will be developed. Physical models for bubble, slug, and annular flow were developed, while the churn flow model has not yet been modeled because of its complexity and was treated as part of slug flow.

Bubble flow model

Because of the uniform distribution of gas bubbles in this phase and no-slippage between gas and oil phase, dispersed bubble flow can be approximated as a pseudo-single phase.

$$\rho_{TP} = \rho_L\lambda_L + \rho_g\left(1 - \lambda_L\right)$$

$$\mu_{TP} = \mu_L\lambda_L + \mu_g\left(1 - \lambda_L\right) \qquad \&$$

$$V_{TP} = V_M V_{sL} + V_{sg} \qquad \text{where; } \lambda_L = \frac{V_{sL}}{V_M}$$

Slippage velocity can be expressed as follows

$$V_s = V_{sg} - 1.2V_M$$

Holdup equation for bubble flow can be implicitly written as

$$\rho_{TP} = \rho_L H_L + \rho_g (1 - H_L) \;\&\; \mu_{TP} = \mu_L H_L + \mu_g (1 - H_L)$$

Now the pressure gradient can be calculated as

$$\left(\frac{dP}{dL}\right) = \left(\frac{dP}{dL}\right)_e + \left(\frac{dP}{dL}\right)_f + \left(\frac{dP}{dL}\right)_{acc}$$

The elevation pressure gradient is given by

$$\left(\frac{dP}{dL}\right)_e = \rho_{TP} g \sin\theta$$

& the friction component is given also by

$$\left(\frac{dP}{dL}\right)_f = \frac{f_{TP} \rho_{TP} V_{TP}^2}{2d}$$

Where f_{TP} is obtained from a Moody diagram for a Reynolds number defined by

$$N_{\mathrm{Re}_{TP}} = \frac{\rho_{TP} V_{TP} d}{\mu_{TP}}$$

Slug Flow Model

The overall gas and liquid mass balances gives

$$V_{sg} = \beta V_{gTB}(1 - H_{LTB}) + (1 - \beta) V_{gLS}(1 - H_{LLS})$$

Where; H_{LLS} = average holdup of liquid slug, and

$$V_{sL} = (1 - \beta) V_{LLS} H_{LLS} - \beta V_{LTB} H_{LTB}$$

Where; $\beta = L_{TB} / L_{SU}$ = length ratio

L_{TB} = length of Taylor bubbles along the pipe

L_{SU} = length of slug unit along the pipe

Mass balances for liquid and gas from liquid slug to Taylor bubble give

$$(V_{TB}cc - V_{LLS})H_{LLS} = (V_{TB} - (-V_{LTB}))H_{LTB} \quad \&$$

$$(V_{TB}cc - V_{gLS})(1 - H_{LLS}) = (V_{TB} - V_{gTB})(1 - H_{LTB})$$

The Taylor bubble-rise velocity is equal to the centerline velocity plus the Taylor bubble-rise velocity in a stagnant liquid column

$$V_{TB} = 1.2V_M + 0.35\left[gd\left(\rho_L - \rho_g\right)/\rho_L\right]^{0.5}$$

Similarly, the velocity of the gas bubbles in the liquid slug is

$$V_{gLS} = 1.2V_M + 1.53\left[g\sigma_L\left(\rho_L - \rho_g\right)/\rho_L^2\right]^{0.25} \mathrm{H}_{\mathrm{LLS}}^{0.5}$$

The pressure gradients can be calculated after solving model equations and by taking into consideration the effect of varying film thickness and neglecting the effect of friction along the Taylor bubble.

The elevation component occurring across a slug unit is given by

$$\left(\frac{dP}{dL}\right)_e = \left[(1-\beta)\rho_{LS} + \beta\rho_g\right]g\sin\theta$$

Where; $\rho_{LS} = \rho_L H_{LLS} + \rho_g(1 - H_{LLS})$

The elevation component for developing slug flow is given by

$$\left(\frac{dP}{dL}\right)_e = \left[(1-\beta^*)\rho_{LS} + \beta^*\rho_{TBA}\right]g\sin\theta$$

Where ρ_{TBA} is based on average void fraction in the Taylor bubble section with varying film section

$$\rho_{TBA} = \rho_L H_{LTBA} + \rho_g(1 - H_{LTBA})$$

$$H_{LTBA} = \left(\frac{2(V_{TB} - V_{LLS})H_{LLS}}{\sqrt{2gL_{TB}^*}} \right)$$

Where L_{TB}^* = length of Taylor bubbles in developing slug flow

The friction component can be obtained by

$$\left(\frac{dP}{dL}\right)_f = \frac{f_{LS}\rho_{LS}V_M^2}{2d}(1-\beta)$$

It is worth noting that β should be replaced with β^* for developing slug flow.

& f_{LS} can be calculated from

$$\mathrm{Re}_{LS} = \frac{\rho_{LS}V_M d}{\mu_{LS}}$$

Annular Flow Model

The fully developed annular flow model considers a core contains a homogeneous mixture of gas and liquid.

The conservation of momentum applied separately to the core and the film

$$A_c\left(\frac{dP}{dL}\right)_c - \tau_i S_i - \rho_c A_c g \sin\theta = 0.0$$

$$A_f\left(\frac{dP}{dL}\right)_F + \tau_i S_i - \tau_F S_F - \rho_F A_F g \sin\theta = 0.0$$

$$\rho_c = \rho_L \lambda_{LC} + \rho_g(1-\lambda_{LC}), \quad \text{Where; } \lambda_{LC} = \frac{F_E V_{SL}}{V_{Sg} + F_E V_{SL}}$$

& $F_E = 1 - \exp\left[-0.125(V_{Crit} - 1.5)\right]$ & $V_{Crit} = 10{,}000\dfrac{V_{Sg}\mu_g}{\sigma_L}\left(\dfrac{\rho_g}{\rho_L}\right)^{0.5}$

The shear stress in the film can be expressed as

$\tau_F = f_F \rho_L \dfrac{V_F^2}{8}$ & f_F is obtained from a Moody diagram

$$\mathrm{Re}_F = \frac{\rho_L V_F d_{HF}}{\mu_L} \quad \& \quad V_F = \frac{q_L(1-F_E)}{A_F} = \frac{V_{SL}(1-F_E)}{4\bar{\delta}(1-\bar{\delta})} \ \& \ \mathrm{d_{HF}} = 4\bar{\delta}(1-\bar{\delta})d$$

Thus;

$$\tau_F = \frac{f_F}{8}(1-F_E)^2 \rho_L \left[\frac{V_{SL}}{4\bar{\delta}(1-\bar{\delta})}\right]^2 = \frac{\mathrm{d}}{4} \left[\frac{(1-F_E)^2}{4\bar{\delta}(1-\bar{\delta})}\right]^2 \frac{f_F}{f_{SL}} \left(\frac{\mathrm{dP}}{\mathrm{dL}}\right)_{\mathrm{SL}}$$

The superficial liquid friction pressure is given by

$$\left(\frac{\mathrm{dP}}{\mathrm{dL}}\right)_{\mathrm{SL}} = \frac{f_{SL}\rho_L V_{SL}^2}{2d}, \quad \text{where } f_{SL} = \textit{friction factor} \text{ for interfacial liquid velocity}$$

Shear stress at the interface can be represented as

$$\tau_i = \frac{f_i \rho_c V_c^2}{8}, \text{ where } \mathrm{V_c} \approx \mathrm{V_{sc}} \Big/ (1-2\bar{\delta})^2 \quad \& \quad f_i = f_{SC} Z$$

& Z = correlating factor for interfacial friction and the film thickness

$$Z = 1 + 300\bar{\delta} \text{ for } \mathrm{F_E} > 0.9$$

$$Z = 1 + 24\left(\frac{\rho_L}{\rho_g}\right)^{1/3} \bar{\delta} \quad \text{for } \mathrm{F_E} < 0.9$$

Combining the last three equations yields

$$\tau_i = \frac{d}{4} \frac{Z}{(1-2\bar{\delta})^4} \left(\frac{dP}{dL}\right)_{SC}$$

The superficial friction pressure gradient in the core can be obtained by the following equation

$$\left(\frac{\mathrm{dP}}{\mathrm{dL}}\right)_{\mathrm{SC}} = \frac{f_{SC}\rho_C V_{SC}^2}{2d}, \quad \text{where } f_{SC} \text{ can be obtained from a Moody diagram}$$

The pressure gradient for annular flow can be calculated then as

$$\left(\frac{\mathrm{dP}}{\mathrm{dL}}\right)_{\mathrm{C}} = \frac{Z}{(1-2\bar{\delta})^5} \left(\frac{\mathrm{dP}}{\mathrm{dL}}\right)_{\mathrm{SC}} + \rho_c g \sin\theta \quad \&$$

$$\left(\frac{\mathrm{dP}}{\mathrm{dL}}\right)_{\mathrm{F}} = \frac{(1-F_E)^2}{64\bar{\delta}^3(1-\bar{\delta})^3}\left(\frac{f_F}{f_{SL}}\right)\left(\frac{\mathrm{dP}}{\mathrm{dL}}\right)_{\mathrm{SL}} - \frac{Z}{4(1-\bar{\delta})(1-2\bar{\delta})^5}\left(\frac{\mathrm{dP}}{\mathrm{dL}}\right)_{\mathrm{SC}} + \rho_L g \sin\theta$$

Solving for the only unknown $\bar{\delta}$ by making use of dimensionless approach and Newton-Raphson method, the total pressure gradient can be estimated.

A.2.3 Chokshi *et al*. *Model (1996)*

A data from 324 well that covered wide range of flow rates were gathered for this model. The tests were conducted on an air-Water system in a 3.5 in. diameter, 1348 ft long, vertical test section. Each data set consists of flow rate measurements, pressure and temperature measurements at eight locations along the test section, and non-intrusive holdup measurement at 490 ft below the surface. The model considers three flow patterns; those are: bubble, slug and annular.

Bubble to Slug Transition

This is defined at the void fraction of 0.25. The rise velocity of a bubble swarm in a static liquid, relative to the average liquid velocity is defined by the following equation

$$V_{bs} = V_G - V_L = \frac{V_{SG}}{\alpha} - C_O V_M$$

Applying the transition criteria α =0.25 and simplifying by defining $V_M = V_{SL} - V_{SG}$

$$V_{SG} = 0.37V_{SL} + 0.34V_{bs}$$

Transition from Annular Flow

This occurs as a result of two mechanisms; blockage of the gas core by liquid in the annular film, or instability of the liquid film at low liquid rates. The first mechanism can be stated mathematically as

$$\left(H_{LF} + \lambda_{LC} \frac{A_C}{A_P} \right) = 0.12$$

Pressure Gradient Prediction Models

All three pressure gradient predictions models (bubble, slug, and annular) are presented below

Bubble Flow Model

The rise velocity can be expressed in terms of liquid holdup as

$$H_L = 1 - \alpha = 1 - \frac{V_{SG}}{(C_O V_M + V_{bs})}$$

The elevation pressure can be estimated as

$$\left(\frac{dP}{dL} \right)_e = \rho_M g \sin\theta$$

& the friction component is given also by

$$\left(\frac{dP}{dL} \right)_f = \frac{f_M \rho_M V_M^2}{2d}$$

Where; $f_M = f_M \left(\frac{\rho_M V_M D}{\mu_M} \right)$

The mixture fluid properties are weighted on liquid holdup

$$\rho_M = \rho_L H_L + \rho_G (1 - H_L)$$

$$\mu_M = \mu_L H_L + \mu_G (1 - H_L)$$

Slug Flow Model

An overall liquid mass balance can be expressed as

$$V_{SL} = V_{TBf} \frac{L_{LS}}{L_{SU}} (1 - H_{GLS}) + V_{TBf} \left(1 - \frac{L_{LS}}{L_{SU}} \right) (1 - H_{GTB}) - (V_{TBf} - V_{LLS})(1 - H_{GLS})$$

Applying a mixture balance on a liquid slug zone cross section

$$V_M = V_{LLS}\left(1 - H_{GLS}\right) + V_{GLS} H_{GLS}$$

The bubble front velocity is stated as

$$V_{TBf} = 1.2V_M + V_{TBs} = 1.2V_M + 0.345\sqrt{\frac{gd\left(\rho_L - \rho_G\right)}{\rho_L}}$$

& the velocity of the falling liquid film is expressed as

$$V_{LTB} = -9.916\sqrt{gd\left(1 - \sqrt{H_{GTB}}\right)}$$

The velocity of the dispersed bubbles in the liquid slug is treated as

$$V_{GLS} = V_{LLS} + V_{bs} = V_{LLS} + 1.41\left[\frac{g\sigma_L\left(\rho_L - \rho_G\right)}{\rho_L^2}\right]^{1/4}$$

The elevation pressure gradient a cross the slug unit is given by

$$\left(\frac{dP}{dL}\right)_e = \frac{L_{LS}}{L_{SU}} \rho_{LS} g \sin\theta$$

The friction pressure gradient across the slug unit is given by

$$\left(\frac{dP}{dL}\right)_f = \frac{L_{LS}}{L_{SU}} \frac{f_M \rho_{LS} V_M^2}{2d}$$

The acceleration pressure gradient is neglected

Annular Flow Model

A linear momentum balance on the liquid film is given by

$$-A_F\left[\frac{dP}{dL}\right]_F - \tau_F S_F + \tau_C S_C - -\rho_L A_F g \sin\theta = 0.0$$

& the balance on the liquid-laden gas core yields

$$-A_C\left[\frac{dP}{dL}\right]_C - \tau_C S_C - \rho_C A_C g \sin\theta = 0.0$$

Various geometric parameters were implemented to solve for the uniformity of the film thickness and diameter. The shear stress between the liquid film and the pipe wall is given by the Moody's friction factor

$$\tau_F = \frac{f_F \rho_L V_{FL}^2}{8}$$

The frictional pressure gradient for the superficial liquid phase is given by

$$\left(\frac{dP}{dL}\right)_{SL} = \frac{f_{SL} \rho_L V_{SL}^2}{2d}$$

The interfacial shear stress between the gas core and the liquid film is given by

$$\tau_C = \frac{f_C \rho_C V_C^2}{8}$$

The frictional pressure gradient for the superficial core is defined as

$$\left(\frac{dP}{dL}\right)_{SC} = \frac{f_{SC} \rho_C V_{SC}^2}{2d}$$

Various assumptions were used for the mass balance including the incompressibility assumptions for both liquid and core.

A.2.4 Gomez *et al. Model (1999)*

They presented a unified mechanistic model that deals with liquid holdup, flow pattern identification, and pressure drop in wellbores and pipelines. The model consists of a unified flow pattern prediction model and unified individual models for stratified, slug, bubble, annular and dispersed bubble flow, applicable to all inclination angles ranging from 0^0 to 90^0.

Unified Flow Pattern Prediction Model

The authors presented first the transition criteria for their study, which includes the stratified to non-stratified, slug to dispersed bubble, annular to slug, bubble to slug flow.

Stratified to Non-Stratified Transition

This criterion was firstly introduced by Taitel and Dukler[66]**.** It is based on a simplified stability analysis given by

$$F^2\left[\frac{1}{\left(1-\tilde{h}_L\right)^2}\frac{\tilde{V}_g^{\,2}\,d\tilde{A}_L/d\tilde{h}_L}{\tilde{A}_g}\right]\geq 1 \quad \text{, where F is a dimensionless group}$$

$$F=\sqrt{\frac{\rho_g}{\left(\rho_L-\rho_g\right)}}\frac{V_{sg}}{\sqrt{dg\cos\theta}}$$

Slug to Dispersed Bubble Transition

The maximum bubble size can be determined from the following equation

$$d_{\max}=\left[4.15\left(\frac{V_{sg}}{V_M}\right)^{0.5}+0.725\right]\left(\frac{\sigma}{\rho_L}\right)^{0.6}\left(\frac{2f_M V_M^3}{d}\right)^{-0.4}$$

Two critical bubble diameters were considered; the one below which bubble do not deform and the other is applicable to shallow inclinations

$$d_{CD}=2\left[\frac{0.4\sigma}{\left(\rho_L-\rho_g\right)g}\right]^{1/2}$$

$$d_{CB}=\frac{3}{8}\frac{\rho_L}{\left(\rho_L-\rho_g\right)}\frac{f_M V_M^2}{g\cos\theta}$$

It is worth noting that transition to dispersed bubble flow will occur only when the maximum possible bubble diameter is less than any critical diameters mentioned lastly.

Annular to Slug Transition

This transition criterion might be caused as a result of instability of the liquid film or because of wave growth on the interface due to large liquid supply from the film. The first reason may be stated as

$$Y = \frac{1+75H_L}{(1-H_L)^{2.5}H_L} - \frac{1}{H_L^3}X^2$$

$$Y \geq \frac{2-\frac{3}{2}H_L}{H_L^3\left(1-\frac{3}{2}H_L\right)}X^2$$

Where X is the Lockhart and Martinelli parameter and Y is a dimensionless gravity group defined as

$$X^2 = \frac{\frac{4C_L}{d}\left(\frac{\rho_L V_{SL} d}{\mu_L}\right)^{-n}}{\frac{4C_g}{d}\left(\frac{\rho_g V_{sg} d}{\mu_g}\right)^{-m}} \frac{\frac{\rho_L V_{SL}^2}{2}\left(\frac{dP}{dL}\right)_{SL}}{\frac{\rho_g V_{sg}^2}{2}\left(\frac{dP}{dL}\right)_{sg}}$$

$$Y = \frac{(\rho_L - \rho_g)g\sin\theta}{\left(\frac{dP}{dL}\right)_{sg}}$$

The second case occurs as a result of the following condition

$$H_L \geq 0.24$$

Bubble to Slug Transition

This transition is caused by coalescence of bubbles at a critical gas void fraction of $\alpha = 0.25$, as follows

$$V_{SL} = \frac{1-\alpha}{\alpha} V_{sg} - 1.53(1-\alpha)^{0.5} \left[\frac{g(\rho_L - \rho_g)\sigma}{\rho_L^2} \right]^{1/4} \sin\theta$$

The authors suggested different techniques to smoothen the transition because predictions of pressure traverses in multiphase flow are tarnished for creating such discontinuities.

Unified Stratified Flow Model

This model utilized the theory of the model presented by Taitel *et al.*[66] the model calculates the momentum balances and closure relationships, basically as follows

Momentum Balances

The force balances for the liquid and gas phases are given as

$$-A_L \frac{dP}{dL} - \tau_{WL} S_L + \tau_I S_I - \rho_L A_L g \sin\theta = 0.0$$
$$-A_G \frac{dP}{dL} - \tau_{WG} S_G + \tau_I S_I - \rho_G A_G g \sin\theta = 0.0$$

Eliminating the pressure gradient from the last two equations yields

$$\tau_{WL} \frac{S_L}{A_L} - \tau_{WG} \frac{S_G}{A_G} - \tau_I S_I \left(\frac{1}{A_L} + \frac{1}{A_G} \right) + (\rho_L - \rho_G) g \sin\theta = 0.0$$

Trial and errors procedure is needed to solve for the geometrical variables. After determination of liquid level, the liquid holdup can be estimated as follows

$$H_L = \pi - \cos^{-1}\left(2\frac{h_L}{d} - 1\right) + \left(2\frac{h_L}{d} - 1\right)\sqrt{1 - \left(2\frac{h_L}{d} - 1\right)^2}$$

The pressure gradient now can be calculated from any one of the balance equations providing that acceleration term is neglected.

Closure Relationships

This deals with determination of wall shear stresses for each phase. Fanning friction factor formula is used

$$\tau_{WL} = f_L \frac{\rho_L V_L^2}{2} \& \tau_{WG} = f_G \frac{\rho_G V_G^2}{2}$$

The hydraulic numbers are determined based on the following formula

$$d_L = \frac{4A_L}{S_L} \& d_G = \frac{4A_G}{S_G + S_I}$$

Moreover, the Reynolds number of each of the phases is

$$\mathrm{Re}_L = \frac{d_L \rho_L V_L}{\mu_L} \& \mathrm{Re}_G = \frac{d_G \rho_G V_L}{\mu_G}$$

Where;

τ_{WL} = liquid wall shear stress, (lbf/ft^2)

τ_{WG} = gas wall shear stress, (lbf/ft^2)

S_L = liquid perimeter, (ft)

S_G = gas perimeter, (ft)

S_I = perimeter interface, (ft)

τ_I = shear stress interface, (lbf/ft^2)

h_L = liquid level height, (ft)

Unified Slug Flow Model

The model simplifies the assumptions that were used by Taitel and Barnea [68] by avoiding the need for a numerical integration along the liquid film region.

Mass Balance

An overall liquid mass balance is calculated as follows

$$V_{SL} = V_{LLS} H_{LLS} \frac{L_S}{L_U} + V_{LTB} H_{LTB} \frac{L_F}{L_U}$$

A mass balance can be applied between two cross sectional areas

$$(V_{TB} - V_{LLS}) H_{LLS} = (V_{TB} - V_{LTB}) H_{LTB}$$

Applying this balance on cross sections in the liquid slug body and in the liquid film region gives

$$V_M = V_{SL} + V_{SG} = V_{LLS} H_{LLS} + V_{GLS} (1 - H_{LLS})$$

$$V_M = V_{LTB} H_{LTB} + V_{GTB} (1 - H_{LTB})$$

The last two equations can be used to determine V_{LLS} . All velocities can be determined from the previous formula.

The average liquid holdup in a slug unit is defined as

$$H_{LSU} = \frac{H_{LLS} L_S + H_{LTB} L_F}{L_U}$$

From the above expressions, the liquid holdup appears independent of the lengths of the different slug zones, as shown below

$$H_{LSU} = \frac{V_{TB} H_{LLS} + V_{GLS} (1 - H_{LLS}) - V_{SG}}{V_{TB}}$$

Where;

V_{SL} = superficial liquid velocity, (ft/s)

V_{SG} = superficial gas velocity, (ft/s)

V_{LLS} = liquid slug velocity, (ft/s)

V_{GLS} = gas slug velocity, (ft/s)

V_{TB} = Taylor's bubbles velocity, (ft/s)

H_{LTB} = liquid holdup for Taylor bubbles

H_{LLS} = liquid slug holdup

V_M = mixture velocity, (ft/s)

L_U = total slug unit length, (ft)

L_F = film length, (ft)

L_S = slug body length, (ft)

Pressure Drop Calculations

This can be calculated using a global force balance along a slug unit.

$$\frac{dP}{dL} = \rho_U g \sin\theta + \frac{\tau_S \pi d}{A}\frac{L_S}{L_U} + \frac{\tau_{WF} S_F + \tau_{WG} S_G}{A}\frac{L_F}{L_U}$$

Where; ρ_U is the average density of the slug unit given by

$$\rho_U = H_{LSU}\rho_L + (1 - H_{LSU})\rho_G$$

&; τ_S = slug body shear stress, (lbf/ft^2)

τ_{WF} = vertical wall shear stress, (lbf/ft^2)

H_{LSU} = liquid slug unit holdup

The first term in the pressure gradient equation is the gravitational pressure gradient, whereas the second and third terms represent the frictional pressure gradient. No acceleration pressure drop occurs.

Closure Relationships

The proposed model requires two closure relationships; the liquid slug length and the liquid holdup in the slug unit.

Assuming a constant length of L_S = 30d and L_S = 20d is used for fully developed and stable slug in horizontal and vertical pipes, respectively.

For horizontal and near horizontal large diameter pipes (d > 2 inch), Scott *et al.*[69] correlation is used, as given below

$$\ln(L_S) = -24.5 + 28.5[\ln(d)]^{0.1}$$

Where d is expressed in inches and L_S is in feet

Gomez et al unified correlation was used to predict the liquid holdup in the slug body as follows

$$H_{LLS} = 1.0e^{-(0.45\theta_R + 2.48\times10^{-6}\,\mathrm{Re}_{LS})} \quad \& \quad 0 \le \theta_R \le 1.57$$

Where; $\theta_R = \left(\pi/180\right)\times\theta$ is the inclination angle in radians and the slug Reynolds number is calculated as follows

$$\mathrm{Re}_{LS} = \frac{\rho_L V_M d}{\pi_L}$$

Unified Annular Flow Model

This model is an extension of the model that developed by Alves *et al.*[70]**.** The equations used for developing this model is the same like ones used for stratified model. Slight differences between the formulations of each one are detected.

Momentum Balances

$$-\tau_{WF}\frac{S_F}{A_F} + \tau_I\frac{S_I}{A_F} - \left[\frac{dP}{dL}\right]_F - \rho_L g\sin\theta = 0.0$$

$$-\tau_I\frac{S_I}{A_C} - \left[\frac{dP}{dL}\right]_C - \rho_C g\sin\theta = 0.0$$

Eliminating the pressure gradients from the last two equations result in the combined momentum equation

$$\tau_{WF}\frac{S_F}{A_F}-\tau_I S_I-\left[\frac{1}{A_F}+\frac{1}{A_C}\right]+(\rho_L-\rho_C)g\sin\theta=0.0$$

Mass Balances

The velocities of the liquid film and gas core are estimated from the following equations

$$V_F=V_{SL}\frac{(1-E)d^2}{4\delta(d-\delta)}$$

$$V_C=\frac{(V_{SG}+V_{SL}E)d^2}{(d-2\delta)^2}$$

The gas void fraction in the core and the core average density and viscosity are given, respectively, by

$$\alpha_C=\frac{V_{SG}}{(V_{SG}+V_{SL}E)}$$

$$\rho_C=\rho_G\alpha_C+\rho_L(1-\alpha_C)$$

$$\mu_C=\mu_G\alpha_C+\mu_L(1-\alpha_C)$$

Closure Relationships

The liquid shear stress is found through single-phase flow calculations as follows

$$\tau_I=f_I\rho_C\frac{(V_C-V_F)^2}{2}$$

The interfacial friction factor is obtained by Alves *et al.* [70].

$$f_I=f_{CS}I$$

Where;

f_{CS} is the friction factor

The parameter I is an average between a horizontal and vertical factor.

$$I_\theta=I_H\cos^2\theta+I_V\sin^2\theta$$

The horizontal correction is applied as follows

$$I_H = 1 + 800F_A \quad \&$$
$$F_A = \frac{\left[\left(0.707\mathrm{Re}_{\mathrm{SL}}^{0.5}\right)^{2.5} + \left(0.0379\mathrm{Re}_{\mathrm{SL}}^{0.9}\right)^{2.5}\right]^{0.4}}{\mathrm{Re}_{\mathrm{SG}}^{0.9}} \left(\frac{V_L}{V_G}\right)\left(\frac{\rho_L}{\rho_G}\right)^{0.5}$$

Where;

$\mathrm{Re}_{SL}, \mathrm{Re}_{SG}$ are the liquid and gas superficial Reynolds numbers, respectively.

Another correction is applied for vertical interfacial annular parameter as follows

$$I_V = 1 + 300\frac{\delta}{d}$$

The entrainment factor, E is calculated as

$$E = 1 - e^{-[0.125(\phi - 1.5)]} \quad \& \phi = 10^4 \frac{V_{SG}\mu_G}{\sigma}\left(\frac{\rho_G}{\rho_L}\right)^{0.5}$$

Unified Bubble Flow Model

The gas velocity is given by

$$V_G = C_O V_M + V_{O\infty} \sin\theta H_L^{0.5}$$

C_O, is the velocity distribution coefficient and $V_{O\infty}$ is the bubble rise velocity and $H_L^{0.5}$ is a correction for bubble swarm

The bubble rise velocity is found by the following formula

$$V_{O\infty} = 1.53\left[\frac{g\sigma(\rho_L - \rho_G)}{\rho_L^2}\right]^{0.25}$$

Substituting for the gas velocity in terms of the superficial velocity results

$$\frac{V_{SG}}{1 - H_L} = C_O V_M + V_{O\infty} \sin\theta H_L^{0.5}$$

APPENDIX B

DATA ORGANIZATION

APPENDIX B

Table B1: Output Layer Weight Matrix.

j/i	**1**
1	-1.6075
2	-3.2712
3	0.074458
bias	-0.67909

Table B2: Evaluating the Last Hidden Layer's Weight Matrix (from Hidden Layer to the Output).

j/i	**1**	**2**	**3**
1	-1.1748	0.077237	1.7844
2	-1.4527	-0.82596	-0.62623
3	-0.40211	1.7704	0.71356
bias	2.2969	-0.73163	2.019

Table B3: Evaluating the second hidden layer's weight matrix (from second hidden layer to the third hidden layer).

j/i	1	2	3
1	-1.1685	0.26346	0.4865
2	0.72774	1.1319	-1.2523
3	0.48866	-0.10124	-1.1615
4	-0.16686	-0.42124	-0.1333
5	-0.44263	-0.65305	-0.28248
6	-0.71261	0.5908	-0.55617
bias	1.7373	0.31668	1.3796

Table B4: Evaluating the first hidden layer's weight matrix (from the first hidden layer to the second hidden layer).

j/i	1	2	3	4	5	6
Q_O	0.21703	0.42328	0.27097	0.024631	-0.45208	-0.7808
Qg	0.23111	0.34952	0.054396	0.68871	-0.05302	-0.57623
Q_W	-0.07782	0.29298	0.076347	-1.0624	-0.51491	0.11992
TBG	-0.24883	0.034517	-0.29101	-1.3784	0.024062	0.63569
DEPTH	0.1651	0.5038	0.1219	0.13544	-0.11959	0.003489
API	0.22712	-0.19885	0.046515	0.032684	1.2305	0.30829
STM	0.40123	-0.04843	0.033292	-0.28476	0.34449	-0.25808
BTM	-0.23678	-0.21024	0.14112	-0.67677	1.3555	-0.04366
P_{wh}	-0.84889	0.243	-0.00319	-0.64737	-0.76269	0.16645
bias	-2.7259	2.6103	-0.40373	-0.31208	1.41	-1.9444

Table B5: NORMALIZED DATA.

S.N	MBHP	Q_O	Qg	Q_W	TBG	DEPTH	API	STM	BTM	P_{wh}
1	1.0424	-0.35604	-0.23553	2.9716	0.42946	0.46114	-0.50577	-0.90061	0.49296	-0.95125
2	-0.40056	-1.1626	-0.97912	-0.50124	-3.5956	-0.15693	-0.50577	-0.90061	0.49296	-0.5931
3	-0.48329	0.47454	0.26541	-0.07161	-0.05334	-0.11632	1.1768	1.2427	0.25707	-0.23494
4	-1.0856	-0.69047	-0.77987	-0.64266	0.32103	-0.02626	-0.41948	-0.90061	-1.3941	-0.65822
5	-0.662	-0.52315	-0.54306	0.39239	0.42946	-0.03509	-0.50577	-0.90061	0.49296	-0.72333
6	0.50292	-1.0842	-0.91989	-0.64445	-4.7471	0.36224	0.96107	1.2427	0.43399	-0.5931
7	0.25141	1.7171	1.5127	-0.517	0.32103	0.27925	0.96107	1.2752	0.37501	-0.46286
8	0.41688	-0.58354	-0.47173	1.1099	0.32103	0.51764	-0.50577	-0.90061	0.49296	-0.00702
9	1.3204	-1.1047	-0.9455	0.075182	0.32103	0.55649	-0.50577	-0.90061	0.49296	0.90466
10	-0.13249	-0.67661	-0.51988	0.1074	0.32103	0.64832	1.1768	1.1128	0.49296	-0.46286
11	-0.28472	0.41208	0.3481	0.36232	0.42946	-0.06511	-0.50577	-0.90061	0.49296	-0.56054
12	-1.5423	0.92872	0.56183	-0.96668	0.42946	0.5406	-0.50577	-0.90061	0.49296	-0.2675
13	-1.4563	-0.1728	-0.14049	-0.07233	0.42946	0.75957	-0.50577	-0.90061	0.49296	-0.78845
14	-0.4502	1.0319	0.82593	-0.96668	0.42946	0.34105	-0.50577	-0.90061	0.49296	0.51394
15	-1.8435	-1.0921	-1.0726	-0.96668	-0.05334	-2.4915	-1.6275	-0.57587	-2.4556	-0.69078
16	0.5989	-0.28221	-0.22079	2.0408	0.32103	0.52824	-0.50577	-0.90061	0.49296	-0.46286
17	0.51947	0.20237	0.92794	-0.63013	-2.173	-0.01743	1.3925	1.2102	0.31604	1.4582
18	-0.24501	0.55396	0.43976	0.25062	0.32103	0.4576	-0.50577	-0.90061	0.49296	-0.39774
19	0.73789	1.9965	1.7553	-0.9631	-0.05334	0.61477	0.96107	1.3401	0.49296	0.058102
20	0.40033	-0.43877	0.18294	-0.60865	-3.5956	-0.0757	1.3925	1.1128	0.37501	1.2628
21	0.62868	1.9541	3.3066	-0.96668	-0.05334	0.35871	1.3925	1.2752	0.43399	1.6861
22	-1.079	-1.0739	-1.0691	-0.96668	-0.05334	-2.465	-1.6275	-0.12123	-2.4556	0.12322

Table B5, Continued

23	-0.05637	1.5097	0.96863	-0.96668	-0.05334	-0.02626	1.1768	1.2752	0.25707	-0.20238
24	0.36062	0.051391	0.53142	-0.96668	0.42946	0.092059	-0.50577	-0.90061	0.49296	2.9885
25	0.9497	0.71941	1.643	0.78766	0.32103	0.61654	1.3925	1.2427	0.49296	1.7512
26	1.8168	-0.96616	-0.69667	1.5932	0.32103	1.1092	-0.50577	-0.90061	0.49296	-0.52798
27	0.92984	2.6987	2.4849	-0.96668	-0.05334	0.69953	0.96107	1.3726	0.55193	-0.16982
28	2.4092	-1.0098	-0.8449	2.8946	0.32103	1.1428	-0.50577	-0.90061	0.49296	-0.20238
29	-0.44689	-0.49544	-0.38862	0.1697	0.32103	1.2699	-0.50577	-0.90061	0.49296	-0.82101
30	0.1455	1.8139	3.0035	-0.96668	0.32103	-0.57369	1.3925	1.3076	0.080156	1.6861
31	1.2178	-0.76182	-0.45647	1.9548	0.32103	0.41346	1.1768	1.2427	0.43399	-0.33262
32	0.46983	-0.57217	-0.70214	-0.84996	0.42946	0.028486	-0.41948	-0.90061	-1.3941	1.621
33	-0.13911	-0.12875	-0.11035	1.1385	0.32103	0.037316	1.1768	1.2102	0.31604	-0.85357
34	0.46983	-0.9978	-0.95628	-0.96668	0.42946	-0.01919	-0.41948	-0.90061	-1.3941	1.8163
35	1.509	-0.83172	-0.71589	1.5753	0.32103	1.005	-0.50577	-0.90061	0.49296	-0.46286
36	-1.2908	-1.0675	-1.0679	-0.96668	-0.05334	-2.2637	-1.6275	0.17104	-2.4556	-0.12423
37	-0.00011	0.20671	0.19895	0.52737	0.32103	0.33576	0.96107	1.3076	0.37501	-0.05911
38	-0.32113	0.38851	0.34048	-0.44754	-0.05334	0.32339	1.1768	1.1778	0.37501	-0.00702
39	-0.82747	1.4257	0.70559	-0.85927	0.32103	-0.08806	-0.50577	-0.90061	0.49296	-0.52798
40	-0.1358	0.016232	-0.03913	0.68025	0.32103	0.53707	1.1768	1.1778	0.49296	-0.78845
41	-1.4728	-0.07353	-0.87998	-0.96668	-0.05334	-3.1961	-1.6275	0.30094	-2.3967	0.30556
42	-0.13911	1.5852	1.2478	-0.92622	-0.05334	0.4682	1.1768	1.2427	0.43399	-0.75589
43	0.31759	-0.57796	-0.66413	-0.96668	0.42946	0.37814	-0.76462	-0.90061	-0.80442	2.0768
44	0.40364	1.6381	1.0682	-0.96668	-0.05334	0.87789	1.1768	1.2752	0.31604	-0.72333
45	1.5454	-0.8431	-0.67758	2.3619	0.32103	0.31456	-0.50577	-0.90061	0.49296	0.3837

Table B5, Continued

46	-1.6548	-0.55996	-0.97196	-0.88899	-0.32103	-2.3131	-1.6275	0.23599	-2.4556	-1.4136
47	0.22493	-0.15274	-0.15648	1.4479	0.42946	0.30927	-0.50577	-0.90061	0.49296	-0.75589
48	-0.11925	-0.60422	-0.35982	1.8617	-0.05334	-0.52601	1.1768	1.1778	0.13913	-0.78845
49	-0.21854	0.10723	0.2019	0.85139	0.32103	0.15387	1.1768	1.1778	0.31604	-0.95125
50	-0.79107	-0.33536	-0.32099	0.64445	0.32103	0.7066	-0.50577	-0.90061	0.49296	-0.91869
51	-1.2147	0.49998	0.37688	-0.12567	0.32103	0.70483	-0.50577	-0.90061	0.49296	-0.78845
52	0.7743	-0.88963	-0.8052	1.2273	0.32103	0.39933	1.1768	1.2102	0.43399	-0.75589
53	0.83387	2.4381	2.0977	-0.60937	0.42946	0.68894	-0.50577	-0.90061	0.49296	-0.72333
54	2.0385	-1.084	-0.87732	1.6254	0.32103	0.15916	-0.50577	-0.90061	0.49296	0.83954
55	0.6353	-1.0385	-0.88535	0.28642	0.32103	1.0156	-0.50577	-0.90061	0.49296	-0.46286
56	0.04622	1.6625	1.2267	-0.96668	0.32103	0.65539	1.1768	1.2752	0.49296	-0.5931
57	0.9497	-0.79656	-0.61512	2.0694	0.32103	0.005529	-0.50577	-0.90061	0.49296	-0.30006
58	-0.98964	-1.1029	-1.0746	-0.9631	0.32103	-2.3131	-1.6275	-0.38102	-2.5146	-0.25447
59	0.049529	0.078278	0.16957	-0.68026	0.42946	0.014359	-0.50577	-0.90061	0.49296	1.9466
60	-0.27811	-0.43608	-0.56477	0.71605	0.32103	-0.04921	-0.50577	-0.90061	0.49296	-0.52798
61	-1.079	-0.85509	-1.0278	-0.96668	-0.05334	-2.4897	-1.6275	-0.4135	-2.4556	0.51394
62	0.6353	-0.51488	-0.32979	2.4049	0.32103	0.49469	-0.50577	-0.90061	0.49296	-0.85357
63	-0.28803	-0.6884	-0.64039	1.0483	0.32103	0.28101	-0.50577	-0.90061	0.49296	-0.72333
64	0.17198	-0.66627	-0.53056	0.93087	0.32103	0.78253	-0.50577	-0.90061	0.49296	-0.72333
65	0.58897	2.54	2.2758	-0.77657	-0.05334	0.24746	1.1768	1.3076	0.37501	-0.78845
66	0.13227	-0.53184	-0.31525	0.18402	0.32103	0.82315	1.1768	1.1453	0.55193	0.12322
67	0.75113	1.4226	2.5433	-0.96668	-0.05334	0.82315	1.3925	1.2102	0.66987	2.8583
68	1.2045	0.80214	1.7455	0.42963	0.32103	0.94853	1.3925	1.2427	0.6109	1.621

Table B5, Continued

69	-0.78776	0.72831	0.20715	-0.20873	0.32103	-0.11102	-0.50577	-0.90061	0.49296	-0.46286
70	0.17529	2.4455	2.1452	-0.96668	0.32103	0.010827	0.96107	1.3726	0.31604	-0.33262
71	-0.40386	1.2547	0.83559	-0.67596	0.32103	0.45584	-0.50577	-0.90061	0.49296	0.3837
72	-1.443	0.46358	0.1117	-0.29538	0.32103	0.086761	-0.50577	-0.90061	0.49296	-0.39774
73	1.5289	-1.0799	-0.91323	0.89507	0.32103	0.15387	-0.50577	-0.90061	0.49296	-0.00702
74	0.052839	-1.2406	-1.0081	-0.56605	-4.7471	1.307	1.3925	1.2102	0.66987	-1.5699
75	-0.64876	1.7634	0.25173	-0.96668	0.32103	-0.22934	-0.50577	-0.90061	0.49296	-0.20238
76	-0.32444	0.24518	0.35462	-0.96668	0.32103	0.31986	1.1768	1.2427	0.37501	1.4907
77	-0.75136	1.5318	1.24	-0.96668	-0.05334	-0.64433	1.1768	1.2752	0.080156	-0.65822
78	0.47645	-0.48013	-0.30767	1.001	0.32103	0.23333	1.1768	1.2102	0.37501	0.18834
79	-0.60574	1.4544	0.83274	-0.96668	0.42946	0.27571	-0.50577	-0.90061	0.49296	-0.23494
80	-0.60574	-0.54218	-0.51762	-0.38667	0.32103	0.005529	-0.50577	-0.90061	0.49296	0.12322
81	-1.539	-1.2495	-1.1023	-0.96668	-0.05334	-2.2566	-1.6275	-1.3553	-2.4556	-1.5178
82	-0.50977	0.028435	-0.45243	-0.96668	0.32103	0.87259	-0.41948	-0.90061	-1.3941	0.44882
83	-0.30789	-0.49813	-0.61722	-0.9631	0.32103	0.2351	-0.41948	-0.90061	-1.3941	1.0089
84	-1.2643	-0.82138	-1.0214	-0.92443	0.32103	-2.3131	-1.6275	-0.08875	-2.4556	-0.78845
85	1.3402	-0.90246	-0.73043	1.2527	0.32103	0.4735	1.1768	1.2427	0.43399	0.96978
86	-1.0029	0.0274	-0.12502	-0.79017	0.32103	0.66245	-0.50577	-0.90061	0.49296	0.64418
87	0.6717	-1.1242	-0.82484	1.0304	0.32103	0.73838	1.1768	1.2102	0.25707	-0.65822
88	-0.76128	0.8948	0.3402	-0.54313	0.32103	0.2351	-0.50577	-0.90061	0.49296	-0.00702
89	0.17198	-0.78519	-0.73624	-0.73074	-2.173	0.87259	-0.76462	-0.90061	-0.80442	0.51394
90	0.43673	0.61104	0.68541	1.044	0.32103	0.57945	0.96107	1.3076	0.49296	-0.65822
91	-0.69841	-0.4518	-0.92454	-0.96668	0.32103	-2.0677	-1.6275	-0.67329	-2.4556	0.18834

Table B5, Continued

92	0.23817	1.2565	2.3532	-0.36806	-0.05334	-0.34765	1.3925	1.2427	0.1981	1.621
93	0.8438	-0.68695	-0.33114	-0.96668	-4.7471	0.16623	1.3925	1.1453	0.1981	0.96978
94	-1.1518	0.2398	0.008314	0.12602	0.32103	-0.03332	-0.50577	-0.90061	0.49296	-0.72333
95	0.9166	-1.2363	-1.0556	0.44968	0.32103	0.1627	1.1768	1.0479	0.37501	-0.88613
96	-1.1981	0.35397	-0.79914	-0.96668	-0.05334	-2.2248	-1.6275	0.56074	-2.4556	-1.1792
97	0.83056	-1.0607	-0.80731	-0.96668	-4.7471	0.41875	1.3925	1.1778	0.43399	1.5559
98	-0.01666	-0.74093	-0.66697	0.24238	0.32103	0.30573	1.1768	1.1453	0.37501	-0.23494
99	1.1549	0.30371	0.67087	0.9971	0.32103	0.89025	-0.50577	-0.90061	0.49296	0.35114
100	0.65185	-0.1182	0.19845	1.2889	-0.05334	0.60241	1.1768	1.1128	0.49296	-0.65822
101	-0.4866	1.0483	0.5571	-0.53346	-0.05334	-0.08453	1.1768	1.2752	0.25707	-0.78845
102	0.60221	2.75	2.0579	-0.96668	-0.05334	0.24569	0.96107	1.0479	0.37501	-0.33262
103	-4.1766	-1.124	-0.94939	-0.87645	-0.05334	-0.28231	1.1768	1.0479	0.1981	-1.1141
104	-0.11925	-0.33536	-0.29446	1.0383	0.32103	0.31986	-0.50577	-0.90061	0.49296	-0.65822
105	1.2376	0.67805	1.5304	0.25062	-0.05334	1.1799	1.3925	1.2102	0.66987	1.9466
106	0.27126	0.098546	-0.0602	1.0394	0.32103	0.79313	-0.50577	-0.90061	0.49296	-0.56054
107	0.73127	-0.69688	-0.60821	-0.92013	-4.7471	0.47703	0.96107	1.3076	0.43399	-0.91869
108	-1.3471	-0.82138	-1.0888	-0.96668	0.32103	-2.276	-1.6275	0.30094	-2.4556	-0.62566
109	1.4362	-0.07394	-0.05184	2.2634	0.32103	0.95206	-0.50577	-0.90061	0.49296	-0.65822
110	0.64854	1.567	1.5364	-0.95128	-0.05334	0.39226	1.1768	1.2102	0.43399	1.7512
111	-2.1579	-1.1833	-1.0156	-0.68026	0.42946	-1.3118	-0.76462	-0.90061	-0.80442	-0.78845
112	-1.6482	-0.86812	-0.7636	-0.68885	0.32103	0.24393	-0.50577	-0.90061	0.49296	-0.75589
113	-0.01666	-0.32295	-0.31438	1.3032	0.32103	0.24746	1.1768	1.2427	0.37501	-0.91869
114	-1.3404	-0.28572	-0.9201	-0.96668	-0.05334	-3.0195	-1.6275	0.17104	-2.7505	0.44882

Table B5, Continued

115	2.0385	-1.084	-0.89401	1.6254	0.32103	0.14857	1.1768	1.0479	0.31604	0.83954
116	-0.02328	0.76078	0.61397	0.14321	-0.05334	-0.04215	1.1768	1.2102	0.25707	-0.78845
117	0.6353	-1.0385	-0.8074	0.33081	-0.05334	1.005	1.1768	1.0803	0.6109	-0.46286
118	0.50623	-0.32233	-0.17544	0.40672	0.32103	0.96442	-0.50577	-0.90061	0.49296	1.1651
119	-1.2544	1.021	-0.67302	-0.96668	0.32103	-2.3131	-1.6275	-0.47845	-2.4556	-1.2443
120	-1.7012	-1.1126	-1.0765	-0.96668	-0.05334	-2.4915	-1.6275	-0.60834	-2.4556	-0.56054
121	0.92653	-0.71942	-0.62848	-0.29538	0.42946	0.64832	-0.50577	-0.90061	0.49296	1.2954
122	0.72135	1.7328	2.9588	-0.68026	0.32103	0.74368	1.3925	1.2427	0.55193	1.4256
123	0.9166	-0.6762	-0.54137	-0.92801	-4.7471	0.51941	0.96107	1.3401	0.49296	-0.13726
124	-0.72819	1.5167	1.361	-0.96668	0.32103	-0.40946	1.1768	1.2102	0.13913	-0.65822
125	1.3667	-0.9796	-0.78338	-0.05442	0.42946	0.35695	-0.50577	-0.90061	0.49296	0.7093
126	-0.59581	0.98683	0.77873	-0.40171	0.32103	0.15563	-0.50577	-0.90061	0.49296	-0.13726
127	0.10579	-0.97918	-0.83796	-0.69923	0.32103	-0.71143	-0.50577	-0.90061	0.49296	1.1651
128	0.29112	-0.63214	-0.42116	-0.28285	0.42946	-0.17283	-0.50577	-0.90061	0.49296	0.83954
129	0.20176	-0.09069	-0.04538	1.233	0.32103	0.26865	-0.50577	-0.90061	0.49296	-0.5931
130	0.13888	-1.0476	-0.84928	-0.02363	-0.05334	-0.13221	0.96107	1.0479	0.25707	2.8583
131	-1.913	-0.91652	-1.0394	-0.96668	0.32103	-2.2248	-1.6275	-0.31607	-2.4556	-1.4722
132	0.92653	1.8983	2.9885	-0.96668	0.32103	0.91144	1.3925	1.3076	0.6109	1.4256
133	1.1119	1.7535	2.9865	-0.96668	-0.05334	0.83727	1.3925	1.2102	0.66987	3.1187
134	-0.19868	1.9303	1.3254	-0.86392	0.32103	-0.0916	1.1768	1.3076	0.25707	-0.2675
135	-0.71826	-0.48013	-0.4054	0.15896	0.32103	0.41346	-0.50577	-0.90061	0.49296	-0.65822
136	1.4792	-0.98332	-0.69673	1.6512	0.32103	0.71896	-0.50577	-0.90061	0.49296	-0.52798
137	0.75775	-0.35604	-0.34426	1.5037	0.32103	0.25982	-0.50577	-0.90061	0.49296	-0.36518

Table B5, Continued

138	0.15874	-0.50185	-0.03107	-0.21482	0.32103	0.83727	-0.50577	-0.90061	0.49296	0.77442
139	-1.8004	-0.74548	-1.085	-0.96668	0.32103	-2.276	-1.6275	0.56074	-2.4556	-1.3094
140	-1.2378	0.77505	0.49959	-0.32438	0.32103	0.13621	-0.50577	-0.90061	0.49296	-0.52798
141	2.1014	-1.1626	-0.97937	0.89507	0.32103	1.1269	-0.50577	-0.90061	0.49296	-0.20238
142	-0.66531	1.3159	0.91222	-0.80449	0.32103	-0.51012	1.1768	1.2752	0.13913	-0.13726
143	-1.2809	-0.72314	-1.0028	-0.96668	-0.05334	-2.465	-1.6275	0.00867	-2.4556	-0.20238
144	-1.0459	-1.1668	-1.0867	-0.96668	-0.05334	-2.2637	-1.6275	-0.25113	-2.4556	0.29253
145	-0.52962	0.34714	0.10869	-0.96668	0.32103	0.49822	-0.50577	-0.90061	0.49296	0.96978
146	-0.21854	0.2396	0.3664	-0.96632	-2.173	0.081464	0.96107	1.2427	0.31604	-0.91869
147	-0.1358	1.2437	0.89669	-0.58251	-0.05334	0.40816	1.1768	1.2427	0.43399	-0.65822
148	-0.62891	0.6582	1.3801	-0.56569	-0.05334	-0.34765	1.3925	1.2102	0.1981	0.83954
149	-0.02328	-0.749	-0.62154	1.3963	0.42946	-0.0916	-0.50577	-0.90061	0.49296	-0.72333
150	1.4263	-0.70763	-0.61415	2.363	0.32103	0.78253	-0.50577	-0.90061	0.49296	-0.72333
151	1.2806	-1.1833	-1.0582	-0.17902	0.32103	0.95559	-0.41948	-0.90061	-1.3941	-1.1792
152	0.1091	0.015405	0.27703	0.91511	-0.05334	0.74192	1.1768	1.2102	0.55193	-0.85357
153	-1.0988	0.73306	-0.66315	-0.96668	0.32103	-2.0677	-1.6275	0.20352	-2.4556	-0.8666
154	1.9822	-1.2104	-1.0037	0.92908	0.32103	0.67481	-0.50577	-0.90061	0.49296	-0.1047
155	1.4263	0.70287	1.1666	1.0257	0.32103	0.86023	-0.50577	-0.90061	0.49296	0.31858
156	1.1383	-0.76968	-0.67179	0.39383	0.32103	0.66422	-0.50577	-0.90061	0.49296	0.90466
157	-0.75136	-1.0514	-0.88569	-0.15252	0.32103	-0.97102	-0.50577	-0.90061	0.49296	-0.00702
158	1.0457	2.2588	1.8931	-0.71749	-0.05334	0.62537	0.96107	1.3726	0.49296	-0.00702
159	0.026363	-0.14922	0.043778	0.96667	-0.05334	0.24393	1.1768	1.1128	0.37501	-0.78845
160	-0.21854	0.10723	0.10642	0.85139	0.42946	0.15387	-0.50577	-0.90061	0.49296	-0.95125

Table B5, Continued

161	-0.39394	-0.85282	-0.7729	0.18975	0.32103	0.34458	-0.50577	-0.90061	0.49296	-0.72333
162	1.8499	-1.1459	-0.97869	-0.56175	0.32103	0.60064	-0.50577	-0.90061	0.49296	1.5559
163	1.3535	-0.92376	-0.59339	-0.96668	-3.5956	1.2064	1.3925	1.0479	0.37501	4.1606
164	0.15212	-0.27331	-0.3231	0.89507	0.32103	0.49292	-0.50577	-0.90061	0.49296	-0.07214
165	-0.63884	-0.23195	-0.26751	0.42963	0.32103	0.73662	-0.50577	-0.90061	0.49296	-0.78845
166	-0.98302	-0.81993	-1.0211	-0.96668	-0.05334	-2.1789	-1.6275	-0.08875	-2.4556	0.28602
167	1.4726	-0.92893	-0.77307	0.057281	0.32103	0.50881	-0.50577	-0.90061	0.49296	1.6535
168	-1.2478	-0.47868	-0.95659	-0.96668	-0.05334	-2.1789	-1.6275	0.17104	-2.4556	-0.16982
169	-0.46343	1.4985	0.94948	-0.60435	0.32103	0.19095	-0.50577	-0.90061	0.49296	-0.39774
170	0.96625	-0.80711	-0.70432	1.001	0.42946	0.98561	-0.50577	-0.90061	0.49296	-0.30006
171	-0.42703	-0.5732	-0.54425	0.66235	0.32103	0.86376	-0.50577	-0.90061	0.49296	-0.5931
172	-1.3206	0.93244	0.55817	-0.96668	0.42946	0.27218	-0.50577	-0.90061	0.49296	-0.20238
173	0.70149	-0.93513	-0.74728	1.3605	0.32103	-0.1587	-0.50577	-0.90061	0.49296	-0.2675
174	0.55918	0.31364	0.26597	-0.76905	0.32103	-0.13398	-0.50577	-0.90061	0.49296	2.2071
175	-0.89697	1.392	0.68697	-0.91691	0.42946	0.081464	-0.50577	-0.90061	0.49296	-0.52798
176	-0.5197	-0.75313	-0.64165	-0.13212	0.32103	0.27571	1.1768	1.0803	0.37501	-0.85357
177	0.21169	-0.19431	-0.16662	1.1897	0.32103	0.63949	-0.50577	-0.90061	0.49296	-0.5931
178	-1.3537	-0.47496	-0.95588	-0.96668	-0.05334	-2.4897	-1.6275	0.20352	-2.4556	-0.00702
179	0.64523	1.9742	1.4774	-0.72071	-0.05334	0.47526	1.1768	1.2752	0.43399	-0.52798
180	0.62868	0.22305	0.23106	1.8259	0.32103	0.000231	-0.50577	-0.90061	0.49296	-0.72333
181	0.006506	0.44848	0.32548	0.95271	-0.05334	-0.49246	1.1768	1.1778	0.13913	-0.82101
182	-1.9295	-0.39265	-0.45301	-0.14751	0.32103	0.17329	-0.50577	-0.90061	0.49296	-0.91869
183	-0.79107	-0.33536	-0.31235	0.64445	0.32103	0.15916	-0.50577	-0.90061	0.49296	-0.91869

Table B5, Continued

184	-1.3437	-0.65489	-0.98991	-0.96668	-0.05334	-3.1961	-1.6275	0.10609	-2.3967	0.73535
185	1.5752	-0.31468	-0.28353	2.7926	0.32103	0.60064	-0.50577	-0.90061	0.49296	-0.2675
186	-1.0624	-0.56141	-0.74832	-0.36591	0.32103	0.056741	-0.41948	-0.90061	-1.3941	-0.69078
187	-1.635	-0.04561	-0.11368	-0.03473	0.32103	-0.32999	-0.50577	-0.90061	0.49296	-0.78845
188	0.44666	0.35645	0.45982	0.51126	-0.05334	0.46467	0.96107	1.3401	0.43399	-0.65822
189	-0.40386	1.464	1.4371	-0.02542	-0.05334	-0.941	1.1768	1.2427	-0.03779	-0.5931
190	0.354	-0.56286	-0.50321	0.28642	0.32103	0.84787	1.1768	1.1453	0.55193	0.18834
191	0.72797	-0.23319	-0.21856	1.3806	0.32103	0.55473	-0.50577	-0.90061	0.49296	-0.23494
192	-1.1683	-1.0758	-1.0695	-0.96668	-0.05334	-2.2637	-1.6275	-0.05628	-2.4556	0.071126
193	1.6381	-1.1337	-0.95041	-0.55137	0.32103	0.30397	-0.50577	-0.90061	0.49296	1.4256
194	1.0953	0.74051	1.5845	0.64301	-0.05334	0.9291	1.3925	1.2102	0.6109	1.4256
195	-0.39394	-0.112	-0.10432	0.89829	0.32103	0.98738	-0.50577	-0.90061	0.49296	-0.91869
196	0.049529	0.2003	0.11024	0.43106	-0.05334	0.24746	1.1768	1.2752	0.37501	-0.2675
197	0.27457	-0.22368	-0.24017	0.42104	0.32103	0.72955	-0.50577	-0.90061	0.49296	0.15578
198	0.75444	-0.41809	-0.20492	-0.14321	0.32103	-0.60901	-0.50577	-0.90061	0.49296	2.7931
199	0.69487	0.61456	0.42825	1.3172	0.32103	0.070868	1.1768	1.3401	0.31604	-0.65822
200	-1.3404	-0.31447	-0.65277	-0.96668	0.42946	-0.20285	-0.41948	-0.90061	-1.3941	-0.13726
201	-0.58588	-0.3246	0.12255	-3.48E-06	-0.05334	-0.31763	1.3925	1.1128	0.25707	0.51394
202	-0.01997	2.0921	1.5383	-0.96668	0.32103	0.11855	1.1768	1.3076	0.31604	-0.2675
203	-0.14904	1.0753	1.5225	-0.36412	0.32103	0.016125	1.1768	1.2752	0.31604	0.51394
204	0.24479	-0.56286	-0.3631	-0.34013	0.32103	-0.17636	-0.50577	-0.90061	0.49296	2.0768
205	1.1019	-0.70267	-0.64666	1.7755	0.32103	1.0121	-0.50577	-0.90061	0.49296	-0.62566
206	-0.46343	1.5113	0.56929	-0.8027	0.32103	-0.13221	-0.50577	-0.90061	0.49296	-0.2675

Table B6: DATA USED FOR TRAINING NETWORK.

S.N	MBHP	Q_O	Qg	Q_W	TBG	DEPTH	API	STM	BTM	P_{wh}
1	2804	4600	2693.37	11000	4	6621	32.6	90	212	175
2	2368	700	411.69	1300	2.441	6271	32.6	90	212	230
3	2343	8616	4230.46	2500	3.813	6294	36.5	156	208	285
4	2161	2983	1023.09	905	3.958	6345	32.8	90	180	220
5	2289	3792	1749.74	3796	4	6340	32.6	90	212	210
6	2641	1079	593.45	900	1.995	6565	36	156	211	230
7	2565	14624	8057.82	1256	3.958	6518	36	157	210	250
8	2615	3500	1968.61	5800	3.958	6653	32.6	90	212	320
9	2888	980	514.85	2910	3.958	6675	32.6	90	212	460
10	2449	3050	1820.85	3000	3.958	6727	36.5	152	212	250
11	2403	8314	4484.19	3712	4	6323	32.6	90	212	235
12	2023	10812	5140.02	0	4	6666	32.6	90	212	280
13	2049	5486	2984.98	2498	4	6790	32.6	90	212	200
14	2353	11311	5950.39	0	4	6553	32.6	90	212	400
15	1932	1041	124.92	0	3.813	4949	30	100	162	215
16	2670	4957	2738.60	8400	3.958	6659	32.6	90	212	250
17	2646	7300	6263.40	940	2.992	6350	37	155	209	545
18	2415	9000	4765.46	3400	3.958	6619	32.6	90	212	260
19	2712	15975	8802.23	10	3.813	6708	36	159	212	330
20	2610	4200	3977.40	1000	2.441	6317	37	152	210	515
21	2679	15770	13562.20	0	3.813	6563	37	157	211	580
22	2163	1129	135.48	0	3.813	4964	30	114	162	340

Table B6, Continued

23	2472	13621	6388.25	0	3.813	6345	36.5	157	208	290
24	2598	6570	5046.70	0	4	6412	32.6	90	212	780
25	2776	9800	8457.40	4900	3.958	6709	37	156	212	590
26	3038	1650	1278.39	7150	3.958	6988	32.6	90	212	240
27	2770	19370	11040.90	0	3.813	6756	36	160	213	295
28	3217	1439	823.54	10785	3.958	7007	32.6	90	212	290
29	2354	3926	2223.61	3174	3.958	7079	32.6	90	212	195
30	2533	15092	12632.00	0	3.958	6035	37	158	205	580
31	2857	2638	2015.43	8160	3.958	6594	36.5	156	211	270
32	2631	3555	1261.60	326	4	6376	32.8	90	180	570
33	2447	5699	3077.46	5880	3.958	6381	36.5	155	209	190
34	2631	1497	481.78	0	4	6349	32.8	90	180	600
35	2945	2300	1219.40	7100	3.958	6929	32.6	90	212	250
36	2099	1160	139.20	0	3.813	5078	30	123	162	302
37	2489	7321	4026.55	4173	3.958	6550	36	158	210	312
38	2392	8200	4460.80	1450	3.813	6543	36.5	154	210	320
39	2239	13215	5581.13	300	3.958	6310	32.6	90	212	240
40	2448	6400	3296.00	4600	3.958	6664	36.5	154	212	200
41	2044	5966	715.92	0	3.813	4550	30	127	163	368
42	2447	13986	7244.75	113	3.813	6625	36.5	156	211	205
43	2585	3527	1378.24	0	4	6574	32	90	190	640
44	2611	14242	6693.74	0	3.813	6857	36.5	157	209	210
45	2956	2245	1336.96	9297	3.958	6538	32.6	90	212	380
46	1989	3614	433.68	217	3.958	5050	30	125	162	104

Table B6, Continued

47	2557	5583	2935.93	6744	4	6535	32.6	90	212	205
48	2453	3400	2312.00	7900	3.813	6062	36.5	154	206	200
49	2423	6840	4035.60	5078	3.958	6447	36.5	154	209	175
50	2250	4700	2431.14	4500	3.958	6760	32.6	90	212	180
51	2122	8739	4572.49	2349	3.958	6759	32.6	90	212	200
52	2723	2020	945.36	6128	3.958	6586	36.5	155	211	205
53	2741	18110	9852.85	998	4	6750	32.6	90	212	210
54	3105	1080	724.08	7240	3.958	6450	32.6	90	212	450
55	2681	1300	699.42	3500	3.958	6935	32.6	90	212	250
56	2503	14360	7180.00	0	3.958	6731	36.5	157	212	230
57	2776	2470	1528.62	8480	3.958	6363	32.6	90	212	275
58	2190	989	118.68	10	3.958	5050	30	106	161	282
59	2504	6700	3936.40	800	4	6368	32.6	90	212	620
60	2405	4213	1683.09	4700	3.958	6332	32.6	90	212	240
61	2163	2187	262.44	0	3.813	4950	30	105	162	400
62	2681	3832	2404.12	9417	3.958	6640	32.6	90	212	190
63	2402	2993	1451.07	5628	3.958	6519	32.6	90	212	210
64	2541	3100	1788.09	5300	3.958	6803	32.6	90	212	210
65	2667	18603	10399.08	531	3.813	6500	36.5	158	210	200
66	2529	3750	2448.75	3214	3.958	6826	36.5	153	213	340
67	2716	13200	11220.00	0	3.813	6826	37	155	215	760
68	2853	10200	8772.00	3900	3.958	6897	37	156	214	570
69	2251	9843	4051.71	2117	3.958	6297	32.6	90	212	250

Table B6, Continued

70	2542	18146	9998.45	0	3.958	6366	36	160	209	270	X252
71	2367	12388	5980.02	812	3.958	6618	32.6	90	212	380	C031
72	2053	8563	3758.81	1875	3.958	6409	32.6	90	212	260	C090
73	2951	1100	613.89	5200	3.958	6447	32.6	90	212	320	C003
74	2505	323	322.68	1119	1.995	7100	37	155	215	80	X312
75	2293	14848	4188.49	0	3.958	6230	32.6	90	212	290	C150
76	2391	7507	4504.20	0	3.958	6541	36.5	156	210	550	X036
77	2262	13728	7220.93	0	3.813	5995	36.5	157	205	220	X047
78	2633	4000	2472.00	5496	3.958	6492	36.5	155	210	350	X050
79	2306	13354	5971.29	0	4	6516	32.6	90	212	285	C147
80	2306	3700	1827.80	1620	3.958	6363	32.6	90	212	340	C054
81	2024	280	33.60	0	3.813	5082	30	76	162	88	X402
82	2335	6459	2027.82	0	3.958	6854	32.8	90	180	390	A008
83	2396	3913	1522.16	10	3.958	6493	32.8	90	180	476	A015
84	2107	2350	282.00	118	3.958	5050	30	115	162	200	X389
85	2894	1958	1174.80	6199	3.958	6628	36.5	156	211	470	X034
86	2186	6454	3032.46	493	3.958	6735	32.6	90	212	420	C109
87	2692	886	885.11	5578	3.958	6778	36.5	155	208	220	X015
88	2259	10648	4459.96	1183	3.958	6493	32.6	90	212	320	C075
89	2541	2525	1156.97	659	2.992	6854	32	90	190	400	B002
90	2621	9276	5519.22	5616	3.958	6688	36	158	212	220	X249
91	2278	4137	579.18	0	3.958	5189	30	97	162	350	X380
92	2561	12397	10636.63	1672	3.813	6163	37	156	207	570	X344

Table B6, Continued

93	2744	3000	2400.00	0	1.995	6454	37	153	207	470
94	2141	7481	3441.58	3052	3.958	6341	32.6	90	212	210
95	2766	344	177.16	3956	3.958	6452	36.5	150	210	185
96	2127	8033	963.96	0	3.813	5100	30	135	162	140
97	2740	1193	938.89	0	1.995	6597	37	154	211	560
98	2484	2739	1369.50	3377	3.958	6533	36.5	153	210	285
99	2838	7790	5474.61	5485	3.958	6864	32.6	90	212	375
100	2686	5750	4025.00	6300	3.813	6701	36.5	152	212	220
101	2342	11390	5125.50	1210	3.813	6312	36.5	157	208	200
102	2671	19618	9730.53	0	3.813	6499	36	150	210	270
103	1227	887	502.93	252	3.813	6200	36.5	150	207	150
104	2453	4700	2512.54	5600	3.958	6541	32.6	90	212	220
105	2863	9600	8112.00	3400	3.813	7028	37	155	215	620
106	2571	6798	3231.34	5603	3.958	6809	32.6	90	212	235
107	2710	2952	1549.80	130	1.995	6630	36	158	211	180
108	2082	2350	75.20	0	3.958	5071	30	127	162	225
109	2923	5964	3257.01	9022	3.958	6899	32.6	90	212	220
110	2685	13898	8130.33	43	3.813	6582	36.5	155	211	590
111	1837	600	299.88	800	4	5617	32	90	190	200
112	1991	2124	1073.00	776	3.958	6498	32.6	90	212	205
113	2484	4760	2451.40	6340	3.958	6500	36.5	156	210	180
114	2084	4940	592.80	0	3.813	4650	30	123	157	390
115	3105	1080	672.84	7240	3.958	6444	36.5	150	209	450

Table B6, Continued

116	2482	10000	5300.00	3100	3.813	6336	36.5	155	208	200	X144
117	2681	1300	938.60	3624	3.813	6929	36.5	151	214	250	X062
118	2642	4763	2877.73	3836	3.958	6906	32.6	90	212	500	C023
119	2110	11258	1350.96	0	3.958	5050	30	103	162	130	X370
120	1975	942	113.04	0	3.813	4949	30	99	162	235	X403
121	2769	2843	1487.63	1875	4	6727	32.6	90	212	520	C044
122	2707	14700	12495.00	800	3.958	6781	37	156	213	540	X325
123	2766	3052	1754.90	108	1.995	6654	36	159	212	300	X231
124	2269	13655	7592.18	0	3.958	6128	36.5	155	206	220	X013

Table B7: DATA USED FOR VALIDATING NETWORK.

S.N	MBHP	Q_O	Qg	Q_W	TBG	DEPTH	API	STM	BTM	P_{wh}	NWELL
1	2902	1585	1012.30	2548	4	6562	32.6	90	212	430	C193
2	2309	11093	5805.54	1578	3.958	6448	32.6	90	212	300	C091
3	2521	1587	844.86	747	3.958	5957	32.6	90	212	500	C252
4	2577	3265	2123.77	1910	4	6262	32.6	90	212	450	C152
5	2550	5883	3276.83	6144	3.958	6512	32.6	90	212	230	C203
6	2531	1256	810.12	2634	3.813	6285	36	150	208	760	X205
7	1911	1890	226.80	0	3.958	5100	30	108	162	95	X408
8	2769	15500	12586.00	0	3.958	6876	37	158	214	540	X337
9	2825	14800	12580.00	0	3.813	6834	37	155	215	800	X320
10	2429	15655	7483.09	287	3.958	6308	36.5	158	208	280	X032
11	2272	4000	2172.13	3144	3.958	6594	32.6	90	212	220	C102
12	2936	1567	1278.21	7312	3.958	6767	32.6	90	212	240	C280
13	2718	4600	2359.74	6900	3.958	6507	32.6	90	212	265	C011
14	2537	3895	3320.73	2100	3.958	6834	32.6	90	212	440	C032
15	1945	2717	86.94	0	3.958	5071	30	135	162	120	X379
16	2115	10069	4949.02	1794	3.958	6437	32.6	90	212	240	C065
17	3124	700	410.92	5200	3.958	6998	32.6	90	212	290	C272
18	2288	12684	6215.16	453	3.958	6071	36.5	157	206	300	X090
19	2102	2825	339.00	0	3.813	4964	30	118	162	290	X399
20	2173	680	81.60	0	3.813	5078	30	110	162	366	X395
21	2329	8000	3749.59	0	3.958	6642	32.6	90	212	470	C224
22	2423	7480	4540.36	1	2.992	6406	36	156	209	180	X230

Table B7, Continued

23	2448	12335	6167.50	1073	3.813	6591	36.5	156	211	220	X117
24	2299	9504	7650.72	1120	3.813	6163	37	155	207	450	X345
25	2482	2700	1508.92	6600	4	6308	32.6	90	212	210	C285
26	2920	2900	1531.59	9300	3.958	6803	32.6	90	212	210	C089
27	2876	600	169.09	2200	3.958	6901	32.8	90	180	140	A004
28	2522	6396	4266.13	5256	3.813	6780	36.5	155	213	190	X105
29	2157	9866	1381.24	0	3.958	5189	30	124	162	188	X382
30	3088	469	336.41	5295	3.958	6742	32.6	90	212	305	C197
31	2920	9720	6995.71	5565	3.958	6847	32.6	90	212	370	C062
32	2833	2600	1354.72	3800	3.958	6736	32.6	90	212	460	C174
33	2262	1238	698.38	2274	3.958	5810	32.6	90	212	320	C127
34	2805	17243	9225.01	696	3.813	6714	36	160	212	320	X268
35	2497	5600	3550.40	5400	3.813	6498	36.5	152	210	200	X024
36	2423	6840	3742.63	5078	4	6447	32.6	90	212	175	C235
37	2370	2198	1044.47	3230	3.958	6555	32.6	90	212	210	C163
38	3048	781	413.03	1131	3.958	6700	32.6	90	212	560	C254
39	2898	1855	1595.30	0	2.441	7043	37	150	210	960	X363
40	2535	5000	2424.66	5200	3.958	6639	32.6	90	212	310	C026
41	2296	5200	2595.22	3900	3.958	6777	32.6	90	212	200	C050

Table B8: DATA USED FOR TESTING NETWORK.

S.N	MBHP	Q_O	Qg	Q_W	TBG	DEPTH	API	STM	BTM	P_{wh}	NWELL
1	2192	2357	282.84	0	3.813	5126	30	115	162	365	X392
2	2934	1830	1043.94	2860	3.958	6648	32.6	90	212	575	C245
3	2112	4007	480.84	0	3.813	5126	30	123	162	295	X393
4	2349	13567	6329.51	1012	3.958	6468	32.6	90	212	260	C230
5	2781	2419	1254.90	5496	4	6918	32.6	90	212	275	C276
6	2360	3550	1746.09	4550	3.958	6849	32.6	90	212	230	C035
7	2090	10830	5128.77	0	4	6514	32.6	90	212	290	C144
8	2701	1800	1123.08	6500	3.958	6270	32.6	90	212	280	C297
9	2658	7838	4232.18	552	3.958	6284	32.6	90	212	660	C095
10	2218	13052	5523.98	139	4	6406	32.6	90	212	240	C131
11	2332	2680	1447.20	2331	3.958	6516	36.5	151	210	190	X081
12	2553	5382	2904.80	6023	3.958	6722	32.6	90	212	230	C290
13	2080	4025	483.00	0	3.813	4950	30	124	162	320	X375
14	2684	15867	7949.37	687	3.813	6629	36.5	157	211	240	X156
15	2679	7400	4125.06	7800	3.958	6360	32.6	90	212	210	C191
16	2491	8490	4414.80	5361	3.813	6081	36.5	154	206	195	X024
17	1906	4423	2026.03	2288	3.958	6458	32.6	90	212	180	C027
18	2250	4700	2457.65	4500	3.958	6450	32.6	90	212	180	C072
19	2083	3155	378.60	0	3.813	4550	30	121	163	434	X371
20	2965	4800	2546.07	10500	3.958	6700	32.6	90	212	280	C002
21	2168	3607	1119.88	1678	3.958	6392	32.8	90	180	215	A005

Table B8, Continued

22	1995	6101	3067.24	2603	3.958	6173	32.6	90	212	200	C232
23	2624	8045	4827.00	4128	3.813	6623	36	159	211	220	X259
24	2367	13400	7825.60	2629	3.813	5827	36.5	156	203	230	X112
25	2596	3600	1872.00	3500	3.958	6840	36.5	153	213	350	X086
26	2709	5194	2745.43	6556	3.958	6674	32.6	90	212	285	C018
27	2136	1120	134.40	0	3.813	5078	30	116	162	332	X396
28	2984	840	499.78	1160	3.958	6532	32.6	90	212	540	C110
29	2820	9902	8278.07	4496	3.813	6886	37	155	214	540	X336
30	2370	5780	3095.98	5209	3.958	6919	32.6	90	212	180	C289
31	2504	7290	3754.35	3904	3.813	6500	36.5	157	210	280	X103
32	2572	5240	2679.14	3876	3.958	6773	32.6	90	212	345	C021
33	2717	4300	2787.29	2300	3.958	6015	32.6	90	212	750	C014
34	2699	9293	4730.14	6379	3.958	6400	36.5	159	209	220	X030
35	2084	4801	1413.09	0	4	6245	32.8	90	180	300	A012
36	2312	4752	3792.10	2700	3.813	6180	37	152	208	400	X326
37	2483	16437	8136.32	0	3.958	6427	36.5	158	209	280	X100
38	2444	11521	8087.74	1683	3.958	6369	36.5	157	209	400	X037
39	2563	3600	2301.92	1750	3.958	6260	32.6	90	212	640	C049
40	2822	2924	1431.85	7659	3.958	6933	32.6	90	212	225	C060
41	2349	13629	5162.91	458	3.958	6285	32.6	90	212	280	C137

Table B9: STATISTICAL DESCRIPTION OF THE INPUT DATA USED FOR TRAINING (124 POINTS).

	MBHP	Q_O	Qg	Q_W	TBG	DEPTH	API	STM	BTM	P_{wh}
Minimum	1227	280	33.6	0	1.995	4550	30	76	157	80
Maximum	3217	19618	13562.2	11000	4	7100	37	160	215	780
Mean	2222	9949	6797.9	5500	2.9975	5825	33.5	118	186	430
STDEV	995	9669	6764.3	5500	1.0025	1275	3.5	42	29	350
Skewness	0.71362	0.05316	0.00913	0	0.00929	-1.0314	-1.7926	0.18135	-1.5156	0.40254

Table B10: STATISTICAL DESCRIPTION OF THE INPUT DATA USED FOR VALIDATION (41 POINTS).

	MBHP	Q_O	Qg	Q_W	TBG	DEPTH	API	STM	BTM	P_{wh}
Minimum	1911	469	81.6	0	2.441	4964	30	90	162	95
Maximum	3124	17243	12586	9300	4	7043	37	160	215	960
Mean	2517.5	8856	6333.8	4650	3.2205	6003.5	33.5	125	188.5	527.5
STDEV	606.5	8387	6252.2	4650	0.7795	1039.5	3.5	35	26.5	432.5
Skewness	-0.8358	0.10247	0.02397	0	-0.8255	-1.3971	-1.7926	-0.4753	-1.6105	0.38808

Table B11: STATISTICAL DESCRIPTION OF THE INPUT DATA USED FOR TESTING (41 POINTS).

	MBHP	Q_O	Qg	Q_W	TBG	DEPTH	API	STM	BTM	P_{wh}
Minimum	1906	840	134.4	0	3.813	4550	30	90	162	180
Maximum	2984	16437	8278.07	10500	4	6933	37	159	214	750
Mean	2445	8638.5	4206.24	5250	3.9065	5741.5	33.5	124.5	188	465
STDEV	539	7798.5	4071.84	5250	0.0935	1191.5	3.5	34.5	26	285
Skewness	-1.0179	0.19603	0.06058	0	-1.9904	-1.1282	-1.7926	-0.5021	-1.6238	0.84748

APPENDIX C

PROGRAM LISTING

APPENDIX C

PROGRAM LISTING

MAIN MODEL PROGRAM

```
close all; %close all figure windows
clear all; %Clears all variables and other classes of data too.
% To reduce the risk of confusing errors.
% Step(1) Processing of the data:
% ==============================
% Step (2) Reading the input file
% ==============================
% Loads data and prepares it for a neural network.
ndata= xlsread('main_file.xls');
%
% Step (3) Normalizing the trainning data
% ======================================
% Putting the data in the range of zero and one.
% ********************************************
for i=1:10
   meana(1,i)=mean(ndata(1:165,i));
   stda(1,i)=std(ndata(1:165,i));
   anormal(:,i)=(ndata(:,i)-meana(1,i))/stda(1,i);
end
%
%60% of data will be used for trainning
%20% of data will be used for cross-validation
%20% of data will be used for testing
for i=1:124
   atr(i,:)=anormal(i,:);
end
for i=125:165
   aval(i-124,:)=anormal(i,:);
end
%
for i=166:length(anormal)
   atest(i-165,:)=anormal(i,:);
end
% Step (4) Generating Network structure
% ====================================
% Back propagation: Batch gradient descent method with momentum
% ************************************************************
%
T=atr(:,1)';
```

```
P=atr(:,2:10)';
TV.P=atest(:,2:10)';
TV.T=atest(:,1)';
VV.T=aval(:,1)';
VV.P=aval(:,2:10)';
%
S1=6; % Number of neurons in the first hidden layer
S2=3; % Number of neurons in the second hidden layer
S3=3; % Number of neurons in the third hidden layer
S4=1; % Number of output variables (in our case PBHP)

net=newff(minmax(P),[S1 S2 S3 S4],{'tansig' 'tansig' 'tansig' 'purelin'},'trainbfg');
net=init(net);
net.trainParam.epochs = 350;          %Max number of iterations
net.trainParam.goal = 0.0;            %Error tolerance; stopping criterion
net.trainParam.max_fail =15   ;       %Maximum validation failures
net.trainParam.mem_reduc = 3          %Factor to use for memory/speed tradeoff
net.trainParam.min_grad = 1e-15       %Minimum performance gradient
net.trainParam.mu = 0.5               %Initial Mu
net.trainParam.mu_dec = 0.9           %Mu decrease factor
net.trainParam.mu_inc = 10            %Mu increase factor
net.trainParam.mu_max = 1e10          %Maximum Mu
net.trainParam.show = 5;              %The result is shown at every 5th iteration
                                        (epoch)
net.trainParam.time = inf             %Maximum time to train in seconds
net.trainParam.lr_inc = 0.25
net.trainParam.lr = 0.750;           %Learning rate used in some gradient schemes

[net,tr]=train(net,P,T,[],[],VV,TV);

% Plotting the network error progress for training, testing, and validation
% data
figure
plot(tr.epoch,tr.perf,tr.epoch,tr.vperf,tr.epoch,tr.tperf)
legend('Training','Validation','Test',-1);
title('Training, Validation, Test Progress')
ylabel('Squared Error');
xlabel('Epoch')
set(gcf, 'color', 'white')
grid off
%
% Detect whether the net simulates the input data
% for testing data only
% **********************
figure
y1=sim(net,TV.P);

plot(TV.T,'-r*');
refline(0,0)
hold
```

```
plot(y1,':ko');
grid off
set(gcf, 'color', 'white')
title('Graph of Simulated network for Testing set')
xlabel('Data Point No')
ylabel('output of network and errors')
legend('Actual BHP','ref. line','Predicted BHP')

% Detect whether the net simulates the input data
% for training data only
% **********************
figure
y2=sim(net,P);

plot(T,'-r*');
refline(0,0)
hold
plot(y2,':ko');
grid off
set(gcf, 'color', 'white')
title('Graph of Simulated network for Training set')
xlabel('Data Point No')
ylabel('output of network and errors')
legend('Actual BHP','ref. line','Predicted BHP')
% Detect whether the net simulates the input data
% for validation data only
% **********************
figure
y3=sim(net,VV.P);

plot(VV.T,'-r*');
refline(0,0)
hold
plot(y3,':ko');
grid off
set(gcf, 'color', 'white')
title('Graph of Simulated network for Validation set')
xlabel('Data Point No')
ylabel('output of network and errors')
legend('Actual BHP','ref. line','Predicted BHP')
colormap gray

% Evaluation of actual and estimated targets
% ---------------------------------------

% firstly, for testing set:
% ========================
Pred_tt=(y1*stda(1,1))+meana(1,1);
Calc_tt=ndata(166:length(ndata),1);
```

```
% secondly, for validation set:
% ============================
Pred_v=(y3*stda(1,1))+meana(1,1);
Calc_v=ndata(125:165,1);

% thirdly, for training set:
% ============================
Pred_t=(y2*stda(1,1))+meana(1,1);
Calc_t=ndata(1:124,1);


% Evaluating Relative Error for training set:
%=========================================

Et=(Calc_t'-Pred_t)./Calc_t'*100;
[q,z] = size(Et);
figure
%
plot(Calc_t',Pred_t,'o')
grid off
set(gcf, 'color', 'white')
%axis ([1500,3500,1500,3500])

title('Graph of Predicted HP vs. Calculated HP');
xlabel('Calculated BHP "psig"');
ylabel('Predicted BHP "psig"')
legend('Training set')
% Addding Reference Line with 45 degree slope
refline(1,0)

% Evaluating the correlation coefficient for training set:
% ======================================================
Rt=corrcoef(Pred_t,Calc_t);
Rt2=min(Rt(:,2));
gtext(['correlation coefficient = (' num2str(Rt2) ')']);

% Evaluating Relative Error for validation set:
%=========================================

Ev=(Calc_v'-Pred_v)./Calc_v'*100;
[m,n] = size(Ev);
figure
%
plot(Calc_v',Pred_v,'o')
grid off
set(gcf, 'color', 'white')
%axis ([1500,3500,1500,3500])

title('Graph of Predicted BHP vs. Calculated BHP');
xlabel('Calculated BHP "psig"');
```

```
ylabel('Predicted BHP "psig"')
legend('Validation set')
% Addding Reference Line with 45 degree slope
refline(1,0)

% Evaluating the correlation coefficient for validation set:
% ========================================================
Rv=corrcoef(Pred_v,Calc_v);
Rv2=min(Rv(:,2));
gtext(['correlation coefficient = (' num2str(Rv2) ')']);

% Evaluating Relative Error for testing set:
%=========================================

Ett=(Calc_tt'-Pred_tt)./Calc_tt'*100;
[m,n] = size(Ett);
figure
%
plot(Calc_tt',Pred_tt,'o')
grid off
set(gcf, 'color', 'white')
%axis ([1500,3500,1500,3500])

title('Graph of BHP vs.Calculated BHP');
xlabel('Calculated BHP "psig"');
ylabel('Predicted BHP "psig"')
legend('Testing set')
% Addding Reference Line with 45 degree slope
refline(1,0)

% Evaluating the correlation coefficient for testing set:
% ========================================================
Rtt=corrcoef(Pred_tt,Calc_tt);
Rtt2=min(Rtt(:,2));
gtext(['correlation coefficient = (' num2str(Rtt2) ')']);

% plotting the histogram of the errors for training set:
% ========================================================
figure
histfit(Et,10)
h = findobj(gca,'Type','patch');
set(h,'FaceColor','w','EdgeColor','k')
title('Graph of Histogram');
legend('Training set')
xlabel('Error');
ylabel('Frequency')
set(gcf, 'color', 'white')

% plotting the histogram of the errors for validation set:
% ========================================================
```

```
figure
histfit(Ev,10)
h = findobj(gca,'Type','patch');
set(h,'FaceColor','w','EdgeColor','k')
title('Graph of Histogram');
legend('Validation set')
xlabel('Error');
ylabel('Frequency')
set(gcf, 'color', 'white')
% plotting the histogram of the errors for testing set:
% ====================================================
figure
histfit(Ett,10)
h = findobj(gca,'Type','patch');
set(h,'FaceColor','w','EdgeColor','k')
title('Graph of Histogram');
legend('Testing set')
xlabel('Error');
ylabel('Frequency')
set(gcf, 'color', 'white')
%
% Estimating the residuals for training set:
% ========================================
figure
Errort = Pred_t-Calc_t';
plot(Errort,':ro');
grid off
set(gcf, 'color', 'white')
title('Neural Network Model')
legend('training set')
xlabel('Data Point No')
ylabel('Errors')

% Estimating the residuals for validation set:
% ========================================
figure
Errorv = Pred_v-Calc_v';
plot(Errorv,':ro');
grid off
set(gcf, 'color', 'white')
title('Neural Network Model')
legend('validation set')
xlabel('Data Point No')
ylabel('Errors')

% Estimating the residuals for testing set:
% ========================================
figure
Errortt = Pred_tt-Calc_tt';
plot(Errortt,':ro');
```

```
grid off
set(gcf, 'color', 'white')
title('Neural Network Model')
legend('testing set')
xlabel('Data Point No')
ylabel('Errors')

% ********************
% STATISTICAL ANALYSIS:
% ********************
% Training set:
% =============
% Determining the Maximum Absolute Percent Relative Error
MaxErrt = max(abs(Et));

% Evaluating the average error

Etavg = 1/z*sum(Et);

% Evaluating the standard deviation
STDT = std(Errort)

% Determining the Minimum Absolute Percent Relative Error
MinErrt = min(abs(Et));


% Evaluating Average Absolute Percent Relative Error
% ================================================
AAPET = sum(abs(Et))/z;

% Evaluating Average Percent Relative Error
% =======================================
APET = 1/z*sum(Et);

% Evaluating Root Mean Square
% ==========================
RMSET = sqrt(sum(abs(Et).^2)/z);

% Validation set:
% ===============
% Determining the Maximum Absolute Percent Relative Error
MaxErrv = max(abs(Ev));

% Determining the Minimum Absolute Percent Relative Error
MinErrv = min(abs(Ev));

% Evaluating the average error

Evavg = 1/n*sum(Ev);
```

```
% Evaluating the standard deviation
STDV = std(Errorv)


% Evaluating Average Absolute Percent Relative Error
% ================================================
AAPEV = sum(abs(Ev))/n;


% Evaluating Average Percent Relative Error
% ========================================
APEV = 1/n*sum(Ev);

% Evaluating Root Mean Square
% ==========================
RMSEV = sqrt(sum(abs(Ev).^2)/n);

% Testing set:
% ============
% Determining the Maximum Absolute Percent Relative Error
MaxErrtt = max(abs(Ett));

% Determining the Minimum Absolute Percent Relative Error
MinErrtt = min(abs(Ett));

% Evaluating the average error

Ettavg = 1/n*sum(Ett);

% Evaluating the standard deviation
STDTT = std(Errortt)

% Evaluating Average Absolute Percent Relative Error
% ================================================
AAPETT = sum(abs(Ett))/n;

% Evaluating Average Percent Relative Error
% ========================================
APETT = 1/n*sum(Ett);

% Evaluating Root Mean Square
% ==========================
RMSETT = sqrt(sum(abs(Ett).^2)/n);

% net parameters:
% * * * * * * * *

% Evaluating the input weight matrix (from input to hidden laeyrs)
X1=net.IW{1,1};
```

```
% Evaluating the first hidden layer's weight matrix (from the first hidden layer to the
2nd one)
X2=net.LW{2,1};

% Evaluating the second hidden layer's weight matrix (from 2nd hidden layer to the
3rd one)
X3=net.LW{3,2};

% Evaluating the last hidden layer's weight matrix (from hidden layer to the output)
X4=net.LW{4,3};

% Evaluating the input bias vector
X5=net.b{1};

% Evaluating the first hidden layer's bias vector
X6=net.b{2};

% Evaluating the second hidden layer's bias vector
X7=net.b{3};

% Evaluating the third hidden layer's bias vector
X8=net.b{4};
```

Executable Program

```
load data

% Enter the bottomhole pressure or leave the first column empty
% Enter the oil rate in the second column
% Enter the gas rate in the third column
% Enter the water rate in the fourth column
% Enter the tubing diameter in the fifth column
% Eneter the depth in the sixth column
% Enter the API in the seventh column
% Enter the surface temperature in the eighth column
% Enter the bottomhole temperature in the ninth column
% Enter the surface (wellhead)pressure in the tenth column

%Loads data and prepares it for a neural network from the mat file.
% Step (3) Normalizing the trainning data
% ======================================
for i=1:10
  % meana=mean(ndata(:,i));
   % stda=std(ndata(:,i));
   anormal(:,i)=(ndata(:,i)-meana(1,i))/stda(1,i);
end

for i=1:length(anormal)
   atest(i,:)=anormal(i,:);
end


P = ndata(:,2:10)';
TV.P = atest(:,2:10)';

%Insert the network parameters
S1 = 6; % Number of neurons in the first hidden layer
S2 = 3; % Number of neurons in the 2ND hidden layer
S3 = 3; % Number of neurons in the 3RD hidden layer
S4 = 1; % Number of output variables (in our case PBHP)


net=newff(minmax(P),[S1 S2 S3 S4],{'tansig' 'tansig' 'tansig' 'purelin'});
```

```
net.IW{1,1} = X1;

% Evaluating the first hidden layer's weight matrix (from the first hidden layer to the
2nd one)
net.LW{2,1} = X2;

% Evaluating the second hidden layer's weight matrix (from 2nd hidden layer to the
3rd one)
net.LW{3,2} = X3;

% Evaluating the last hidden layer's weight matrix (from hidden layer to the output)
net.LW{4,3} = X4;

% Evaluating the input bias vector
net.b{1} = X5;

% Evaluating the first hidden layer's bias vector
net.b{2} = X6;

% Evaluating the second hidden layer's bias vector
net.b{3} = X7;

% Evaluating the third hidden layer's bias vector
net.b{4} = X8;


% Detect whether the net simulates the input data
% for testing data only
% **********************
figure
y1=sim(net,TV.P);

plot(y1,':ko');
grid off
set(gcf, 'color', 'white')
title('Graph of Simulated network for Testing set')
xlabel('Data Point No')
ylabel('output of network and errors')
legend('Actual BHP','ref. line','Predicted BHP')

Pred_BHP=(y1*stda(1,1))+meana(1,1);

% Remove the comment from the next lines if you have the value of BHP

%Calc_BHP=ndata(1:length(ndata),1);
%plot(Calc_t',Pred_t,'o')
%grid off
%set(gcf, 'color', 'white')
%title('Graph of Predicted HP vs. Calculated HP');
%xlabel('Calculated BHP "psia"');
```

```
%ylabel('Predicted BHP "psia"')
%legend('Training set')
%Addding Reference Line with 45 degree slope
%refline(1,0)

% Evaluating Relative Error for testing set:
%=========================================
%Ett=(Calc_tt'-Pred_tt)./Calc_tt'*100;
%[m,n] = size(Ett);
%figure
%
%plot(Calc_tt',Pred_tt,'o')
%grid off
%set(gcf, 'color', 'white')

% plotting the histogram of the errors for testing set:
% ====================================================
%figure
%histfit(Ett,10)
%h = findobj(gca,'Type','patch');
%set(h,'FaceColor','w','EdgeColor','k')
%title('Graph of Histogram');
%legend('Testing set')
%xlabel('Error');
%ylabel('Frequency')
%set(gcf, 'color', 'white')

% Estimating the residuals for testing set:
% =========================================
%figure
%Errortt = Pred_tt-Calc_tt';
%plot(Errortt,':ro');
%grid off
%set(gcf, 'color', 'white')
%title('Neural Network Model')
%legend('testing set')
%xlabel('Data Point No')
%ylabel('Errors')

% Stattistical Analysis:
%======================
% Testing set:
% ============
% Determining the Maximum Absolute Percent Relative Error
%MaxErrtt = max(abs(Ett));

% Determining the Minimum Absolute Percent Relative Error
%MinErrtt = min(abs(Ett));

% Evaluating the average error
```

```
%Ettavg = 1/n*sum(Ett);

% Evaluating the standard deviation
%STDTT = std(Errortt)

% Evaluating Average Absolute Percent Relative Error
% ================================================
%AAPETT = sum(abs(Ett))/n;

% Evaluating Average Percent Relative Error
% ========================================
%APETT = 1/n*sum(Ett);

% Evaluating Root Mean Square
% ==========================
%RMSETT = sqrt(sum(abs(Ett).^2)/n);
```